International Committee for Future Accelerators
Sponsored by the Particles and Fields Commission of IUPAP

Beam Dynamics Newsletter

No. 75

Issue Editors:
Zhentang Zhao and Dong-O Jeon

Editor in Chief:
Y. H. Chin

December 2018

Contents

1 Foreword

1.1 From the Chair

Yong Ho Chin, KEK
Mail to: yongho.chin@kek.jp

We have changed the theme of this edition from the previously announced one to the introduction of the two ICFA Advanced Beam Dynamics Workshops due to the regrettable mishandle of this edition. They are the 60th ICFA Advanced Beam Dynamics Workshop on Future Light Sources (FLS2018) and the 61st ICFA Advanced Beam Dynamics Workshop on High-Intensity and High Brightness Hadron Beams (HB2018). Both were held in this year in Asia.

The 60th ICFA Advanced Beam Dynamics Workshop on Future Light Sources (FLS2018) was held very successfully on March 4-9, 2018, at the Hotel Equatorial Shanghai, China. About 150 participants from all over the world gathered together to exchange ideas and best practices about accelerator based light sources, their new development trend and related key technologies. The proceedings was published on the JACoW website (http://www.jacow.org/index.php?n=Main.Proceedings).

The 61st ICFA Advanced Beam Dynamics Workshop on High-Intensity and High Brightness Hadron Beams (HB2018) was also held very successfully on June 17-22, 2018, in Daejeon, Korea. About 150 participants from all over the world gathered together to exchange ideas and best practices about hadron machines, their new development trend and related key technologies. The proceedings was published on the JACoW website (http://www.jacow.org/index.php?n=Main.Proceedings).

We have selected three and four outstanding plenary presentations from FLS2018 and HB2018, respectively. They indicate hot topics in the light source and hadron beam communities.

Following the endorsement of ILC operating at 250 GeV by ICFA, the Japanese Ministry of Education, Culture, Sports, Science and Technology (MEXT) renewed its activities with the ILC working groups to discuss physical merits of ILC at 250GeV and the technical and cost aspects. The final reports were already made and sent to the Japanese government.

The editors of this issue are Zhentang Zhao and Dong-O Jeon, the workshop chairs of FLS2018 and HB2018, respectively. I want to thank them for editing a valuable and formidable newsletter of high quality for the accelerator community.

2 THE 60TH ICFA ADVANCED BEAM DYNAMICS WORKSHOP ON FUTURE LIGHT SOURCES (FLS2018)

2.1 Foreword From the Chairs

Zhentang Zhao (*) and Yong Ho Chin (**)

Mail to: zhaozt@sinap.ac.cn
yongho.chin@kek.jp

(*) Shanghai Institute of Applied Physics (SINAP), Shanghai, China
(**) High Energy Accelerator Research Organization (KEK), Tsukuba, Japan

The 60th ICFA Advanced Beam Dynamics Workshop on Future Light Sources, FLS2018, was held on 5-9 March, 2018 at the Hotel Equatorial, Shanghai, China. There were 148 participants representing institutions from Asia, Europe and America. After a lapse of 6 years, FLS2018 restarts the Future Light Sources series.

The scientific program of the workshop was decided by the International Organizing Committee, chaired by Yong Ho Chin (KEK), and the conference was chaired by Zhentang Zhao (SINAP). The workshop was hosted by SINAP - the Shanghai Institute of Applied Physics, CAS. Its Local Organizing Committee was chaired by Zhengchi Hou (SINAP). Eighty-six talks were presented during the plenary and parallel working group (WG) sessions, including 8 plenary, 45 invited and 33 contributed talks. They covered a wide spectrum of topics on accelerator and laser based light sources and related key technologies during the past six years since the last FLS workshop gathering at JLab, USA, in 2012. The talks were well researched, highly informative and well received by the audience.

The four working groups were themed as follows: WG1: Linac based light sources, convened by T. Raubenheimer (SLAC), L. Giannessi (Elettra) and W. Decking (DESY); WG2: Ring based light sources, convened by R. Walker (DLS), Y. Li (BNL) and Q. Qin (IHEP); WG3: Compact light sources, convened by Chunguang Jing (Euclidtechlabs), M.E. Couprie (SOLEIL) and H. Zen (Kyoto University), and WG4: Key technologies, convened by John Byrd (ANL), Joachim Pflueger (European XFEL) and Y.B. Leng (SINAP). The four topics generated heated interest in all breakout sessions and the WG conveners showed strong leadership to engage all participants in the discussions.

The poster session was also a huge success with 38 posters presented. The detailed program and talks are available via the workshop website (https://indico.sinap.ac.cn/e/fls2018). The workshop proceedings are published at the JACoW site.

During the IOC meeting at FLS2018 it was decided to organize the next workshop (FLS2021) at PSI, in Switzerland.

Zhentang Zhao
FLS2018 Workshop Chair

Yong Ho Chin
FLS2018 IOC Chair

ISBN: 978-3-95450-206-6 doi:10.18429/JACoW-FLS2018-MOA2PL03

REVIEW OF NEW DEVELOPMENTS IN SUPERCONDUCTING UNDULATOR TECHNOLOGY AT THE APS*

J.D. Fuerst†, Y. Ivanyushenkov, Q. Hasse, M. Kasa, I. Kesgin, Y. Shiroyanagi, E. Gluskin,
Argonne National Laboratory, Argonne, IL, USA

Abstract

Superconducting undulator technology for storage ring light sources has evolved from proof of principle to the working insertion device level. Both planar and helical magnet topologies using NbTi superconductor have been successfully incorporated into functional devices operating in the Advanced Photon Source (APS) storage ring at liquid helium temperatures using cryocooler-based, zero-boil-off refrigeration systems. Development work on higher field magnets using Nb_3Sn superconductor is ongoing at the APS, as are concepts for FEL-specific magnets and cryostats for future light sources.

BACKGROUND – EXISTING DEVICES

The APS currently operates three SCUs in the storage ring. Two are nominally identical vertical gap planar devices with period length 1.8 cm and overall active length 1.1 m. These devices reside in Sectors 1 and 6. The third is a helically wound, circularly polarizing device located in Sector 7 with period length 3.15 cm and overall active length 1.2 m. Device parameters are listed in Table 1.

Table 1: Parameters for SCUs Installed at APS

Parameter	Value	
	Planar	Helical
Cryostat length [m]	2.06	1.85
Magnetic length [m]	1.1	1.2
Period [mm]	18	31.5
Magnetic gap [mm]	9.5	29 (diameter)
Beam chamber aperture [mm]	7.2	8(V) x 26(H)
Peak field [T]	0.97	0.42 (B_x=B_y)
K value	1.63	1.2 (K_x=K_y)

Additional details regarding the existing devices as well as a fourth planar device developed for LCLS R&D are provided in [1,2]. For details on magnetic performance see [3]. Table 2 lists the operational statistics for planar device SCU18-1 which has operated in Sector 1 of the APS storage ring since May 2015. Device performance has been highly reliable, with overall availability of 99.99%. Figures 1 and 2 show the devices installed in the APS storage ring.

*Work supported by the U.S. Department of Energy, Office of Science under Contract No. DE-AC02-06CH11357
† fuerst@anl.gov

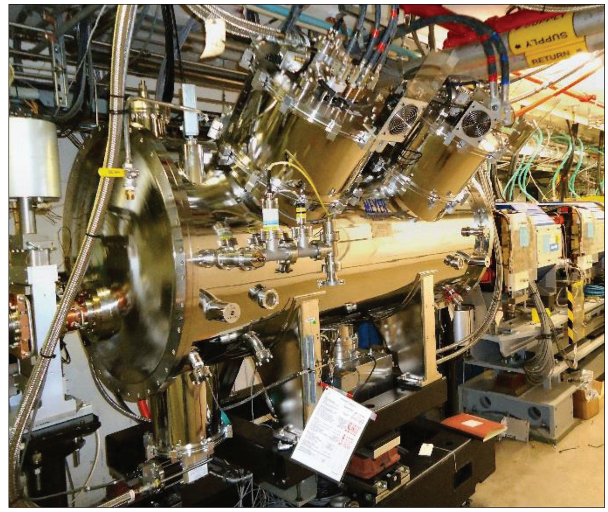

Figure 1: Planar SCU installed in the APS ring, Sector 1.

Figure 2: Helical SCU installed in Sector 7.

Table 2: Operating Statistics for SCU18-1

Year	SCU hours operating	Availability %
2015	3059	99.997
2016	4585	99.990
2017	4818	99.984

ISBN: 978-3-95450-206-6 doi:10.18429/JACoW-FLS2018-MOA2PL03

NEW MAGNET DESIGNS

Planar Polarizing

The APS continues to explore the feasibility of alternative superconductors for SCU magnets such as Nb_3Sn although this activity is in the very early stages. Recent developments in planar magnet mechanical design have focussed on minimizing phase error via tight machining tolerances, gap control, and overall magnet straightness for magnetic lengths beyond 1.5 m. As part of the APS Upgrade a new planar magnet design based on 1.8 m magnetic length is in development. Target phase error will be 2-3 degrees rms with period length 16.5 mm and target field strength approximately 1.1 T. Several features of the existing 1.1-meter magnets will be retained, including: conductor winding technique, liquid helium cooling strategy, gap separation mechanism, control of magnet straightness, and beam vacuum chamber support with thermal isolation from the 4.2 K magnets. Verifying the extension of these techniques to longer magnetic lengths is a crucial element of our development activity. Figure 3 shows a CAD model of a 1.8-meter planar magnet pair.

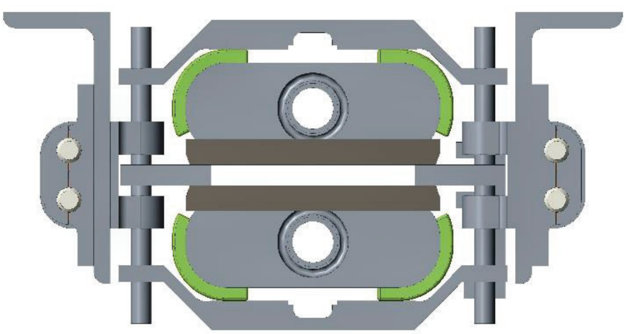

Figure 3: Cross-section of planar magnet pair showing magnet cores with helium cooling passages, pole pieces, gap separator system, and magnet support system. Superconducting wire is not shown.

Circular Polarizing

The helical SCU presently in operation was designed to be compatible with the APS storage ring. Future development of this magnet type will likely focus on free electron laser (FEL) applications where a very small "magnetic gap" is allowed and the subsequent magnetic field is large. These magnets would be installed in a multi-undulator array as opposed to individually as in a storage ring. In that regard their design can be tailored to provide an optimal magnetic length for field tapering. The superconductor in the existing helical SCU is wound continuously into a double-helical "2-lead" rectangular-thread groove machined into the magnet core. Magnet performance is strongly dependent on the machining accuracy of the groove depth and pitch. Future devices may benefit from precision thread grinding, perhaps as a finishing step following the multi-axis CNC milling process. Figure 4 shows a helical magnet core wound with superconducting wire and prepared for epoxy impregnation.

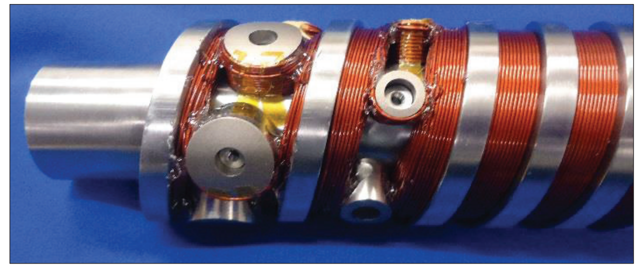

Figure 4: Closeup of the helical SCU wound core showing conductor end turn-around detail.

Universal Polarizing

Development work continues on a universal superconducting undulator capable of arbitrary polarization. At the APS this work takes the acronym SCAPE (Superconducting Arbitrarily Polarizing Emitter) and consists of two orthogonal planar magnet pairs with roughly triangular cross-section, offset longitudinally by ¼-period. The four magnet cores are arranged around an X-shaped beam vacuum chamber. The chamber operates at a higher temperature than the cores and is thermally isolated from them. Two views of the SCAPE geometry are shown in Figs. 5 and 6 while Fig. 7 shows a prototype SCAPE magnet core after winding with NbTi superconductor.

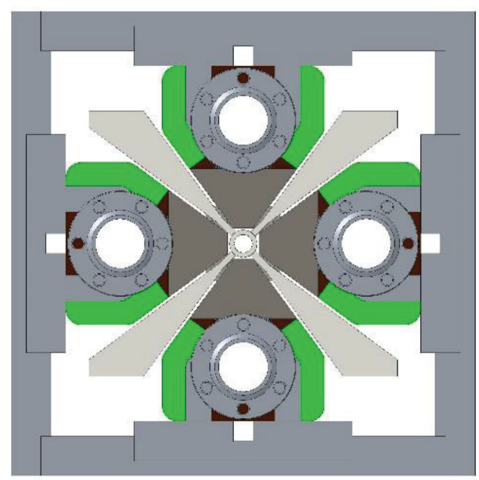

Figure 5: End view of the SCAPE SCU concept.

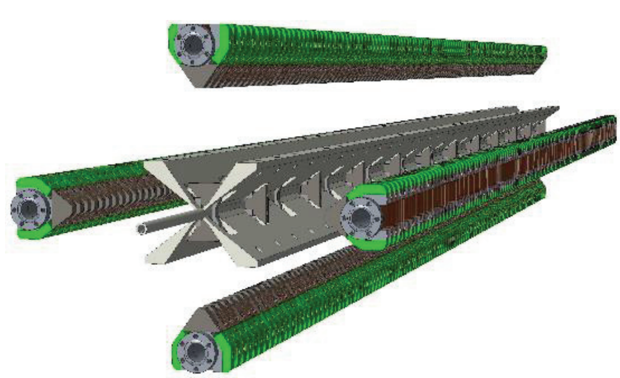

Figure 6: Exploded view of the SCAPE magnet/vacuum chamber concept.

ISBN: 978-3-95450-206-6 doi:10.18429/JACoW-FLS2018-MOA2PL03

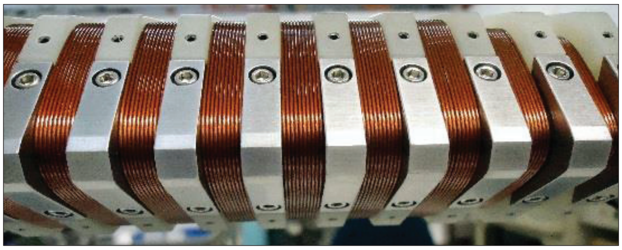

Figure 7: (top) Close-up view of a prototype SCAPE core after winding with superconducting wire.

This magnet technology has application for both storage ring and FEL light sources, providing planar horizontal through circular to planar vertical (as well as intermediate elliptical) polarizations. As in the storage ring-based planar devices, the SCAPE vacuum chamber can operate at elevated temperature relative to the magnets in order to intercept both electron- and photon-based heating and maintain a reasonable 4.2 K heat load to the magnets.

Correctors

Existing SCUs use both internally wound and externally mounted magnets to perform first and second integral correction. Future multi-magnet SCUs will require either dipole chicanes for phase shifting or (for storage ring applications with multiple straight section end stations) canting magnets between the undulator magnets. These devices may be superconducting or cryogenically cooled/normal conducting depending on magnet current requirements and installation complexity. Figure 8 shows a closeup of the helical SCU dipole correctors.

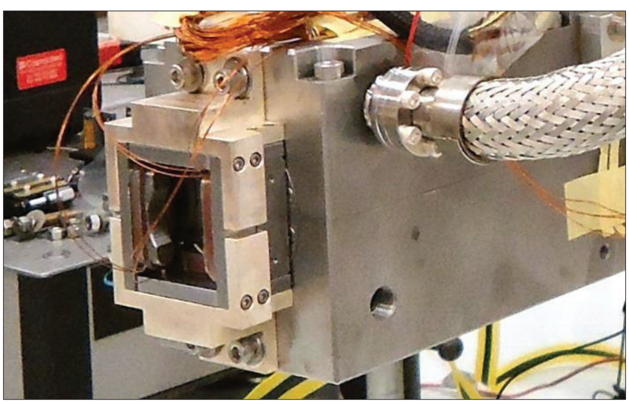

Figure 8: Conduction-cooled helical SCU superconducting horizontal and vertical dipole correction package mounted to the end of the main magnet.

NEW CRYOSTAT DESIGNS

Storage Ring-Specific

Cooling Systems The existing APS SCU cryostat design descends from liquid helium-based, cryocooler-cooled insertion devices developed at the Budker Institute for Nuclear Physics (BINP), Novosibirsk [4]. The relatively sparse and isolated nature of today's storage-ring-based SCU installations argues in favour of individually cooled units (in contrast to a central helium refrigeration plant plus cryogenic distribution system) in terms of capital cost. Careful management of cryogenic heat leak permits use of a reasonable number of 1.5 W, 4.2 K cryocoolers while maintaining zero-boil-off operation. Future plans include pursuit of alternative cryocooler technologies such as a new 2-W class of 4.2 K pulse-tube cryocoolers. Cryogen-free designs present an attractive option by eliminating liquid helium and the associated pressure system and cryogenic leak issues. Regardless of architecture, the cooling system must provide some capacity overhead to allow for recovery from magnet quench within a reasonable interval. During routine operation the excess capacity is dissipated with a regulated heater. The heater power level provides an excellent diagnostic with respect to the overall health of the system.

Alignment Systems Alignment requires precision in both position adjustment and measurement. Development efforts include precise (<10 micron) external adjustment capability for the magnet cold mass with respect to the cryostat when the system is at 4.2 K along with sub-5-micron laser displacement-based position measurement capability [5]. These requirements are particularly important for multi-undulator-magnet cryostats where magnet-to-magnet alignment at the 5-micron level is desirable. Multi-magnet alignment to a common rigid cold mass support is the baseline choice for the APS Upgrade SCU cryostat (see Figure 9) although independent magnet supports with external precision adjustment capability are a potential alternative.

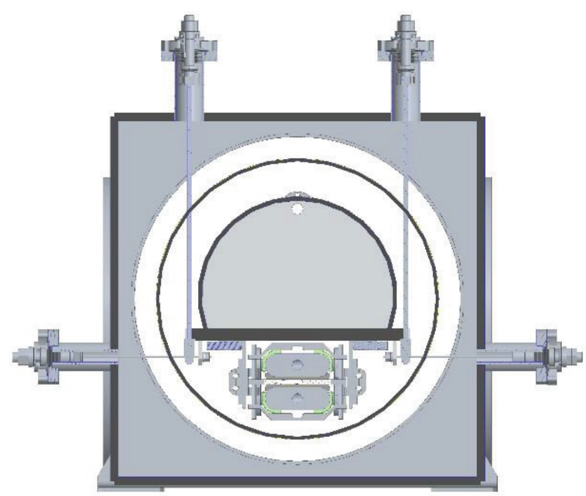

Figure 9: End view of a magnet support and alignment concept for the APS Upgrade SCU cryostat. Externally adjustable low-heat-leak supports provide precise positional control.

Beam Vacuum Chambers SCU magnets must be screened effectively from substantial beam and/or x-ray-induced heating in a storage ring application. An independently cooled beam vacuum chamber provides an adequate screen for planar SCUs. However the helical SCU at the APS is vulnerable to x-ray heating caused by the bending-magnet (BM) beam line immediately upstream. This potentially fatal heat source was mitigated

ISBN: 978-3-95450-206-6 doi:10.18429/JACoW-FLS2018-MOA2PL03

by sophisticated beam orbit correction to steer the BM x-ray fan away from the helical SCU magnet. The vulnerability arises due to the helical magnet core design which completely envelopes the beam vacuum chamber. For the planar geometry, there is no magnet exposure along the horizontal plane of the electron beam orbit (see Figure 3).

FEL-Specific

Cooling Systems An FEL SCU array, perhaps of order 100 m length, lends itself to the use of a centralized cryoplant coupled to a cryogenic distribution system (compared to a very large number of cryocoolers). The 4.2 K heat load per meter is likely around one watt if thermal design discipline similar to the storage-ring-specific cryostat is maintained. However given the available cooling power of even a small liquid helium refrigerator, it is possible to loosen the heat load budget as a means to simplify cryostat design. A small commercial refrigerator is shown in Fig. 10.

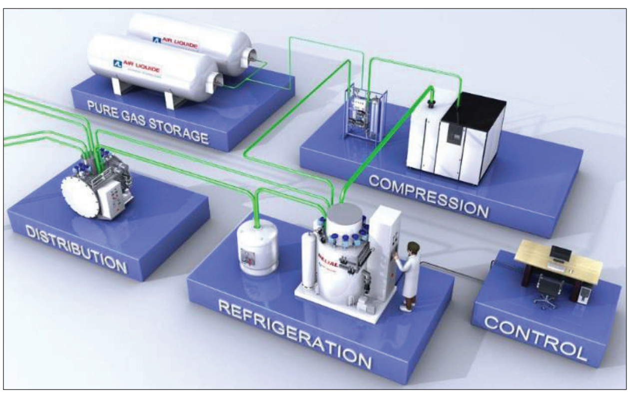

Figure 10: A small helium refrigerator system (from the Air Liquide website).

Alignment Systems FEL requirements push the state of the art and may involve active, beam-based component alignment. Individual control of undulator magnets, focusing quadrupoles and phase shifters may be required. Room-temperature remote adjustment of cold mass supports via cryostat insulating vacuum feed-throughs may be sufficient. Piezo actuators can be located outside of or internal to the insulating vacuum and may find an application for short-distance, fast position adjustment. In the longer term, fiber-optic interferometer-based systems may provide improved precision and multi-channel capability for real-time magnet location measurement as part of an active positioning system

Beam Vacuum Chambers A 4.2 K beam vacuum chamber becomes feasible, in part due to the lower expected beam-induced heating relative to a storage ring but also due to the refrigeration capacity inherent in a centralized helium refrigerator. This could enable smaller magnetic gaps and larger magnetic fields for a given magnet operating current.

Array Segmentation Cryogenic distribution may be external (for example CEBAF at JLab [6]) or internal (LCLS-II [7] and European X-FEL [8]) depending on overall cooling power, capital cost, and maintenance strategy (individually removable cryostats compared to a full-system warm-up for cryostat removal). Figures 11 and 12 illustrate the minimal-segmentation concept where the distribution system resides internal to the cryostat.

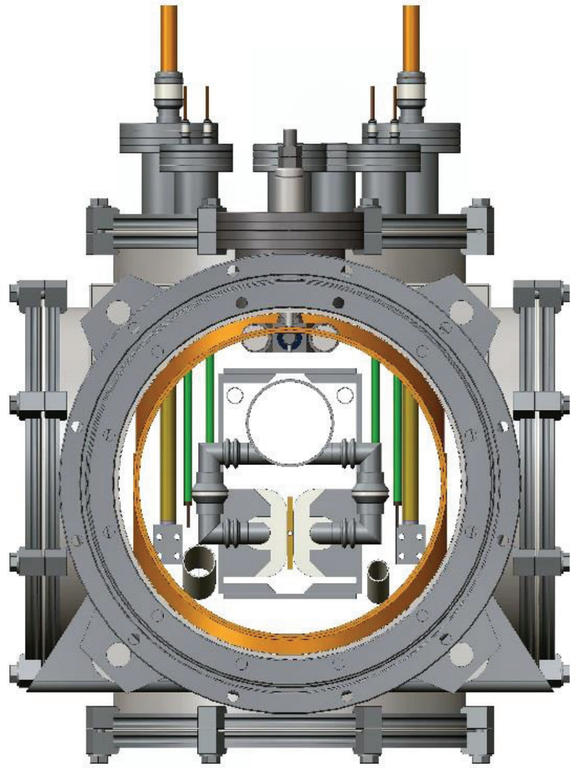

Figure 11: End-section view of a minimally-segmented SCU cryostat showing horizontal-gap planar magnets packaged with internal helium cryogenic distribution.

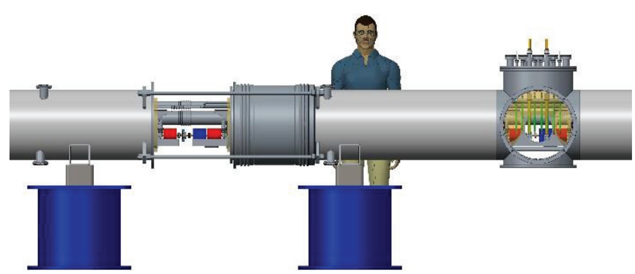

Figure 12: Concept representation of multiple cryostats connected in a minimally-segmented FEL array. The inter-cryostat vacuum vessel spool is shown in the retracted (assembly) position.

Multi-line FEL Cryostats An SCU cryostat represents a space-efficient means of packaging an undulator magnet. As such, it is possible to design a single cryostat capable of housing multiple undulator lines in parallel. Figure 13 shows a cryostat concept containing four parallel helical SCU magnet arrays in parallel, each with an independent beam vacuum chamber. This represents a packing capability which is likely unachievable using permanent magnet undulator technology.

ISBN: 978-3-95450-206-6 doi:10.18429/JACoW-FLS2018-MOA2PL03

Figure 13: FEL helical SCU concept containing four independently powered SCU arrays in a common cryostat.

CONCLUSION

The APS is working to develop the next generation of superconducting undulator (SCU) technology for future storage ring and FEL light sources. At present there are three SCUs operating in the APS storage ring (two planar, one circular polarizing). Development is underway for a new generation of SCUs for the APS Upgrade. SCU technology is well-suited to FEL applications and development work on FEL-specific devices is ongoing.

ACKNOWLEDGMENT

The submitted manuscript has been created by UChicago Argonne, LLC, Operator of Argonne National Laboratory (“Argonne”). Argonne, a U.S. Department of Energy Office of Science laboratory, is operated under Contract No. DE-AC02 -06CH11357. The U.S. Government retains for itself, and others acting on its behalf, a paid-up nonexclusive, irrevocable worldwide license in said article to reproduce, prepare derivative works, distribute copies to the public, and perform publicly and display publicly, by or on behalf of the Government.The Department of Energy will provide public access to these results of federally sponsored research in accordance with the DOE Public Access Plan.

REFERENCES

[1] Gluskin, E., “Development and performance of superconducting undulators at the Advanced Photon Source,” in *Synchrotron Radiation News*, 28:3, 4-8.

[2] Ivanyushenkov, Y. et al., “Status of the development of superconducting undulators at the Advanced Photon Source,” in *Proceedings of IPAC2017*, Copenhagen, Denmark, p. 2499-2502.

[3] Kasa. M. et al., “Progress on the magnetic performance of planar superconducting undulators,” in *Proceedings of NA-PAC2016*, Chicago, IL, USA, p. 477-479.

[4] Mezentsev, N. and Wallen, E., “Superconducting wigglers,” in *Synchrotron Radiation News*, 24:3, 3-9.

[5] Jansma, W.G. et al., “Precision 2D laser scanning: overview and applications,”in *Journal of the CMSC*, Vol. 12, No. 2 (2017) p. 6-13.

[6] Weisend II, J.G. (Ed.), “Cryostat Design,” *International Cryogenics Monograph Series*, Springer (2016), p.149.

[7] Peterson, T. et al., “LCLS-II 1.3 GHz cryomodule design – modified TESLA-style cryomodule for CW operation,” in *Proceedings of SRF2015*, Whistler, BC, Canada, p. 1417-1421.

[8] Bozhko, Y. et al., “Commissioning and first cooldown of XFEL linac,” in *IOP Conf. Ser.: Mater. Sci. Eng* **278** 012100 (2017).

ISBN: 978-3-95450-206-6 doi:10.18429/JACoW-FLS2018-WEA1PL02

DIELECTRIC AND OTHER NON-PLASMA ACCELERATOR BASED COMPACT LIGHT SOURCES*

R. J. England†, Z. Huang
SLAC National Accelerator Laboratory, Menlo Park, CA 94025, USA

Abstract

We review recent experimental progress in developing nanofabricated dielectric laser-driven accelerators and discuss the possibility of utilizing the unique sub-femtosecond electron pulse format these accelerators would provide to create ultra-compact EUV and X-ray radiation sources.

INTRODUCTION

Particle acceleration in dielectric structures driven by ultrafast infrared lasers, a technique we refer to as "dielectric laser acceleration" (DLA), is a new and rapidly progressing area of advanced accelerator research that sets the stage for future generations of high-gradient accelerators of reduced cost and unprecedented compactness. In recent years, there have been several critical experiments: the first demonstration of high-field (300 MV/m) speed-of-light electron acceleration in a fused silica structure [1], acceleration at sub-relativistic energies with an open grating [2], demonstration of a compatible optical-scale beam position monitor [3], high-gradient sub-relativistic acceleration at 220 MV/m [4] and at 370 MV/m [5] in silicon microstructures, and high-gradient (700 MV/m) acceleration of relativistic electrons using femtosecond laser pulses [6]. This approach has been colloquially referred to in the press as an "accelerator on a chip." The high-gradient and wafer size of these accelerators make them very attractive for a future generation of high brilliance extreme ultraviolet (EUV) and X-ray sources. The DLA approach has the distinct features to produce attosecond electron bunches and can operate at 10s of MHz repetition rate. However, there are many accelerator science questions and technical challenges to address since the beam parameters for an accelerator based on this concept would be drastically different from both conventional accelerators and other advanced schemes.

The most powerful XUV and x-ray sources today are enabled by relativistic electron beams driven by state-of-the-art microwave linear accelerator facilities such as the Linac Coherent Light Source (LCLS) at SLAC. Recent research into novel dielectric laser accelerators (DLA) has given rise to the potential for new coherent radiative processes with attosecond pulses using dielectric structures with wavelength-scale periodic features excited by lasers at near-infrared wavelengths [1, 7], and with orders of magnitude higher accelerating fields than is possible with conventional microwave technology [6]. This approach has the potential to produce extremely bright electron beams in an ultra-compact footprint that are suitable for driving superradiant EUV light in a similarly optical-scale laser-induced undulator field. Radiation from each undulator/compressor module would add in amplitude but not in pulse length, maintaining the wide bandwidth and attosecond pulse structure. Preliminary calculations presented below suggest that a compact DLA driven by a 2 μm infrared laser may generate a 10-fC, 200-as electron bunch train at 40 MeV particle energy. After passing 100 undulator/compressor modules, EUV radiation could be generated in a train of 660 as pulses separated by 6.6 fs laser period, with a pulse energy of more than 100 nJ. This attosecond pulse train would form an intense EUV frequency comb that would be extremely valuable for precision spectroscopy.

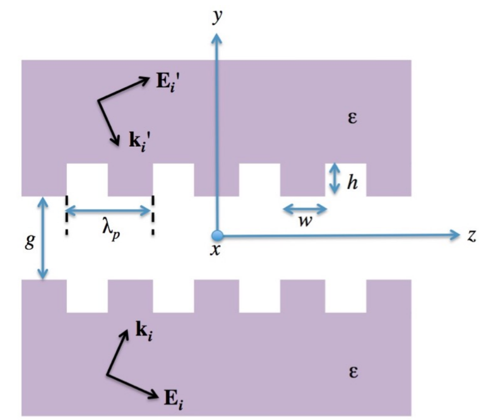

Figure 1: Planar symmetric geometry with periodic variation in z. Two exciting plane waves are shown incident from top and bottom.

LASER-DRIVEN DEFLECTION IN PLANAR STRUCTURE

All DLA structures experimentally tested to date have been of the planar symmetric variety (spatially invariant in one coordinate) and with a longitudinal periodicity along the particle beam axis. We here derive a generic form for the transverse forces in such a geometry which provide some helpful insights regarding development of a compatible laser-driven undulator. The wave equation for a linear material with spatially varying dielectric function $\epsilon(\mathbf{r})$ may be written

$$\nabla^2\mathbf{E} - \nabla(\nabla \cdot \mathbf{E}) = -(\omega/c)^2\mathbf{D} \tag{1}$$

where $\mathbf{D}$ is the electric displacement field, related to the electric field $\mathbf{E}$ and polarization $\mathbf{P}$ by $\mathbf{D} = \mathbf{E} + 4\pi\mathbf{P}$. We assume a dielectric, non-magnetic material ($\mu = 1$), hence $\mathbf{H} = \mathbf{B}$. Solutions to Eq. 1 for given dielectric function

* Work supported by U.S. Dept. of Energy, National Science Foundation, and Moore Foundation.
† england@slac.stanford.edu

ISBN: 978-3-95450-206-6 doi:10.18429/JACoW-FLS2018-WEA1PL02

$\epsilon(\mathbf{r})$ immediately yield the magnetic field via Faraday's law, $\nabla \times \mathbf{E} = i(\omega/c)\mathbf{B}$. By the Floquet theorem, the solutions to Maxwell's equations subject to periodic boundary conditions along z with periodicity $\mathbf{u} = \lambda_p \hat{\mathbf{z}}$ satisfy $\mathbf{E}(\mathbf{r}+\mathbf{u}) = \mathbf{E}(\mathbf{r})e^{i\psi}$, where ψ is the cell-to-cell phase shift. If the fields are excited by an incident plane wave with wavenumber $\mathbf{k}_i = (\omega/c)\sqrt{\epsilon_i}\,\hat{\mathbf{n}}$, then ψ is given by the projection of the incident plane wave onto the fundamental periodicity. If we define θ to be the usual polar angle between $\hat{\mathbf{n}}$ and $\hat{\mathbf{z}}$ then this gives rise to the projection of the incident wave in the first Brillouin zone: $k_0 \equiv |\mathbf{k}_i \cdot \mathbf{u}| = (\omega/c)\sqrt{\epsilon_i}\cos\theta$, and a corresponding set of Floquet space harmonics with wave numbers $k_n = k_0 + nk_p$ where $k_p \equiv 2\pi/\lambda_p$. The phase velocity of the n'th space harmonic, normalized to speed of light c is thus $\beta_n = \omega/(ck_n)$.

For the considered case, illustrated in Fig. 1 by the example of parallel gratings with rectangular teeth, with a planar-symmetric system invariant in x, and a vacuum region occupying the space $|y| < g/2$, two orthogonal polarizations may be defined relative to the plane of y and z wherein there is variation of the fields. We call these S and P polarization, which respectively give rise to transverse electric (TE) and transverse magnetic (TM) modes, relative to excited surface waves propagating in z within the vacuum gap. For a single laser excitation ($\mathbf{E}_i$ in Fig. 1), the solution to Eq. 1 in the vacuum region yields the following non-vanishing components for S- polarization (TE):

$$
\begin{aligned}
E_x &= E_0 \sum_n [a_n e^{\Gamma_n y} + b_n e^{-\Gamma_n y}] e^{ik_n z} \\
B_y &= \frac{c}{\omega} E_0 \sum_n k_n [a_n e^{\Gamma_n y} + b_n e^{-\Gamma_n y}] e^{ik_n z} \\
B_z &= i\frac{c}{\omega} E_0 \sum_n \Gamma_n [a_n e^{\Gamma_n y} - b_n e^{-\Gamma_n y}] e^{ik_n z}
\end{aligned}
\tag{2}
$$

and for P-polarization (TM):

$$
\begin{aligned}
E_y &= -iE_0 \sum_n \frac{k_n}{\Gamma_n} [a_n e^{\Gamma_n y} - b_n e^{-\Gamma_n y}] e^{ik_n z} \\
E_z &= \frac{c}{\omega} E_0 \sum_n k_n [a_n e^{\Gamma_n y} + b_n e^{-\Gamma_n y}] e^{ik_n z} \\
B_x &= iE_0 \sum_n \frac{\omega}{c}\frac{1}{\Gamma_n} [a_n e^{\Gamma_n y} - b_n e^{-\Gamma_n y}] e^{ik_n z}
\end{aligned}
\tag{3}
$$

where $\Gamma_n \equiv \sqrt{k_n^2 - (\omega/c)^2}$ is the transverse decay constant of the n'th space harmonic. The complex coefficients a_n, b_n are determined by boundary condition matching at the dielectric interface and therefore depend upon the specific geometry of the periodic structure. Explicit forms have been derived for a square-tooth grating as depicted in Fig. 1 by, e.g. [8,9]. By virtue of the assumed symmetry, if an otherwise identical plane wave $\mathbf{E}_i'$ propagates from the opposite direction with the same incidence angle, then the resultant mode is of the same form as Eqs. 2 - 3 but with the substitution $a_n \leftrightarrow b_n$. The superposition of the fields excited by both plane waves has the form of Eqs. 2 - 3 but with the replacements

$$
[a_n e^{\Gamma_n y} \pm b_n e^{-\Gamma_n y}] \rightarrow 2(a_n + b_n) \left\{ \begin{array}{c} \cosh(\Gamma_n y) \\ \sinh(\Gamma_n y) \end{array} \right. \tag{4}
$$

If the two plane-waves are out of phase by π then the roles of cosh and sinh in Eq. 4 are exchanged and $(a_n + b_n) \rightarrow (a_n - b_n)$. The desired acceleration mode is the in-phase TM mode with $n = 1$, wherein $E_z \propto \cosh(\Gamma y)e^{ik_p z}$. The hyperbolic cosine dependence can be seen to approach a transversely uniform field in the limit where $g \ll \Gamma_n^{-1}$ or the case $\Gamma_n \rightarrow 0$ which implies that $k_n = \omega/c$ and hence that the phase velocity of the mode is equal to c. To instead obtain a uniform deflecting force, we consider modes where the transverse force $\mathbf{F}_\perp$ has a cosh-like dependence on y. From the above considerations we see that two solutions satisfy this condition: the double-sided excitation of TM mode with π out-of-phase plane waves and the TE mode with in-phase plane waves. These yield

$$
\mathbf{F}_\perp = qE_0 \left\{ \begin{array}{c} (1-\beta/\beta_n) \\ -i\frac{k_n}{\Gamma_n}(1-\beta_n\beta) \end{array} \right\} \left\{ \begin{array}{c} \hat{\mathbf{x}} \\ \hat{\mathbf{y}} \end{array} \right\} e^{i(k_n z - \omega t)} \tag{5}
$$

where the top line corresponds to the TE mode and the bottom line is the TM mode. In both cases $F_z = 0$. We have here taken a single mode n from the summation which is assumed to have a phase velocity β_n that is matched to the electron beam, and have assumed the limit $\Gamma_n g \ll 1$ or $\cosh(\Gamma_n y) \approx 1$. Further the constant $a_n \pm b_n$ has been absorbed into the field amplitude E_0. We see from these expressions that the TE mode vanishes for a synchronous particle ($\beta = \beta_n$) while the TM mode instead scales as $1/\gamma_n^2$. Plettner solves this speed-of-light synchronicity problem by rotating the particle axis by an angle α. In the rotated frame of the beam, the resonant velocity of the mode is in the direction of $\mathbf{k}_n$ which is no longer co-linear with z but now has the form $\mathbf{k}_n = k_n(\cos\alpha\,\hat{\mathbf{z}} - \sin\alpha\,\hat{\mathbf{x}})$. Phase synchronicity is therefore accomplished if $\mathbf{k}_n \cdot \hat{\mathbf{z}} = \omega/\beta c$. For normal laser incidence ($\theta = \pi/2$) this leads to the synchronicity condition $\lambda_p = \beta n\lambda\cos\alpha$. Hence, as compared with the unrotated case, the period λ_p of the grating must be decreased by a factor $\cos\alpha$ to remain synchronous with a speed of light particle. This is geometrically obvious since in the rotated frame the apparent spacing between grating teeth is increased along z. Laser-driven dielectric undulators based upon this and similar concepts have been proposed and could attain very short (mm to sub-mm) periods with multi-Tesla field strengths and fabricated using similar photolithographic methods [10–12].

ATTOSECOND RADIATION GENERATION

Combining the high gradient and high brightness of advanced accelerators with novel undulator designs would enable laboratory-scale demonstrations of key concepts needed for future EUV and X-ray lasers that can transform the landscape of ultrasmall and ultrafast sciences. Attosecond electron current modulation would be automatically created by

ISBN: 978-3-95450-206-6 doi:10.18429/JACoW-FLS2018-WEA1PL02

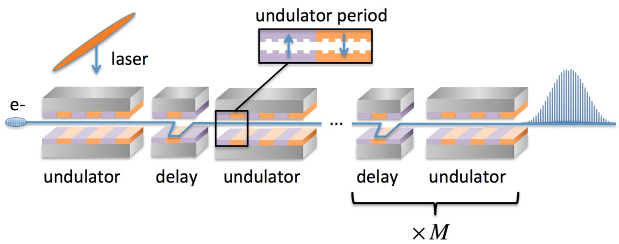

Figure 2: Chain of M laser-driven undulator and delay modules to mode-lock DLA attosecond pulse train.

the DLA structure and phase-locked to the drive laser. The radiative process could then be modelocked via a chain of such laser-driven undulators and compressors as suggested in [13]. This mode-locked radiation would possess the attosecond pulse structure with a well-defined phase within the train. The undulator and delay chain can be made of dielectric structures as well (see, e.g., Ref. [10, 14]), as illustrated in Fig. 2.

In an operating DLA, the optimal bunch charge would be of order a few fC, so we will ingore the FEL gain in the undulator/delay chain. Following Ref. [13] Sec. 3 we rewrite the equations without ρ scaling, yielding the radiation field

$$A(\bar{\nu}) = b_0(\bar{\nu}) N_u \operatorname{sinc}(\pi\bar{\nu}N_u)\,\frac{1-e^{-iM\bar{\nu}\bar{s}}}{1-e^{-i\bar{\nu}\bar{s}}}\,e^{-i\bar{\nu}(\bar{s}-\pi N_u)} \tag{6}$$

The corresponding power spectrum is then $P(\bar{\nu}) \propto |A(\bar{\nu})|^2$. Here $\bar{\nu} = (\omega-\omega_0)/\omega_0$ is the undulator fundamental radiation frequency, N_u is the number of undulator periods per section, M is the number of sections of undulator/delay modules, and $\bar{s} = k_0 R_{56}/2 + 2\pi N_u$ is the total slippage per module in units of $\lambda_0/(2\pi)$. The quantity $b_0(\nu)$ is the initial bunching spectrum and is assumed to be constant in the undulator in absence of FEL interaction.

The sinc function shows the typical undulator radiation behavior, with the FWHM spectral width given by $1/N_u$. The last factor in Eq. (6) introduces spectral modes. In Fig. 3, we show an example when $N_u = 5$, $\bar{s} = 2\pi \times 100$, and $M = 10$. About 20 modes are contained in the full spectral bandwidth, and the intensity of the central mode is enhance by $M^2 = 100$.

As discussed in Ref. [13], the mode will not be locked if the electron bunch is randomly distributed, and can be locked if the bunch is energy or density modulated with a modulation wavelength that matches $\bar{s}/k_0$. In a DLA, the attosecond bunch train is generated by some sort of an optical buncher so the mode locking happens naturally. The mode-locking means the XUV radiation will posess the attosecond pulse train with a well-defined phase within the train. The peak power of the core part of the train (not head or tail which may be subject to transient effects) can be calculated as follows.

We will work in the 1D limit (assuming a large transverse beam size and can consider 3D later), the transverse electric field is (see Eq. (3) of Ref. [15])

$$E_x(z,t) = \eta \sum_{j=1}^{N} \frac{e^{ik_r[z-c(t-t_j)]}}{1-\beta_\parallel} H(z, t-t_j) + \text{c. c.}, \tag{7}$$

where $\eta \equiv ecZ_0K_{JJ}/8\pi\sigma_x^2\gamma$, K_{JJ} is the undulator parameter with the usual Bessel function correction, t_j is the electron arrival time at the undulator entrance $z = 0$, $Z_0 = 377\ \Omega$ is the vacuum impedance, $\beta_\parallel$ is the average longitudinal velocity in the undulator, $\lambda_r = (1-\beta_\parallel)\lambda_u$, and H is 1 when $\beta_\parallel c(t-t_j) < z < c(t-t_j)$ and 0 otherwise to take care of the slippage. Although this expression is derived in 1D, the electric field transverse distribution should follow that of the electron beam as

$$\begin{aligned} E_x(z,t,r) = \eta \textstyle\sum_{j=1}^{N} \frac{e^{ik_r[z-c(t-t_j)]}}{1-\beta_\parallel} H(z,t-t_j) \\ \times \exp(-\tfrac{r^2}{2\sigma_x^2}) + \text{c. c.} \end{aligned} \tag{8}$$

In the DLA example we consider here, we assume the DLA bunches the electron to attosecond durations. This is supported by recent VORPAL simulations that show 10 as bunches formed in a 1-mm DLA structure. As far as XUV radiation (tens of nm wavelength) is concerned, the electron bunch radiates coherently right away in the undulator as a macro point charge. This can be seen from the above equation that the sum of phases yields N, the number of electrons in the attosecond bunch. We have

$$E_x(z,t,r) = \eta \frac{N}{1-\beta_\parallel} e^{ik_r(z-ct)} \exp(-\frac{r^2}{2\sigma_x^2}) + \text{c. c.} \tag{9}$$

Note that the electric field amplitude is independent of N_u (undulator period), only the length of the wavepacket is determined by $N_u\lambda_u$. This agrees with the intuitive picture. The radiated power per module is given by

$$P_0 = \frac{1}{2Z_0}\int |E_x(z,t,r)|^2 d\mathbf{r} = \frac{Z_0 K_{JJ}^2 Q^2 c^2 \gamma^2}{8\pi\sigma_x^2(1+K^2/2)^2}, \tag{10}$$

where $Q = Ne$ is the total charge in the bunch. After M modules, the radiated power becomes

$$P = M^2 P_0\,. \tag{11}$$

For example, consider a compact DLA driven by a 1 μm infrared laser. We assume the charge per bunch is 10 fC, and the fwhm bunch length is 20 as (6 nm) and is shorter than the radiation wavelength (10 nm). Suppose the electrons are accelerated to 50 MeV, and focused to $\sigma_x = 0.2\ \mu$m and then passed through a Byer-Plettner type of dielectric undulator with $\lambda_u = 200\ \mu$m, and $K = 0.15$ is the deflecting parameter. The undulator fundamental wavelength is $\lambda_0 = 10$ nm. Since the electron bunch length is comparable to the radiation wavelength, coherent radiation will be emitted at λ_0 from the beginning. After $N_u = 5$ undulator period, the radiation wavepacket is 50 nm or 166 as. If we simply make the undulator longer, it will only elongate the wavepacket

ISBN: 978-3-95450-206-6 doi:10.18429/JACoW-FLS2018-WEA1PL02

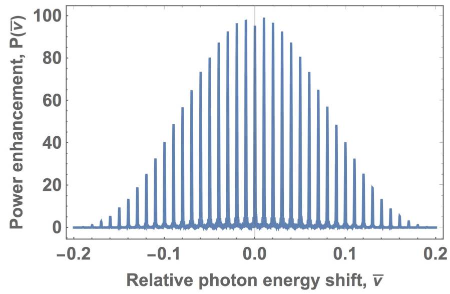

Figure 3: Mode-locked coherent undulator radiation spectrum (see text for details).

and eventually merge the attosecond pulse train. Mode-locking with undulator/chicane module will maintain the wide bandwidth nature and attosecond pulse train. Let us take undulator/chicane module $R_{56}/2 + N_u\lambda_0 = 1\ \mu$m to match the drive laser wavelength and hence the periodicity of the bunch train, then the radiation from adjacent modules will add in amplitude but not in pulse duration. After $M = 10$ such modules, the radiation will maintain 166 as with the peak power given by Eqs. (10) and (11). In this example, $P = 80$ MW, and the single pulse energy is 13 nJ. If the optical laser pulse length is 1 ps, there can be approximately 300 such pulses in each optical pulse (with some transient effects in head/tail of the optical pulse).

Eventually the beam quality (energy spread) limits how many modules can be used in this scheme. Each chicane/undulator module will have $R_{56} \sim 2\ \mu$, so energy spread requirement is

$$\sigma_\delta M R_{56} < 6\text{nm} \quad \text{or} \quad \sigma_\delta < 3 \times 10^{-4}\,. \tag{12}$$

There should be focusing after each module in order to keep the constant beam size in the undulators. Since the undulator radiation is transversely coherent, the emittance of the bunch should be

$$\epsilon_{x,y} \leq \frac{\lambda_0}{4\pi} \sim 1\text{nm}\,. \tag{13}$$

This corresponds to the normalized emittance $\gamma\epsilon_{x,y} = 0.1\ \mu$m.

APPLICATIONS

The DLA approach can produce orders of magnitude higher accelerating fields than is possible with conventional microwave technology. The extreme accelerating environment has the potential to produce extremely bright electron beams that are suitable for driving superradiant EUV light in a similarly optical-scale laser-induced undulator field. Furthermore, because of the few-femtosecond optical cycle of near infrared (NIR) mode-locked lasers, laser-driven X-ray free electron lasers could allow attosecond x-ray laser pulses to probe matter on even shorter time-scales than possible today. Combining the high gradient and high brightness of advanced accelerators with novel undulator designs could enable laboratory-scale demonstrations of key concepts needed for future XUV and X-ray lasers that can transform the landscape of ultrasmall and ultrafast sciences. To realize these laboratory-scale, lower-cost, higher performance radiation sources, critical components of laser-driven free electron lasers need to be developed and demonstrated.

Coherent attosecond radiation could potentially be produced using the same operating principles that produce particle acceleration via the “accelerator on a chip" mechanism. These structures operate optimally with optical-scale pulse formats, making high repetition rate (10s of MHz) attosecond-scale pulses a natural combination. The beam is by necessity very close to the exposed micro-structures and there are fundamental questions regarding the impact of the beam impedance upon itself and the remnant fields back on the device itself. This regime has never been studied before and questions arise as to how well the beam will behave in such structures and how well it will ultimately perform. The theoretical and numerical tools to model these processes need to be developed in order to guide experimental studies of attosecond electron and photon generation.

The FEL process has been studied extensively over a broad range of parameters and is quite well understood; however, this is not true in this new regime of ultrashort, attosecond bunches generating X-rays at relatively low electron beam energies. This presents some interesting new opportunities. As the electron energy becomes lower, the impact of the X-ray photon’s momentum on the electron’s momentum becomes significant and quantum effects start to come into play in a way not before seen or measured in “classical" FELs [16]. This has consequences with respect to, among other things, the fundamental physics of coherence between particles, the causal relationships between these particles, and the momentum exchange difference that occurs between incoherent emission and coherent emission. The FEL operated in such a regime might help answer some of these fundamental questions.

CONCLUSION

A DLA-based light source could generate EUV radiation in the 50 eV photon energy range with even lower beam energies (about 40 MeV using a laser driven undulator with a period of 250 μm). However, at these relatively long wavelengths, radiation will slip outof the very short electron bunch after of order 10 undulator periods, and hence make the device inefficient for generation of high-power, attosecond (as) pulses. In a DLA, attosecond electron current modulation is automatically created by the structure and is phase-locked to the drive laser which can be further stabilized using optical techniques. One possible route to mode-lock the radiative process via a chain of laser-driven undulators and compressors is suggested in Ref. [13]. If successfully mode-locked, the EUV radiation would possess the attosecond pulse structure with a well-defined phase within the train. Radiation from each undulator/compressor module would add in amplitude but not in pulse length, maintaining the wide bandwidth nature and attosecond pulse train.

ISBN: 978-3-95450-206-6 doi:10.18429/JACoW-FLS2018-WEA1PL02

This attosecond pulse train would form an intense EUV frequency comb (see Fig. 3) that could be extremely valuable for precision spectroscopy.

ACKNOWLEDGMENT

This work is supported by the U.S. Department of Energy (DE-AC02-76SF00515), U.S. National Science Foundation (ECS-9731293), and the Moore Foundation (GBMF4744). We also thank R. L. Byer, K. P. Wootton, Y-C. Huang, and L. Schachter for helpful comments and discussions.

REFERENCES

[1] E. A. Peralta, K. Soong, et al. “Demonstration of electron acceleration in a laser-driven dielectric microstructure," *Nature* 503, 91-94 (2013).

[2] J. Breuer and P. Hommelhoff, "Laser-based acceleration of nonrelativistic electrons at a dielectric structure," *Phys. Rev. Lett.* 111, 134803 (2013).

[3] K. Soong, E. Peralta, et al. “Electron beam position monitor for a dielectric microaccelerator," *Optics Letters* 39 (16), 4747-4750 (2014).

[4] K. J. Leedle, R. F. Pease, R. L. Byer, and J. S. Harris, “Laser acceleration and deflection of 96.3 keV electrons with a silicon dielectric structure," *Optica* 2, 158-161 (2015).

[5] K. J. Leedle, A. Ceballos, et al. “Dielectric laser acceleration of sub-100 keV electrons with silicon dual-pillar grating structures," *Optics Letters* 40 (18), 4344 (2015).

[6] K. Wootton, et al. “Demonstration of acceleration of electrons at a dielectric microstructure using femtosecond laser pulses," *Optics Letters* 41 (12), 2672 (2016).

[7] R. J. England, et al. "Dielectric Laser Accelerators" *Rev. Mod. Phys.* 86, 1337 (2014).

[8] L. Pilozzi, A. D’Andrea, and R. Del Sole, "Electromagnetic properties of a dielectrid grating I. Propagating, evanescent, and guided waves," *Phys. Rev. B*, 54 (15), 10751 (1996).

[9] A. Hanuka, W. D. Kimura, I. Pogorelski, and L. Schachter, "Quasi-analytic design of a dielectric acceleration structure," *AIP Conference Proceedings* 1812, 060012 (2017).

[10] T. Plettner and R. L. Byer, "Proposed dielectric-based microstructure laser-driven undulator," *Phys. Rev. ST Accel. Beams* 11, 030704 (2008).

[11] F. Toufexis, T. Tang, and S. G. Tantawi, "A 200 μm-period laser-driven undulator," *Proceedings of FEL 2014, Basel, Switzerland* MOP047 (2014).

[12] K. P. Wootton, et al. "Design and optimisation of dielectric laser deflecting structures," *Proceedings of 2015 International Particle Accelerator Conference* (IPAC‘15), WEPJ012 (2015).

[13] E. Kur *et. al.*, "A wide bandwidth free-electron laser with mode locking using current modulation," *New Journal of Physics* 13, 063012 (2011).

[14] T. Plettner *et. al.*, "Photonic-based laser driven electron beam deflection and focusing structures," *Phys. Rev. ST Accel. Beams* 12, 101302 (2009).

[15] Z. Huang, K.-J. Kim, "Coherent spontaneous emission in high gain free-electron lasers," *Proceedings of 1999 Particle Accelerator Conference* (PAC 1999), 2495 (1999).

[16] R. Bonifacio, N. Piovella, G. R. M. Robb, and A. Schiavi, "Quantum regime of free electron lasers starting from noise," *Phys. Rev. ST - Accel. Beams* 9, 090701 (2006).

60th ICFA Advanced Beam Dynamics Workshop on Future Light Sources FLS2018, Shanghai, China JACoW Publishing
ISBN: 978-3-95450-206-6 doi:10.18429/JACoW-FLS2018-WEA1PL03

ATTOSECOND TIMING

F. X. Kärtner, M. Xin, and K. Safak
Center for Free-Electron Laser Science, Deutsches Elektronen-Synchrotron and
Physics Department and The Hamburg Center for Ultrafast Imaging, Universität Hamburg,
Hamburg, Germany

Abstract

Photon-science facilities such as X-ray free-electron lasers (XFELs) and intense-laser facilities are emerging worldwide with some of them producing sub-fs X-ray pulses. These facilities are in need of a high-precision timing distribution system, which can synchronize various microwave and optical sub-sources across multi-km distances with attosecond precision. Here, we report on a synchronous laser-microwave network that permits attosecond precision across km-scale distances. This was achieved by developing new ultrafast timing metrology devices and carefully balancing the fiber nonlinearities and fundamental noise contributions in the system. New polarization-noise-suppressed balanced optical crosscorrelators and free-space-coupled balanced optical-microwave phase detectors for improved noise performance have been implemented. Residual second- and third-order dispersion in the fiber links are carefully compensated with additional dispersion-compensating fiber to suppress link-induced Gordon-Haus jitter and to minimize output pulse duration; the link power is stabilized to minimize the nonlinearity-induced jitter as well as to maximize the signal to noise ratio for locking..

INTRODUCTION

Recently, several X-ray FELs (XFELs), such as the European XFEL [1] in Hamburg, FERMI [2] in Italy, SwissFEL in Switzerland and Linac Coherent Light Source (LCLS) [3] and LCLS II [4] in Stanford and Dalian Coherent Light Source (DCLS) and SXFEL in China have been built and are in operation. The length of these facilities ranges from few hundred meters to several kilometers. Many of these facilities aim to generate attosecond X-ray pulses [5] with unprecedented brightness to film physical and chemical reactions with sub-atomic-level spatio-temporal resolution [6, 7]. Significant progress in attosecond science, including the time-domain observation of intramolecular charge transfer [8] and the discovery of ultrafast Auger processes altering the chemistry of matter on an attosecond time scale [9, 10], has been made in the past few years. Thus current XFELs technology will move over the next decade into the attosecond regime. As illustrated in Fig. 1, it is advantages to generate attosecond X-ray pulses and perform attosecond- precision pump-probe experiments. This is supported in an optimum way, if all optical/microwave sources in the XFEL, including the electron gun, injector laser, microwave references of the linear accelerator and bunch compressor, most importantly, the seed laser and pump lasers at the end station are synchronized simultaneously with attosecond relative timing jitter. Therefore, a multi-km attosecond-precision synchronization technique is imperative to unleash the full potential of these billion-dollar photon-science facilities.

The timing system consists of a reference providing extremely stable timing signals, a target signal that needs to be synchronized, a detector that can measure the timing difference between the target signal and the reference, and a control box to lock the timing of the target to that of the reference. If the target device is far away from the reference, a timing link is also necessary to deliver the timing signal from the reference to the target. Without exception, the attosecond-precision synchronization technique also requires these key elements.

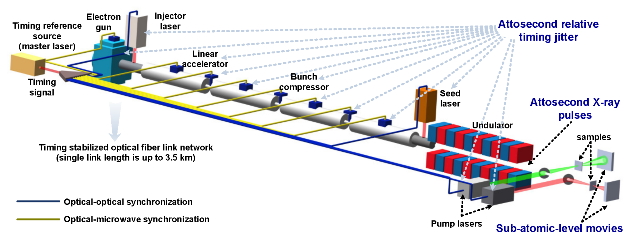

Figure 1: Timing and synchronization system for an attosecond XFEL [11].

The timing reference source in attosecond synchronization can be an atomic clock [12, 13], a continuous-wave (CW) laser [14, 15] or a mode-locked laser [16, 17]. The state-of-the-art technique in each solution can provide an attosecond-jitter-equivalent instability for 1s observation time. In contrast to the other two solutions, a mode-locked laser can simultaneously provide ultralow-noise optical and microwave signals, and the ultrashort optical pulses in time domain can be directly used as time markers for precise timing measurements. So it is an ideal timing source for synchronization applications such as telescope arrays and XFELs, where the target devices are mode-locked lasers and microwave sources.

Another advantage of using mode-locked lasers is that it can provide very high sensitivity during timing detection, thanks to its high pulse peak power. For example, we have developed balanced optical cross-correlators (BOCs) [17, 18] and balanced optical-microwave phase detectors (BOMPDs) [19–21] for optical-optical and optical-microwave timing detection, respectively. Both of them can achieve attosecond precision and >1-ps dynamic range at the same time.

For remote synchronization, the timing link can be implemented as optical fiber link [22]. Optical-fiber-based timing

ISBN: 978-3-95450-206-6 doi:10.18429/JACoW-FLS2018-WEA1PL03

links are very flexible for installation and can be easily fitted into XFELs and other facilities.

Here, we focus on the XFEL application, since it possesses currently the most urgent timing challenge. But the techniques we present here can also easily be adapted to other applications in the future. Based on the discussions above, the best synchronization solution for XFELs, as depicted in Fig. 1, should use a mode-locked laser (master laser) as the timing reference, and optical fiber links to distribute the timing signals to different remote laser/microwave sources. We have been working on this approach over the past decade [22, 23] and already passed the 10-fs precision level [24–26], which is more than an order-of-magnitude better than the best results achieved with traditional microwave signal distribution schemes. In order to meet the strict timing requirements of XFELs, a novel sub-fs-precision timing synchronization system is developed based upon our previous work, and presented here.

JITTER OF THE OPTICAL MASTER OSCILLATOR

Since the optical master oscillator (OMO) in Fig. 1 serves as timing reference for all optical/microwave sub-sources, it must exhibit attosecond-level timing jitter, which needs to be accurately characterized. Here, we use a balanced optical cross-correlator (BOC) [18, 23], which is intrinsically immune to AM-PM noise conversion by directly converting the timing difference of two optical pulses into a voltage signal. The BOC characterization has achieved extremely low noise floors down to 10^{-12} fs^2/Hz for offset frequencies up to the Nyquist frequency of mode-locked lasers [26, 27].

The OMO jitter characterization setup is shown in Fig. 2. The output of two identical lasers (master and slave, with 216.667 MHz repetition rate, 50 mW average power, 170 fs pulse width and 1553 nm center wavelength) were combined by a polarization beam splitter (PBS) and launched into a BOC, which consists of a single 4-mm-long periodically-poled $KTiOPO_4$ (PPKTP) crystal operating in a double-pass configuration with appropriate dichroic beam splitter and mirror (DBS, DM) and a low-noise balanced photodetector (BPD). The BOC output was fed back to the piezoelectric transducer (PZT) of the slave laser (with a sensitivity of 17.4 Hz/V) through a proportional-integral (PI) controller so that the two lasers' repetition rates were locked to each other. Finally, the BOC output was sent to an SSA for jitter characterization.

It can be seen that as feedback gain increases, the low frequency jitter is suppressed below 50 kHz. So in terms of measurement, we can decrease the feedback gain as much as possible (e.g., to -20 dB), then we can obtain the accurate master-laser jitter between 1 kHz and 20 kHz and an upper limit estimate above this frequency range.

The master laser characterization results are displayed in Fig. 3. The top panel shows the jitter spectral density at different feedback gains. As predicted by the simulations, the jitter spectrum is limited by the detector noise floor (grey curve) above 30 kHz. Between 1 kHz and 30 kHz, as the gain decreases, the spectrum approaches the real laser jitter. We choose the lowest gain value (about -15 dB) at which the locking is still stable enough to perform a measurement, and obtain 330 as integrated timing jitter from 1 kHz to 1 MHz, as shown in the bottom panel of Fig. 3. This value gives a very good upper limit estimate of the master laser's jitter. So this laser is definitely capable of providing the reference in an attosecondprecision timing synchronization system.

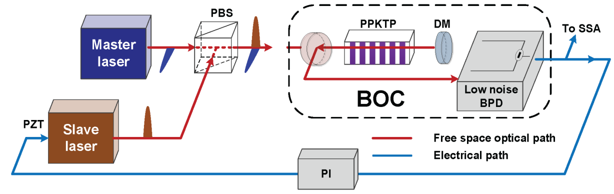

Figure 2: Master-laser (OMO) jitter characterization setup (PBS, polarization beam splitter; DBS, dichroic beam splitter; DM, dichroic mirror; PPKTP, periodically-poled $KTiOPO_4$; PI, proportional-integral controller; BPD, balanced photodetector; PZT, piezoelectric transducer; SSA, signal source analyzer).

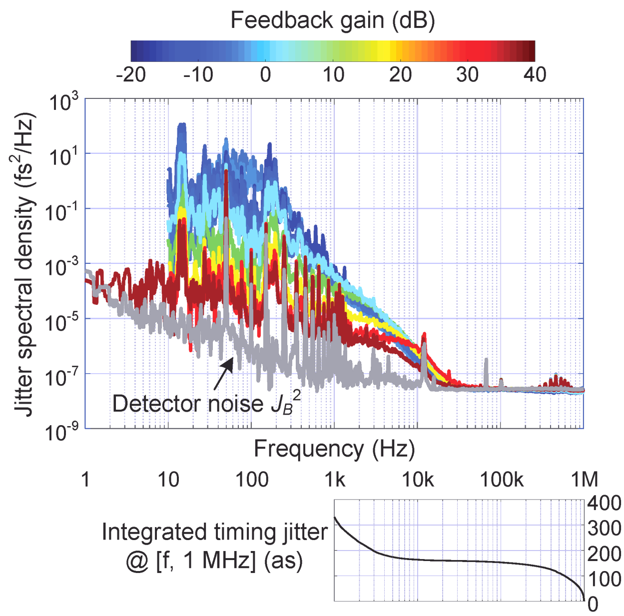

Figure 3: Measured master-laser jitter spectrum and corresponding integrated timing jitter [25].

1550 nm LASER SYNCHRONZATION

To test the local optical-optical synchronization an experimental setup shown in Fig. 4 is constructed. Similar to that in laser characterization, the repetition rates of the slave and master lasers were first locked together with an in-loop BOC, then another out-of-loop BOC was used to evaluate the jitter performance after synchronization. Both of the two BOCs have the same structure as that shown in Fig. 2. In the feedback loop, the output of the in-loop BOC was first filtered

ISBN: 978-3-95450-206-6 doi:10.18429/JACoW-FLS2018-WEA1PL03

by a PI controller. Then the PI output was separated into two paths: the first path was directly sent to the slave laser's PZT without amplification to compensate fast jitter above 10 Hz; the second path was sampled by a data acquisition (DAQ) card, analyzed by a Labview program to generate a DC voltage to compensate slow jitter below 10 Hz, and a voltage amplifier was used to extend the compensation range. This feedback design can effectively optimize the locking bandwidth and compensation range simultaneously.

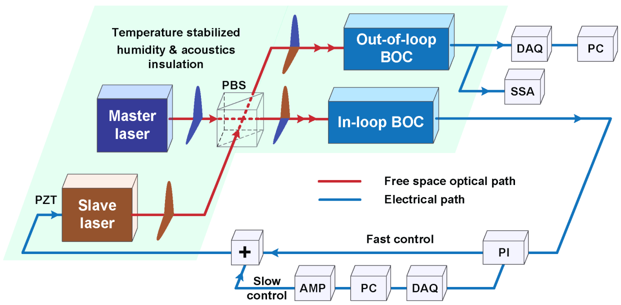

Figure 4: Local optical-optical synchronization (DAQ, data acquisition card; PC, computer, AMP, voltage amplifier; +, voltage summer).

To minimize the thermally-induced timing fluctuations, the two lasers, two BOCs and other free-space optics were mounted on a temperature-stabilized breadboard with a Super-Invar surface sheet. With temperature fluctuations controlled below ±0.05 K, the effective timing instability of free-space beam paths due to thermal expansion is only ±1 as/cm.

Figure 5(a) shows the out-of-loop jitter spectrum from 1 Hz to 1 MHz. The total integrated jitter over this frequency range is only 450 as. A long-term drift measurement was taken and the peak-to-peak drift in 10 hours is 400 as, which gives a root-mean-square (RMS) drift of 71 as (Fig. 6(b)). The Fourier transform of the drift data is also calculated in Fig. 6(c). The integrated drift from 200 μHz to 1 Hz is only 50 as. These results indicate that optical synchronization using BOC can easily achieve attosecond precision. Furthermore, they also provide a precision limit that we can approach in the remote timing synchronization.

SYNCHRONIZATION OF Ti:SAPPHIRE LASERS

In order to investigate the jitter noise limitations in the timing synchronization system, we built a Ti:Sapphire laser synchronization setup on a 4.7-km timing link network [28], as shown in Fig. 5. The same master laser as before was used, and its repetition rate was locked to an RF reference to reduce its drift below ~200 Hz. The slave laser, is a home-built Ti:Sapphire Kerr-lens mode-locked laser operating at 800-nm center wavelength and 1.0833 GHz repetition rate. Then the output of the master laser was split into two separate timing links. Timing link 1 consisted of a 3.5-km polarization-maintaining (PM) dispersion-compensated fiber spool, a PM fiber stretcher, and a fiber-coupled motorized delay line with 560-ps range. Similarly, the components of timing link 2 included a 1.2-km PM fiber spool, a PM fiber stretcher, and a free-space motorized stage with 100-ps range. At the end of each link, there was a fiber-coupled mirror reflecting 10% of the optical power back to the link input. Here, a bidirectional erbium-doped fiber amplifier (EDFA) was also used to provide sufficient power for the backpropagating signal and the link output required for link stabilization and remote synchronization, respectively. At the link inputs, the round-trip pulses were combined with newly emitted ones in one-color (OC)-BOCs. OC-BOCs operate at 1554 nm wavelength and realize the crosscorrelation

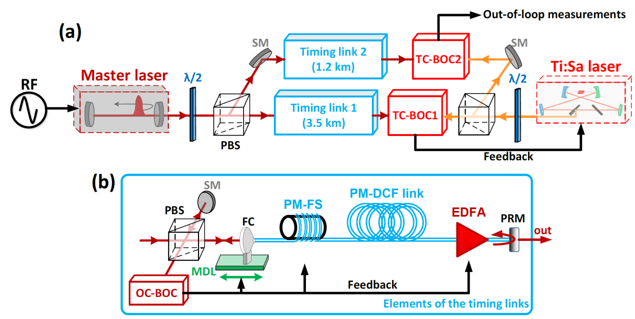

Figure 5: (a) Experimental setup for the synchronization of the Ti:Sa laser on a timing link network with a total length of 4.7 km. (b) Individual elements of the timing stabilized fiber links. Abbreviations: RF: RF reference; FC: fiber collimator; MDL: motorized delay line; PMFS: polarization-maintaining fiber stretcher; PM-DCF: PM dispersion-compensated fiber; EDFA: bidirectional erbium-doped fiber amplifier; PRM: partially reflecting fiber mirror [28].

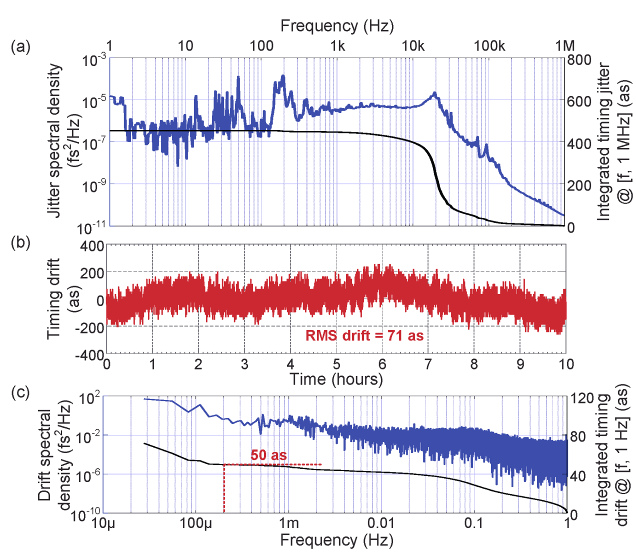

Figure 6: Local optical-optical synchronization measurement results. (a) Out-of-loop jitter spectrum; (b) longterm timing drift (sampling rate: 2 Hz); (c) timing drift spectrum.

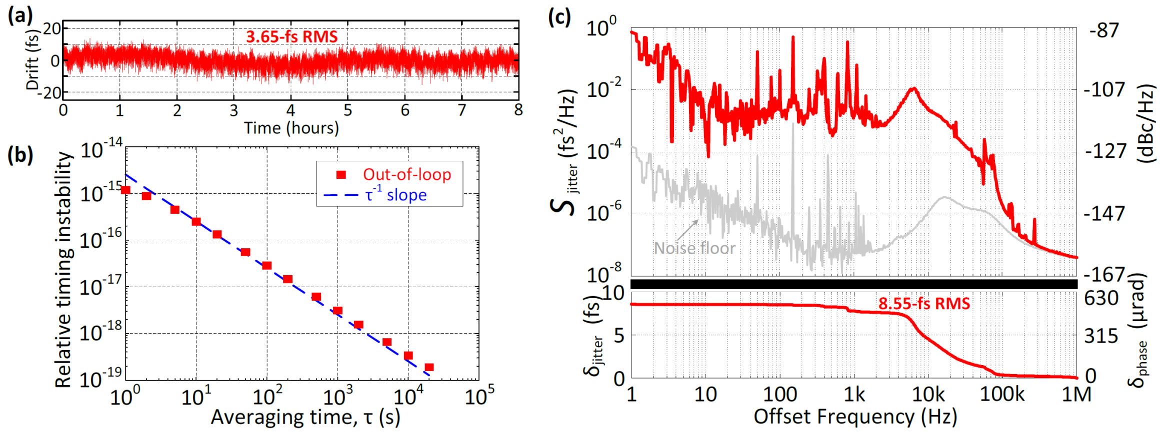

Figure 7: Out-of-loop measurements between the remotely synchronized Ti:Sa laser and timing link 2 output. (a) Timing drift below 1 Hz. (b) Calculated relative timing instability from the drift data. (c) Jitter spectral density S_{jitter} and its integrated jitter δ_{jitter}; right axes: equivalent SSB phase noise $\mathcal{L}$(f) and its integrated phase δ_{phase} scaled to a 10 GHz carrier frequency. The grey curve shows the noise floor of the free-running TC-BOC2 [28].

with the birefringence between two orthogonally polarized input pulses. OC-BOCs measured the propagation delay fluctuations in the links and generated error voltages, which controlled the fiber stretchers and the motorized delays to compensate for fast jitter and long-term drifts, respectively. The Ti:Sapphire laser was placed at the output location of the timing links. As the OMO and Ti:Sapphire laser operate at different central wavelengths, two two-color BOCs (TC-BOCs) [28] were built between each link output and the Ti:Sapphire laser output. Both of the TC-BOCs were realized with type-I sum-frequency generation between 800-nm and 1550-nm central wavelengths in a beta-barium borate (BBO) crystal. TC-BOC1 synchronized the Ti:Sa laser with link 1 output by tuning the repetition rate via its intracavity PZT mirror. Finally, the free-running TC-BOC2 evaluates the timing precision between the synchronized Ti:Sapphire laser and timing link 2 output.

Figure 7(a) shows the out-of-loop timing drift between the remotely synchronized Ti:Sa laser and timing link 2 output. We were able to keep the complete system synchronized for 8 hours continuously, which is limited by the PZT range of the Ti:Sa laser. The observed drift is only 25-fs peak-to-peak and 3.65 fs RMS for the complete duration without any excess locking volatility. We also calculated the relative timing instability (i.e., timing error in terms of overlapping Allan deviation) from the drift data to investigate the system behavior for different averaging times. As Fig. 7(b) illustrates, the relative timing instability is only 1.2×10^{-15} in 1-s averaging time (τ) and falls to 3.36×10^{-19} at 10,000 s following a deterministic slope very close to τ^{-1}.

The timing jitter spectral density for offset frequencies larger than 1 Hz was measured with a baseband analyzer, which Fourier transformed the TC-BOC2 output. The red curve in Fig. 7(c) shows the out-of-loop jitter between the remotely synchronized Ti:Sa laser and timing link 2 output. The integrated jitter for 1 Hz – 1 MHz is 8.55 fs RMS corresponding to a phase error of 0.5 mrad for a 10 GHz carrier.

SUB-FEMTOSECOND PERFORMANCE

Demonstration of sub-femtosecond timing distribution was achieved with the laser-microwave network shown in Fig. 8a. The timing signal from the master laser is distributed through a network that contains two independent fiber links of 1.2-km and 3.5-km length operated in parallel. The link outputs are used to synchronize a remote

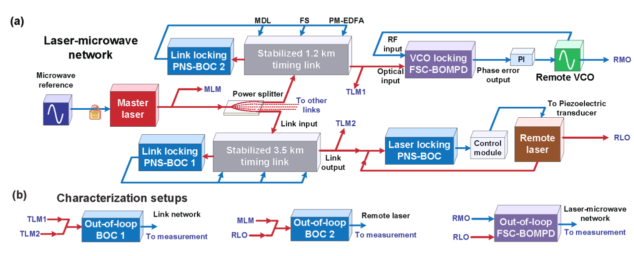

Figure 8: (a) Laser-microwave network (VCO, voltagecontrolled oscillator); (b) Out-of-loop characterization setups [11].

laser (e.g., serving as a pump-probe laser at the FEL end station) and a voltagecontrolled oscillator (VCO) (e.g., serving as a microwave reference of the FEL linear accelerator) simultaneously. New *polarization-noise-suppressed* BOCs (PNS-BOC) and *free-space-coupled balanced optical-microwave phase detectors* (FSC-BOMPD) for improved noise performance have been and implemented. Residual second and third-order dispersion links are carefully compensated with additional dispersion-compensating fiber to suppress link-induced Gordon-Haus jitter and to minimize output pulse duration; the link power is stabilized to minimize the nonlinearity-induced jitter as well as to maximize the SNR for BOC locking. Characterization setups are shown

ISBN: 978-3-95450-206-6 doi:10.18429/JACoW-FLS2018-WEA1PL03

in Fig. 8b, to evaluate the performance of the link network, as shown in Fig. 9.

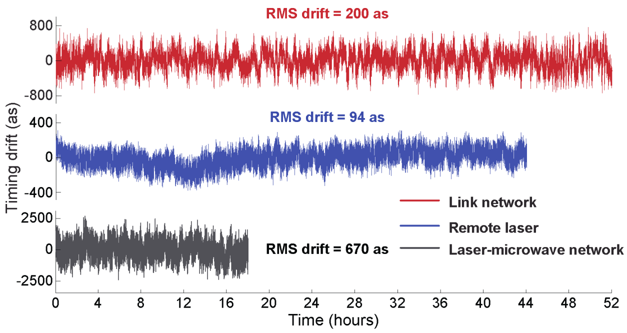

Figure 9: Measured long-term timing drift (sampling rate = 2 Hz).

The residual timing drift between links below 1 Hz is only 200 as RMS (red), and the total integrated timing jitter from 6 µHz to 1 MHz is 580 as (red). Remote laser synchronization over 44 hours without interruption is within 100 as RMS (blue). Overall, an unprecedented long-term precision of 670 as RMS out-of-loop drift over 18 hours (black) [11].

CONCLUSIONS

A sub-femtosecond laser-microwave network has been demonstrated with novel timing devices.

ACKNOWLEDGEMENT

This work was supported by the European Research Council under the European Union's Seventh Framework Program (FP/2007-2013) / ERC Grant Agreement No. 609920 and the Cluster of Excellence "The Hamburg Centre for Ultrafast Imaging–Structure, Dynamics and Control of Matter at the Atomic Scale" of the Deutsche Forschungsgemeinschaft.

REFERENCES

[1] M. Altarelli, R. Brinkmann, M. Chergui, W. Decking, B. Dobson, S. Düsterer, G. Grübel, W. Graeff, H. Graafsma, and J. Hajdu, "XFEL: The European X-Ray Free-Electron Laser", DESY, Technical Design Report, 2006.

[2] E. Allaria *et al.*, "Highly coherent and stable pulses from the FERMI seeded free-electron laser in the extreme ultraviolet", *Nature Photon*, 6 (2012) 699.

[3] P. Emma *et al.*, "First lasing and operation of an ångstrom-wavelength free-electron laser", *Nature Photon*, 4 (2010) 641.

[4] J. Stohr, "Linac Coherent Light Source II (LCLS-II) Conceptual Design Report", SLAC, Design Report, No. SLAC-R-978, 2011.

[5] E. Prat and S. Reiche, "Simple Method to Generate Terawatt-Attosecond X-Ray Free-Electron-Laser Pulses", *Phys. Rev. Lett*. 114 (2015) 244801.

[6] C. Kupitz *et al.*, "Serial time-resolved crystallography of photosystem II using a femtosecond X-ray laser", *Nature* 513 (2014) 261.

[7] H. Öström *et al.*, "Probing the transition state region in catalytic CO oxidation on Ru", *Science* 347 (2015) 978.

[8] F. Calegari, D. Ayuso, A. Trabattoni, L. Belshaw, S. De Camillis, S. Anumula, F. Frassetto, L. Poletto, A. Palacios, P. Decleva, J. B. Greenwood, F. Martín, and M. Nisoli, "Ultrafast electron dynamics in phenylalanine initiated by attosecond pulses", *Science* 346 (2014) 336.

[9] S. K. Son, L. Young, and R. Santra, "Impact of hollow-atom formation on coherent x-ray scattering at high intensity", *Phys. Rev.* A. 83 (2011) 033402.

[10] S. P. Hau-Riege, "Photoelectron dynamics in X-ray free-electronlaser diffractive imaging of biological samples", *Phys. Rev. Lett.* 108 (2012) 238101.

[11] M. Xin, K. Şafak, M. Y. Peng, A. Kalaydzhyan, W. Wang, O. D. Mücke, and F. X. Kärtner, "Attosecond precision multi-km lasermicrowave network", *Light: Science & Applications* 6 (2017) e16187.

[12] C. W. Chou, D. B. Hume, T. Rosenband, and D. J. Wineland, "Optical clocks and relativity", *Science* 329 (2010) 1630.

[13] T. L. Nicholson, S. L. Campbell, R. B. Hutson, G. E. Marti, B. J. Bloom, R. L. McNally, W. Zhang, M. D. Barrett, M. S. Safronova, G. F. Strouse, W. L. Tew, and J. Ye, "Systematic evaluation of an atomic clock at 2×10^{-18} total uncertainty", *Nature Commun.* 6 (2015) 6896.

[14] D. Meiser, J. Ye, D. R. Carlson, and M. J. Holland, "Prospects for a millihertz-linewidth laser", *Phys. Rev. Lett.* 102 (2009) 163601.

[15] C. Hagemann, C. Grebing, C. Lisdat, S. Falke, T. Legero, U. Sterr, F. Riehle, M. J. Martin, and J. Ye, "Ultrastable laser with average fractional frequency drift rate below $5{\times}10^{-19}$/s", *Opt. Lett.* 39 (2014) 5102.

[16] T. K. Kim, Y. Song, K. Jung, C. Kim, H. Kim, C. H. Nam, and J. Kim, "Sub-100-as timing jitter optical pulse trains from mode-locked Er-fiber lasers", *Opt. Lett.* 36 (2011) 4443.

[17] A. J. Benedick, J. G. Fujimoto, and F. X. Kärtner, "Optical flywheels with attosecond jitter", *Nature Photon*. 6 (2012) 97.

[18] T. R. Schibli, J. Kim, O. Kuzucu, J. T. Gopinath, S. N. Tandon, G. S. Petrich, L. A. Kolodziejski, J. G. Fujimoto, E. P. Ippen, and F. X. Kärtner, "Attosecond active synchronization of passively mode-locked lasers by balanced cross correlation", *Opt. Lett.* 28 (2003) 947.

[19] J. Kim, J. Chen, Z. Zhang, F. N. C. Wong, F. X. Kärtner, F. Loehl, and H. Schlarb, "Long-term femtosecond timing link stabilization using a single-crystal balanced cross correlator", *Opt. Lett.* 32 (2007) 1044.

[20] J. Kim, F. X. Kärtner, and F. Ludwig, "Balanced optical–microwave phase detectors for optoelectronic phase-locked loops", *Opt. Lett.* 31 (2006) 3659.

[21] M. Y. Peng, A. Kalaydzhyan, and F. X. Kärtner, "Balanced optical-microwave phase detector for sub-femtosecond optical-RF synchronization", *Opt. Express* 22 (2014) 27102.

[22] J. Kim, J. A. Cox, J. Chen, and F. X. Kärtner, "Drift-free femtosecond timing synchronization of remote optical and microwave sources", *Nature Photon.* 2 (2008) 733.

ISBN: 978-3-95450-206-6 doi:10.18429/JACoW-FLS2018-WEA1PL03

[23] M. Y. Peng, P. T. Callahan, A. H. Nejadmalayeri, S. Valente, M. Xin, L. Grüner-Nielsen, E. M. Monberg, M. Yan, J. M. Fini, and F. X. Kärtner, "Long-term stable, sub-femtosecond timing distribution via a 1.2-km polarization-maintaining fiber link: approaching 10^{-21} link stability", *Opt. Express* 21 (2013) 19982.

[24] M. Xin K. Şafak, M. Y. Peng, P. T. Callahan, and F. X. Kärtner, "One-femtosecond, long-term stable remote laser synchronization over a 3.5-km fiber link", *Opt. Express* 22 (2014) 14904.

[25] K. Şafak, M. Xin, P. T. Callahan, M. Y. Peng, and F. X. Kärtner, "All fiber-coupled, long-term stable timing distribution for free electron lasers with few-femtosecond jitter", *Structural Dynamics* 2 (2015) 041715.

[26] J. Kim, J. Chen, J. Cox, and F. X. Kärtner, "Attosecond-resolution timing jitter characterization of free-running mode-locked lasers", *Opt. Lett.* 32 (2007) 3519.

[27] J. A. Cox, A. H. Nejadmalayeri, J. Kim, and F. X. Kärtner, "Complete characterization of quantum-limited timing jitter in passively mode-locked fiber lasers", *Opt. Lett.* 35 (2010) 3522.

[28] K. Şafak, M. Xin, Q. Zhang, S. Chia, O. D. Mücke, and F. X. Kärtner, "Jitter analysis of timing-distribution and remote-laser synchronization systems", *Opt. Express* 24 (2016) 21752.

3 THE 61ST ICFA ADVANCED BEAM DYNAMICS WORKSHOP ON HIGH-INTENSITY AND HIGH BRIGHTNESS HADRON BEAMS (HB2018)

3.1 Foreword From the Chair

Dong-O Jeon, Institute for Basic Science (IBS), Daejeon, Korea

Mail to: jeond@ibs.re.kr

Welcome to the HB2018!

Welcome to the 61st ICFA Advanced Beam Dynamics Workshop on High-Intensity and High-Brightness Hadron Beams.

It is a great pleasure to have the HB2018 workshop first time in Korea. It is a very nice time to host the HB2018 workshop at the Institute for Basic Science, as the construction of the RAON heavy ion accelerator facility is currently underway.

The construction of the Spallation Neutron Source that started in the year of 1998 presented urgent needs to further the understanding of space-charge mechanisms and the beam loss. And the HB workshop series was conceived in the ICFA (International Committee for Future Accelerators) ABDW (Advanced Beam Dynamics Workshops). The 1st HB workshop was held in the year of 2002 at the Fermilab in the United States. And since then the HB workshop has become the main international event for the high- intensity hadron beam accelerator community.

At the time of the 1st HB workshop, the highest power accelerator had about 0.1 MW beam power. Since then, brilliant progresses have been made. Now the Spallation Neutron Source reached its design power of 1.4 MW and is striving for power-upgrade. The J-PARC reached 0.5 MW and is ramping up the beam power. The beam power of the European Spallation Source is 5 MW which is under construction and the beam power of the IFMIF is 10 MW.

The HB starts with the Monday morning plenary session, followed by two parallel sessions. Also there is one plenary session in Wednesday morning and the poster session in Wednesday afternoon. The HB consists of five working groups: Beam Dynamics in Rings (WG-A), Beam Dynamics in Linacs (WG-B), Accelerator Systems (WG-C), Commissioning and Operations (WG-D) and Beam Instruments and Interactions (WG-E).

The program of the HB is set by the International Organizing Committee (IOC), which selects the plenary speaker and working group conveners. The invited oral programs are formulated by each working groups and approved by the IOC. These committees have done an excellent work in setting up the scientific program.

Daejeon is known as the science city of Korea and is a home to majority of thenational laboratories and several prestigious universities. Daejeon has a population of 1.5-million people and has a rich culture. We hope that you all enjoy the HB2018 workshop and your stay in Daejeon.

ISBN: 978-3-95450-202-8 doi:10.18429/JACoW-HB2018-MOA1PL01

CHALLENGES IN UNDERSTANDING SPACE CHARGE EFFECTS

H. Bartosik*, CERN, Geneva, Switzerland

Abstract

Space charge effects in high intensity and high brightness synchrotrons can lead to undesired beam emittance growth, beam halo formation and particle loss. A series of dedicated machine experiments has been performed over the past decade in order to study these effects in the particular regime of long-term beam storage (10^5-10^6 turns) as required for certain applications. This paper gives an overview of the present understanding of the underlying beam dynamics mechanisms. In particular it focuses on the space charge induced periodic resonance crossing, which has been identified as the main mechanism causing beam degradation in this regime. The challenges in further progressing with the understanding, the modelling and the mitigation of these space charge effects and the resulting beam degradation are discussed. Furthermore, an outlook for possible future directions of studies is presented.

INTRODUCTION

Space charge effects in high intensity and high brightness synchrotrons can lead to undesired beam emittance growth, beam halo formation and particle loss. Some accelerator projects require long-term storage (up to several seconds) of high brightness bunches at injection energy in order to allow accumulating several injections from an upstream machine. This is the case for the Proton Synchrotron (PS) and the Super Proton Synchrotron (SPS) at CERN, which are part of the injector chain for the Large Hadron Collider (LHC). In preparation for the High Luminosity era of the LHC (HL-LHC), the injector chain at CERN is in the course of being upgraded in the framework of the LHC Injectors Upgrade (LIU) [1]. In simplified terms, the aim of this project is to enable the injectors to deliver twice higher intensity at equal emittance, i.e. twice as high brightness, as compared to today's performance. Table 1 shows an overview of the required storage times, the space charge tune shifts and the loss and emittance growth budgets for the various machines of the proton injector chain at CERN. For the heavy ion injector chain, space charge is critical in the Low Energy Ion Ring (LEIR). In the SPS, a space charge tune shift of up to $\Delta Q_y = -0.3$ is achieved and storage times of up to 40 s are required. In this case the beam quality is subject to strong degradation, which has been taken into account for the projection of the LIU-ion target parameters [2].

At the Facility for Antiproton and Ion Research project (FAIR) at GSI, the future SIS100 is required to store high brightness beams with a maximum space charge tune shift of about $\Delta Q_y \approx -0.3$ for about 1 s to accumulate several injections from SIS18 with losses on the percent level [3]. In this case, the tight constraint on beam losses is (at least partially) imposed by dynamic vacuum issues stemming from the large ionization cross section of U^{+28} ions with the residual gas.

Table 1: Target Parameters for LIU Project at CERN

Machine	ΔQ_y	Storage time	Budget for losses / Emittance growth
PSB	-0.5	-	5% / 5%
PS	-0.31	1.2 s	5% / 5%
SPS	-0.21	10.8 s	10% / 10%

Keeping the beam degradation within tight tolerances for long storage times can be quite challenging in presence of large space charge tune spread. A detailed understanding of the underlying beam dynamics mechanisms is required. A series of dedicated machine experiments has been performed over the past decade in collaboration between CERN and GSI in order to study the space charge dynamics in this regime. The aim of this paper is to give an overview of the present understanding, discuss the challenges faced and provide an outlook for future directions of study.

OVERVIEW OF STUDIES AND PRESENT UNDERSTANDING

One-dimensional Resonances

The first systematic experimental study of long-term space charge effects in presence of non-linear resonances was performed at the CERN PS in 2002-2003, as reported in [4] and [5]. In this experiment, the fourth order horizontal resonance $4Q_x = 25$ was deliberately excited by a single octupole. A bunched proton beam with a horizontal (vertical) incoherent direct space charge tune shift of -0.075 (-0.12) was stored at injection energy for about 1 s for different working points. Depending on how the space charge tune spread overlaps the resonance, two regimes of beam degradation could be clearly identified. For bare machine working points only slightly above the resonance, beam loss dominates. At the same time a reduction of both the horizontal emittance as well as the bunch length are observed. For higher machine tunes, losses are reduced but a large halo is formed in the horizontal plane leading to an enlarged emittance.

The beam degradation observed in the PS experiment was explained by trapping and scattering of particle trajectories during the periodic resonance crossing induced by space charge in a bunched beam, as anticipated by a simplified simulation model in 2002 [6]. This picture was refined in the following years [7–9], describing the main features of the phenomenon as follows:

- Space charge couples transverse and longitudinal planes: due to the change of line charge density along

* hannes.bartosik@cern.ch

ISBN: 978-3-95450-202-8 doi:10.18429/JACoW-HB2018-MOA1PL01

the bunch, the instantaneous transverse Coulomb force depends on the particle location in the longitudinal plane. Therefore, the longitudinal motion induces, via space charge, a variation of transverse tunes.

- The presence of a relatively small tune shift compared to the machine tunes ($\Delta Qx/Qx_0$ of a few percent), does not destroy the validity of standard transverse non-linear dynamics, but rather induces a slow modulation of transverse tunes according to twice the synchrotron frequency.
- The transverse-longitudinal space charge coupling determines, via the depression of tunes, the transverse position of the fixed-points generated by the 1D resonance.
- The strength of the resonance determines the tune of particles around the fixed-points and also the resonance island size. The island size is also determined by the detuning created by space charge: a stronger gradient in the amplitude dependent detuning leads to smaller islands,
- The synchrotron tune determines the speed of the resonance crossing. A figure of merit on the speed of the resonance crossing is given by the adiabaticity parameter T, which is obtained as the ratio between the speed of migration of the fixed-points to the maximum speed of rotation of the particle in the island. If this ratio is small ($T \ll 1$) the motion is adiabatic and the particles remain locked to the island. As a consequence, the particle gains large amplitudes (trapping). If instead $T > 1$, a single resonance crossing results in a “kick” to the particle invariant (scattering).
- Particles that periodically cross the resonance will slowly diffuse to large amplitudes to form a halo. Its density and extension depend on the number of particles that cross the resonance, and on the outer position of the islands. If the outer position of islands intercepts the beam pipe or reaches the dynamic aperture, beam loss occurs according to a rate which is function of the distance from the resonance. When the accelerator is tuned close to a resonance (and above it), only particles with large synchrotron amplitude may cross the resonance and therefore become trapped or scattered into a halo and eventually be lost. This leads to a correlation between beam loss and longitudinal beam size such that only particles with large synchrotron amplitude will be lost resulting in a reduction of the bunch length.
- The space charge induced tune modulation due to longitudinal particle motion has twice the synchrotron frequency. The tune modulation introduced by chromaticity, instead, has the same frequency as the synchrotron motion. When maximum space charge detuning and maximum chromaticity detuning are comparable, the resulting slow modulation of the transverse tunes is the composition of these two effects with different frequencies. Consequently, the position of the fixed points is different in the two synchrotron half-periods. The overall effect is that islands are pushed further out (during half of the synchrotron period) and the halo size is increased.

This mechanism was confirmed in a systematic measurement campaign performed at the GSI SIS18 in 2007, where the horizontal third order resonance $3Q_x = 13$ was studied for both coasting and bunched beams with different beam intensities and space charge tune spreads [10]. The strong emittance growth was only observed for the high intensity bunched beam but not for the coasting beam with the same space charge tune shift, since for the coasting beam there is no periodic resonance crossing.

Two-dimensional Sum Resonances

While all the studies reported above concentrated on one-dimensional non-linear resonances, an experiment in 2012 at the CERN PS was dedicated to studying the beam behaviour close to the third order coupled sum resonance $Q_x + 2Q_y = 19$ deliberately excited by a sextupole magnet [11]. The beam was stored for about 1 s. Also in this experiment the loss dominated and the emittance growth dominated regimes were observed depending on the working point. However, the halo formation measured with wire scanners was observed to be very asymmetric between the horizontal and vertical planes. In particular, the beam developed much larger tails in the vertical plane. This observation could not be explained by a naive extension of the one-dimensional model developed earlier, since the particle trajectory on the coupled resonance follows resonant tori in phase space rather than fixed points. These resonant tori, in this context referred to as “fixed lines” [12–14], have a peculiar shape in the 4 dimensional phase space of horizontal and vertical coordinates. In the case of the $Q_x + 2Q_y$ resonance, the projection of the single particle trajectory in the physical $x - y$ space has a larger excursion in the vertical plane and, depending on the phase advance from the driving sextupole to the observation point, follows either a figure-of-eight or a C-shape. This explains the larger vertical halo observed in this experiment at the PS.

It should be mentioned that there is an experimental campaign ongoing at the CERN SPS to study the fixed lines on the $Q_x + 2Q_y$ resonance in the “zero” space charge limit [15]. Furthermore, a general theory of space charge dynamics in the presence of non-linear coupled sum resonance of arbitrary order is being developed [16].

(REMAINING) CHALLENGES

Macroparticle Simulations

Space charge in a synchrotron is usually modelled by alternating space charge interaction (“space charge kicks”) with particle tracking in the magnetic guide field. As the space charge forces depend on the transverse beam sizes,

ISBN: 978-3-95450-202-8 doi:10.18429/JACoW-HB2018-MOA1PL01

the rule of thumb is that about 10 space charge kicks per beam size variation period (sometimes referred to as betatron wavelength) are needed.

The brute force way of calculating the space charge forces is based on the Particle-In-Cell (PIC) algorithm [17]. In this approach the real number of particles is represented by macroparticles (usually about 10^6), where the total beam intensity is equally distributed to the charge of each macroparticle. The charge distribution is binned onto a spatial grid and the Poisson equation is solved numerically on the grid points to obtain the space charge kicks through the electric field. This method is self-consistent, i.e. the evolution of the particle distribution as a function of time is fully taken into account. However, a large number of macroparticles is needed to reduce emittance growth due to numerical noise in the particle distribution [18]. This approach is therefore very demanding in terms of computational power, necessitating the implementation of parallel computing. In addition, there is some artificial emittance growth induced by the grid ("grid heating") [19] and special care needs to be taken to make the calculation symplectic [20], which comes at additional computational cost.

To avoid the issue with noise, simulations with a so-called "frozen" space charge potential are commonly used for long-term simulations. In this approach, the space charge kicks are computed analytically for a chosen (fixed) particle distribution. A closed analytic expression for the electric field generated by a bi-dimensional Gaussian transverse distribution was derived by Bassetti and Erskine [21]. For each particle in the simulation, this formula is evaluated at the position of the particle using the actual horizontal and vertical beam sizes at the location of the space charge interaction and taking the local longitudinal line density into account. Simulations with this approach require only a few thousand particles to study the emittance growth and losses statistically. The drawback of this approach is that coherent collective effects cannot be taken into account. Furthermore the evolution of the particle distribution is not treated self-consistently.

The latter is partially overcome by adapting the beam parameters such as intensity and transverse emittances periodically and recomputing the frozen potential, as implemented in MAD-X [22] and in PyOrbit [23]. PyOrbit allows furthermore to partially account for the generation of halo by representing the beam by two transverse Gaussian distributions with different weights and different transverse emittances.

Some years ago a code-to-code benchmarking suite has been put in place in order to check the space charge induced particle trapping phenomenon [24]. In addition to MICROMAP [25] and SIMPSONS [26], this benchmarking case has been successfully passed by MAD-X [22], PTC-ORBIT [27] and lately also SYNERGIA [28, 29]. It should be highlighted that SYNERGIA is a PIC code and all the features observed in the frozen space charge codes could be reproduced. Even the long term emittance evolution test case was in very good agreement, once a sufficient number of macroparticles was used [30]. Work is presently ongoing to check the frozen space charge module of PyOrbit against this benchmarking case.

A more general overview of space charge code benchmarking can be found in [31, 32].

Quantitative Agreement Between Measurements and Simulations

Achieving quantitative agreement between machine experiments and space charge simulation codes is challenging. In fact, reproducing the evolution of the particle distribution during long-term storage requires several ingredients:

- **Accurate measurement of beam parameters** The measurement of the transverse beam profiles in synchrotrons is particularly challenging, because a high signal to noise ratio is required in order to resolve the beam halo.
- **Good knowledge of machine linear and non-linear errors** The long-term evolution of the particle distribution in the presence of space charge is very sensitive to machine errors and non-linearities. Having a good model of the machine is crucial. In general, the information on magnet errors for machines, which have been in operation for more than two decades, is sparse. In this case an effective non-linear model of the machine can be established from beam-based measurements, as done for example at the SPS [33].
- **Accurate aperture model including misalignments** Reproducing losses relies critically on a good model of the machine aperture, including element misalignments and the closed orbit. This information is unfortunately not always readily available, especially concerning the alignment data.
- **Properly identifying and accounting for interfering effects** To achieve quantitative agreement with simulations it is crucial to identify any effects that contribute to emittance growth and or losses in the machine under study. If these effects cannot be suppressed in the machine, they need to be quantified and eventually taken into account in the simulations. In some cases the interplay between space charge and other effects requires a study on its own. This might become more and more relevant in the future, when the accelerator performances will be pushed further. This aspect will be addressed in more detail later in this paper.

An example where a good quantitative agreement between measurements and simulations could be achieved is the PSB. As reported in [34], a benchmark experiment was performed for a working point slightly above the $2Q_y = 9$ half integer resonance. The beam loss evolution over about 200 ms was studied on a constant energy plateau when switching off the half integer correctors. To reproduce the observed losses in PIC simulations, a very accurate machine model of the

ISBN: 978-3-95450-202-8 doi:10.18429/JACoW-HB2018-MOA1PL01

linear errors had to be developed using beam-based measurements. In the end, even the evolution of the longitudinal bunch profile measured in the experiment was in very good agreement with the simulations.

A similar level of agreement has not yet been reached for the PS. Studies performed in 2013 have shown that high brightness beams suffer from losses for machine working points above $Q_y = 6.25$, while practically no losses are observed for beams with low brightness [35]. Further studies have shown that the non-linear space charge potential of the Gaussian particle distribution drives the 8^{th} order resonance $8Q_y = 50$, because 50 is the strongest harmonic of the PS lattice functions [36, 37]. More recent campaigns concentrated on tune scans in different experimental conditions. However, simulations using a frozen adaptive model in PyOrbit for the ideal PS lattice do not explain the observed losses quantitatively (about a factor 3 higher losses in the measurements for high brightness beams) as shown in Fig. 1 [38]. The space charge tune shift of the beam used in this study was about $\Delta Q_y = -0.25$. As the discrepancy between measurements and simulations is relatively large, detailed investigations on this subject are ongoing. In particular, the interplay with some residual, but yet to be quantified, magnetic resonance excitation at $Q_y = 6.25$ (e.g. octupole components) is being studied. A direct measurement of such residual resonance excitation is however difficult. Furthermore, the aperture model of the machine is being refined (e.g. comparison of model aperture with direct measurement of the effective physical aperture). Finally the importance of other effects like indirect space charge, as recently proposed in [39], and coherent space charge effects is being investigated. It should be mentioned that, since the beam loss at these working points is observed only for high brightness beams, the studies need to be performed with a relatively large tune spread. It could therefore be that multiple resonances are contributing to the beam degradation, which is an additional complication for these studies. In fact, driving term calculations have shown that there are also 8^{th} order coupled sum resonances excited by space charge [40], in addition to third order (skew) resonances in the tune space investigated (as indicated in the top of the graphs in Fig. 1).

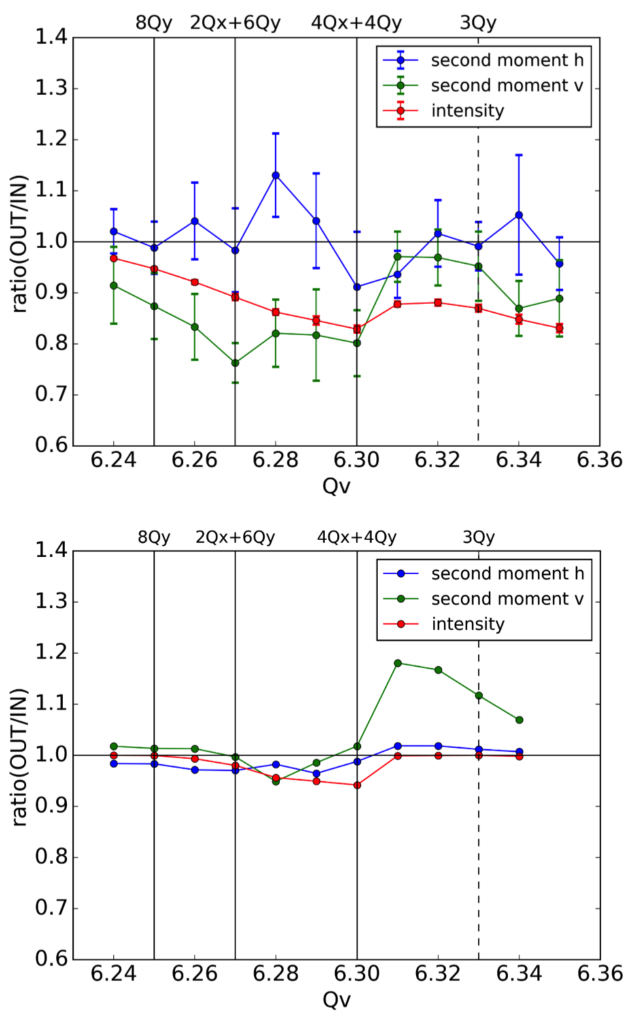

Figure 1: Relative emittance growth and losses as a function of the vertical machine tune in measurements (top) and in simulations (bottom) [38]. The horizontal tune was set to 6.2 in all cases.

Mitigation of Beam Degradation

In view of pushing the accelerator performance further, an important aspect to be addressed is the mitigation of the space charge induced beam degradation. On the one hand, individual non-linear resonances excited by magnetic errors can be compensated in case appropriate corrector magnets are available in the machine (at the expense of possibly further exciting other resonances or reducing the dynamic aperture). Typically two independent correctors with adequate phase advance are needed in order to control the resonance driving term in the complex plane. This has been tested in the PS for third order normal and skew resonances, see for example [38, 40, 41]. Experimental studies in the SIS18 on this subject are summarized in [42]. It seems that after the compensation, some minor residual resonance excitation left. It is not yet clear if this is related to the space charge detuning or to non-ideal resonance compensation settings, or due to another reason.

The other approach could be to try compensating the space charge detuning in the first place. A study in this direction was performed recently based on using electron lenses [43].

FUTURE DIRECTIONS

As described above, the main mechanism for beam degradation of high brightness bunches in the long-term storage regime has been attributed to periodic resonance crossing. Future study efforts could focus on identifying and better understanding the interplay with other collective effects or beam dynamics mechanisms such as:

- Tune modulation induced by power converter ripple
- Intra Beam Scattering (especially for ions)

ISBN: 978-3-95450-202-8 doi:10.18429/JACoW-HB2018-MOA1PL01

- Electron-cloud
- Indirect space charge and impedance

which are encountered in some operational conditions in the CERN injectors. A good example is the SPS, as discussed in more detail below.

Reaching the LIU target beam parameters requires injecting 25 ns beams with unprecedented intensity (about twice compared to today's nominal) and beam brightness. In the past, coherent and incoherent electron cloud effects were encountered in the SPS already with the nominal intensity. Over the years this effect was slowly reduced by beam induced scrubbing. In recent machine studies with high intensity beams (not yet LIU intensity) a strong incoherent emittance growth was observed when storing the beam for about 20 s at injection energy. However, a clear improvement of the beam quality could already be observed after running the machine in this scrubbing configuration for two days [44]. Nevertheless, some residual electron-cloud might always be present in future operation and the interplay with space charge effects could become important.

Other recent studies at the SPS indicate that the tune modulation induced by power converter ripple can play an important role in the beam degradation during the long storage in presence of space charge [45]. Figure 2 (top graph) shows the relative emittance growth and transmission for different working points in the SPS close to excited resonances ($Q_x = 20.33$ deliberately excited using a single sextupole and at $Q_x = 20.40$ most likely driven by space charge itself). Simulations using a frozen potential are far from the experimental observations (middle graph) unless the measured tune ripple induced by the power converters for the main quadrupoles of the SPS is taken into account (bottom graph). Detailed studies on this subject are ongoing.

It should be pointed out that the tune ripple might also play a role for the strong emittance growth and losses observed for the Pb^{82+} ion beam on the SPS injection plateau. This beam has to be stored for more than 40 s for accumulation of several batches from the PS to reach the LIU ion target parameters [2] and the space charge tune shift at injection reaches up to $\Delta Q_y = -0.3$. On the other hand, Intra Beam Scattering is also contributing to emittance growth [46] and the interplay between space charge and Intra Beam Scattering needs to be studied.

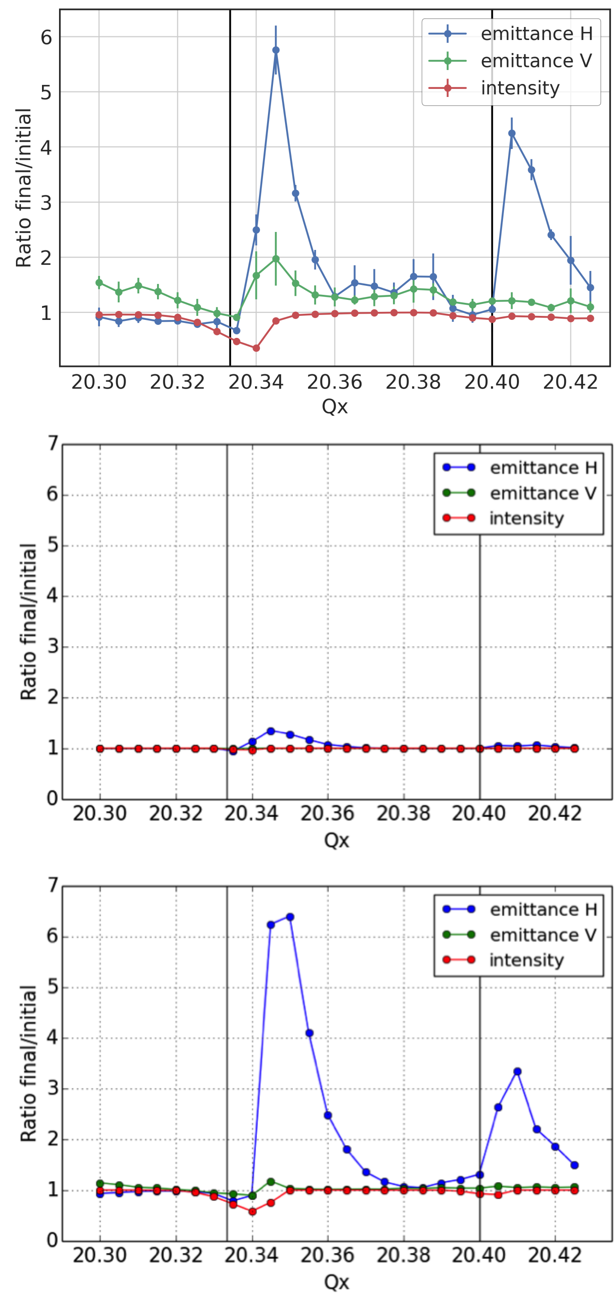

Figure 2: Relative emittance growth and losses as a function of the measured horizontal machine tune in measurements (top), in simulations (middle) and in simulations including the tune ripple induced by power converters in the SPS (bottom).

ACKNOWLEDGEMENTS

The author would like to acknowledge the contributions of Y. Alexahin, F. Asvesta, E. Benedetto, O. Boine-Frankenheim, S. Cousineau, V. Forte, G. Franchetti, S. Gilardoni, I. Hofmann, J. Holmes, A. Huschauer, S. Kostoglou, S. Machida, E. Metral, Y. Papaphilippou, J. Qiang, A. Saa Hernandez, F. Schmidt, A. Shishlo, E. Stern, R. Wasef, and all other colleagues of the CERN space charge collaboration.

REFERENCES

[1] J. Coupard *et al.*, "LIU Technical Design Report - Volume I: Protons", CERN, Geneva, Switzerland, Rep. CERN-ACC-2014-0337, Dec. 2014.

[2] J. Coupard *et al.*, "LIU Technical Design Report - Volume II: Ions", CERN, Geneva, Switzerland, Rep. CERN-ACC-2016-0041, April 2016.

ISBN: 978-3-95450-202-8 doi:10.18429/JACoW-HB2018-MOA1PL01

[3] "Facility for Antiproton and Ion Research", https://fair-center.eu

[4] E. Métral *et al.*, "Observation of octupole driven resonance phenomena with space charge at the CERN Proton Synchrotron", *Nuclear Instruments and Methods in Physics Research* A, vol. 561, pp. 257-265, 2006, doi:10.1016/j.nima.2006.01.029

[5] G. Franchetti, *et al.*, "Space charge and octupole driven resonance trapping observed at the CERN Proton Synchrotron", *Phys. Rev. ST Accel. Beams*, vol. 6, p. 124201, Dec. 2003, doi:10.1103/PhysRevSTAB.6.124201

[6] G. Franchetti and I. Hofmann, "Modeling of Space Charge Induced Resonance Loss", in *Proc. of High Intensity and High Brightness Hadron Beams 2002*, AIP Conf. Proc. No. 642, AIP, New York, 2002, p. 260, doi:10.1063/1.1522641

[7] G. Franchetti and I. Hofmann, "Particle Trapping by Nonlinear Resonances and Space Charge", in *Proc. of High Intensity Beam Dynamics - COULOMB'05*, Senigallia (AN), Italy, 2005.

[8] G. Franchetti and I. Hofmann, "Resonance Trapping due to Space Charge and Synchrotron Motion, in Theory, Simulations and Experiments", in *Proc. of High Intensity and High Brightness Hadron Beams 2006*, Tsukuba, Japan, 2006.

[9] G. Franchetti and I. Hofmann, *Nucl. Instrum. Methods Phys. Res., Sect.* A, vol. 561, p. 195, 2006.

[10] G. Franchetti *et al.*, "Experiment on space charge driven nonlinear resonance crossing in an ion synchrotron", *Phys. Rev. ST Accel. Beams*, vol. 13, p. 114203, 2010, doi:10.1103/PhysRevSTAB.13.114203

[11] G. Franchetti *et al.*, "Space charge effects on the third order coupled resonance", *Phys. Rev. Accel. Beams*, vol. 20, p. 081006, 2017, doi:10.1103/PhysRevAccelBeams.20.081006

[12] F. Schmidt, "Untersuchungen zur dynamischen Akzeptanz von Protonenbeschleunigern und ihre Begrenzung durch chaotische Bewegung", PhD thesis, DESY HERA 88-02, 1988.

[13] G. Franchetti and F. Schmidt, "Extending the Nonlinear-Beam-Dynamics Concept of 1D Fixed Points to 2D Fixed Lines", *Phys. Rev. Lett.*, vol. 114, p. 234801, June 2015, doi:10.1103/PhysRevLett.114.234801

[14] G. Franchetti and F. Schmidt, "Fix-lines and stability domain in the vicinity of the coupled third order resonance", April 2015, http://arxiv.org/abs/1504.04389

[15] H. Bartosik, G. Franchetti, F. Schmidt, M. Titze, private communication.

[16] G. Franchetti, "Sum Resonances with Space Charge", presented at HB2018, Daejeon, Korea, June 2018, paper WEA1WA01, this conference.

[17] R.W Hockney and J.W Eastwood, "Computer Simulation Using Particles", ISBN9780852743928.

[18] F. Kesting and G. Franchetti, "Propagation of numerical noise in particle-in-cell tracking", *Phys. Rev. ST Accel. Beams*, vol. 18, p. 114201, Nov. 2015, doi:10.1103/PhysRevSTAB.18.114201

[19] A. Bruce Langdon, "Effects of the spatial grid in simulation plasmas", *Journal of Computational Physics*, vol. 6, Issue 2, October 1970, pp. 247-267, doi:10.1016/0021-9991(70)90024-0

[20] J. Qiang, "Symplectic multiparticle tracking model for self-consistent space-charge simulation", *Phys. Rev. Accel. Beams*, vol. 20, p. 014203, 2018, doi:10.1103/PhysRevAccelBeams.21.054201

[21] M. Bassetti and G.A. Erskine, "Closed Expression for the Electric Field of a two-dimensional Gaussian Charge", CERN-ISR-TH/80-06, Geneva, March 1980.

[22] Y. Alexahin *et al.*, "Adaptive Space Charge Calculations in MADX-SC", in *Proc. NA-PAC'16*, Chicago, IL, USA, Oct. 2016, paper THPOA15, doi:10.18429/JACoW-NAPAC2016-THPOA15

[23] Andrei Shishlo *et al.*, "The Particle Accelerator Simulation Code PyORBIT", *Procedia Computer Science*, vol. 51, pp. 1272-1281, 2015.

[24] G. Franchetti, "The GSI Bench-Marking Suite", http://web-docs.gsi.de/~giuliano/research_activity/trapping_benchmarking/main.html

[25] G. Franchetti *et al.*, "MICROMAP Library", http://web-docs.gsi.de/~giuliano/micromap_manual/micromap_reference_manual.html

[26] S. Machida, "The Simpsons program 6-D phase space tracking with acceleration", *AIP Conference Proceedings*, vol. 297, p. 459, 1993, doi:10.1063/1.45344

[27] J. Galambos *et al.*, "Orbit - A ring injection code with space charge", ibid, p. 3143.

[28] E. Stern *et al.*, "SYNERGIA", https://cdcvs.fnal.gov/redmine/projects/synergia2/wiki

[29] J. Amundson *et al.*, "High Performance Computing Modeling Advances Accelerator Science for High Energy Physics", *IEEE Comput.Sci.Eng.*, vol. 16, no. 6, pp. 32-41, 2014.

[30] E. Stern, "Studies on space charge compensation", 2nd CERN Space Charge Collaboration Meeting, March 2018, https://indico.cern.ch/event/688897

[31] S. Machida, "Benchmarking and Application of Space Charge Codes for Rings", in *Proc. IPAC'15*, Richmond, VA, USA, 2015, pp. 2402-2407.

[32] F. Schmidt *et al.*, "Code Bench-marking for Long-term Tracking and Adaptive Algorithms, in *Proc. HB'16*, Malmö, Sweden, 2016, paper WEAM1X01, pp. 357-361, ISBN978-3-95450-178-6

[33] H. Bartosik *et al.*, "Improved Methods for the Measurement and Simulation of the CERN SPS Non-linear Optics", in *Proc. IPAC'16*, Busan, Korea, 2016, paper THPMR036, pp. 3464-3467.

[34] V. Forte *et al.*, "CERN Proton Synchrotron booster space charge simulations with a realistic model for alignment and field errors", *Phys. Rev. Accel. Beams*, vol. 19, p. 124202, 2016, doi:10.1103/PhysRevAccelBeams.19.124202

[35] R. Wasef, "PS Experiments and Simulations", 1st CERN Space Charge Collaboration Meeting, CERN, Geneva, May 2014, https://indico.cern.ch/event/292362

[36] S. Machida, "Space charge simulation for 4th order resonance", CERN Space Charge Collaboration Meeting, CERN, Geneva, May 2014, https://indico.cern.ch/event/292362

ISBN: 978-3-95450-202-8 doi:10.18429/JACoW-HB2018-MOA1PL01

[37] R. Wasef, "Space charge in the PS", Machine Studies Working Group meeting, CERN, Geneva, July 2015, https://indico.cern.ch/event/433250/

[38] F. Asvesta *et al.*, "PS: Studies on Qy=6.25 and other resonances", 2nd CERN Space Charge Collaboration Meeting, CERN, Geneva, March 2018, https://indico.cern.ch/event/688897

[39] S. Machida, "About indirect space charge driven resonances", 2nd CERN Space Charge Collaboration Meeting, CERN, Geneva, March 2018, https://indico.cern.ch/event/688897

[40] F. Asvesta *et al.*, "Resonance Identification Studies at the CERN PS", in *Proc. IPAC'18*, Vancouver, BC, Canada , 2018, paper THPAK056.

[41] A. Huschauer *et al.*, "Identification and compensation of resonances in the CERN Proton Synchrotron", presentation at Space Charge 13 workshop, CERN, Geneva, April 2013, https://indico.cern.ch/event/221441/

[42] G. Franchetti, "Resonance Compensation for High Intensity Bunched Beam", in *Proc. IPAC'15*, Richmond, VA, USA, 2015, paper MOPWA028, pp. 159-161.

[43] O. Boine-Frankenheim and W. Stem, "Space charge compensation for intense ions beams in booster synchrotrons", arXiv:1705.01057

[44] G. Rumolo, "Beam Dynamics Challenges for the LHC and Injector Upgrades", presented at HB2018, Daejeon, Korea, June 2018, paper MOA1PL02, this conference.

[45] H. Bartosik *et al.*, "SPS: Power converter ripple and space charge driven resonance", 2nd CERN Space Charge Collaboration Meeting, CERN, Geneva, March 2018, https://indico.cern.ch/event/688897

[46] A. Saa Hernandez *et al.*, "Characterization of Losses and Emittance Growth for Ion Beams on the SPS Injection Plateau", in *Proc. IPAC'18*, Vancouver, BC, Canada, 2018.

ISBN: 978-3-95450-202-8 doi:10.18429/JACoW-HB2018-MOA1PL02

BEAM DYNAMICS CHALLENGES FOR THE LHC AND INJECTOR UPGRADES

G. Rumolo*, CERN, CH-1211 Geneva 23, Switzerland

Abstract

The High Luminosity upgrade of the Large Hadron Collider (HL-LHC) will rely on significantly higher bunch current and brightness to meet the future yearly integrated luminosity target. The implications are twofold. On one side, all the accelerators of the LHC injection chain will have to be upgraded to produce the desired beam parameters. For this purpose, the LHC Injectors Upgrade (LIU) program has been established to implement all the needed modifications for meeting the required beam specifications. These upgrades will lead to the lifting of the main intensity and brightness limitations in the injectors, linked to beam instabilities driven by impedance or electron cloud (e-cloud), and space charge. On the other side, the LHC will have to be able to swallow the new beam parameters. This will mainly require control of impedance driven instabilities and beam-beam effects, and e-cloud mitigation. In this paper, we will focus on proton beams by describing the identified performance limitations of the LHC and its injectors, as well as the actions envisioned to overcome them.

INTRODUCTION

The LHC Injectors Upgrade (LIU) project [1, 2] aims at increasing the intensity and brightness of the beams in the injectors in order to match the beam requirements set out by the High Luminosity LHC (HL-LHC) project [3], while ensuring high availability and reliable operation of the injector complex well into the HL-LHC era (up to about 2037) in synergy with the Consolidation (CONS) project [4]. For the upgrade of the LHC injector proton chain, LIU includes the following principal items:

- The replacement of Linac2, which accelerates protons to 50 MeV, with Linac4, providing 160 MeV H^- ions;
- Proton Synchrotron Booster (PSB): New 160 MeV H^- charge exchange injection, acceleration to 2 GeV from current 1.4 GeV with new power supply and RF system;
- Proton Synchrotron (PS): New 2 GeV injection, broadband longitudinal feedback;
- Super Proton Synchrotron (SPS): Upgrade of the 200 MHz RF system, impedance reduction and e-cloud mitigation, new beam dump and protection devices.

All these upgrades will lead to the production of beams with the challenging HL-LHC parameters and, if not already installed, they will for the most part be implemented during the Long Shutdown 2 (LS2) in 2019-20.

To extend its discovery potential, the LHC will undergo a major upgrade during Long Shutdown 3 (LS3) in 2024-25 under the HL-LHC project. The goal will be to increase the rate of collisions by a factor of 5-7.5 beyond the original LHC design value, leading to a target integrated luminosity of 3000-4000 fb^{-1} over the full HL-LHC run (2026-2037). The new configuration will rely on the replacement of the final focusing quadrupoles at the high luminosity Interaction Points (IPs), which host ATLAS and CMS, with new and more powerful magnets based on the Nb_3Sn technology, as well as a number of key innovations that push accelerator technology beyond its present limits while enabling, or even broadening, the future desired performance reach. Among these are the cutting-edge 11 T superconducting Nb_3Sn-based dipoles, the new superconducting link technology with MgB_2, compact superconducting cavities for transverse beam tilting along the longitudinal axis to compensate for the crossing angle at collision (crab cavities), the upgrade of the cryogenic system and general infrastructure, new technology and material for collimators, the optional use of hollow electron lenses for beam halo cleaning.

The beam dynamics aspects of the LIU and HL-LHC projects are challenging, because during the HL-LHC era:

- The LHC injectors will have to be able to routinely produce, stably control and safely handle beams with unprecedented intensity and brightness;
- The LHC will have to be able to run with the future beams, preserve their stability and make them available for collisions all along the calculated optimum fill length with the desired levelling scheme, ensuring as little as possible beam quality degradation.

Addressing the beam intensity limitations of the LHC and its injectors and illustrating the envisaged strategies to cope with them will be the subject of the next sections.

BEAM PERFORMANCE LIMITATIONS IN THE LHC INJECTORS AND GOALS

In this section we will first present a general overview on the present LHC beam performance of the injectors and the beam requirements for the LIU project. We will only focus on the so called 'standard LHC beam', which is baseline for the projects and produced as follows:

- Two subsequent injections of 4+2 bunches from the four PSB rings into the PS at E_{kin}=1.4 GeV;
- In the PS, triple splitting of the injected bunches at 2.5 GeV, then acceleration to 25 GeV and two consecutive double splittings of all 18 bunches at 25 GeV;
- Four subsequent injections of trains of 72 bunches spaced by 25 ns into the SPS (train spacing 200 ns) at 25 GeV and acceleration to 450 GeV.

Then, we will describe the actions that the LIU project has (planned to) put in place to overcome the intensity/brightness limitations in the various accelerators of the injector chain.

* Giovanni.Rumolo@cern.ch

61st ICFA ABDW on High-Intensity and High-Brightness Hadron Beams HB2018, Daejeon, Korea JACoW Publishing
ISBN: 978-3-95450-202-8 doi:10.18429/JACoW-HB2018-MOA1PL02

Present Performance of the LHC Injector Chain

An upper limit for the brightness of standard LHC beam is determined at the PSB injection, because of the efficiency of the multi-turn injection process as well as the effects of space charge during injection. The normalised transverse emittance has been measured as a function of intensity at the PSB extraction after optimization of the injection settings and for a longitudinal emittance of 1.2 eVs at extraction [5]. The relation is found to be linear and the resulting line defines the "PSB brightness" line. The longitudinal emittance at extraction can be made in principle as high as 2.8 eVs via longitudinal emittance blow up along the PSB cycle [6] compatibly with other constraints coming from the transfer to the PS and further longitudinal beam manipulation in the PS ring. Although this is believed to be beneficial in terms of space charge in the PS since it would allow the transfer of longer bunches with larger momentum spreads, the experimental proof is to date still missing – probably due to other issues related to the transfer of bunches with large momentum spread. The PSB does not have an intensity limitation for the LHC beams, as it already nowadays successfully accelerates to 1.4 GeV beams up to 6 times more intense than the current LHC beams, which are used for fixed target experiments at the ISOLDE facility.
Combining the experience accumulated with operational beams with the outcomes of several dedicated space charge Machine Development (MD) studies conducted throughout 2012 – 2017, it can be assumed that the maximum values of space charge vertical tune spread, ΔQ_y, compatible with the beam loss and emittance blow up budgets reported below, are 0.31 and 0.21 at the PS and SPS injection, respectively. Besides, prior to the LIU upgrade program, due to longitudinal dipolar coupled bunch instabilities on the ramp and at top energy, the PS was not able to produce 25 ns beams with more than 1.8e11 p/b within the longitudinal emittance of 0.35 eVs, which is currently the optmised value to limit capture losses and keep the beam longitudinally stable in the SPS. Finally, due to RF power constraints on the main SPS RF system (200 MHz) and longitudinal coupled bunch instabilities along the cycle, beams with more than 1.3e11 p/b could not be extracted from the SPS with the desired bunch length of 1.6 ns for a basically lossless injection into LHC. E-cloud has been also affecting 25 ns beams in the SPS, but currently the SPS has undergone sufficient beam induced scrubbing to produce beams with 1.3e11 p/b transversely stable and without the characteristic pattern imprinted by e-cloud on the bunch intensities and emittances along the trains. Finally, the onset of the vertical Transverse Mode Coupling Instability (TMCI) limited in the past the bunch intensity to 1.6e11 p/b [7], but this limitation was lifted in 2012 by commissioning a new optics with γ_t lower by 4 units, which increases the TMCI threshold by a factor 2.5 [8].

After including some predefined budgets for emittance blow up and beam loss (5% in the PSB and PS for both, and 10% in the SPS) we can represent in the plane emittance vs. intensity per bunch at the SPS extraction the curves corresponding to PSB brightness, PS and SPS space charge limits, and intensity limitations of the PS and SPS. The regions of inaccessible parameter ranges are shaded. The outcome of this exercise is displayed in Fig. 1, from which we deduce that presently the best standard LHC beam produced by the injectors has 1.3e11 p/b within about 2.7 μm transverse emittance. All the points measured at LHC injection over the years 2015 – 2018 fully confirm this analysis.

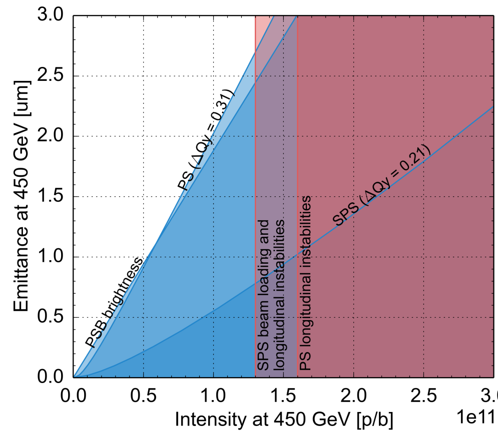

Figure 1: Limitation diagram for the standard LHC beam in the present injectors' chain.

Other methods of LHC beam production exist, which can lead to brighter bunches at the expense of the length of the trains transferred from the PS to the SPS at each cycle. For example, by transferring trains of 48 bunches instead of 72, obtained through a different sequence of batch compression and bunch merging/splitting actions at 2.5 GeV in the PS, the beam brightness can be almost doubled with respect to the scheme discussed above. The beam obtained in this way has been preferred for physics production in the LHC for most of the current run and has been routinely employed since the beginning of 2018. More details about alternative LHC beam production schemes can be found in [9–11].

HL-LHC Beam Requirements

The HL-LHC upgrade aims at accumulating an integrated luminosity of 250 fb^{-1}/year at the high luminosity IPs. Assuming 50% HL-LHC performance efficiency, this goal can be achieved assuming a standard LHC beam with bunch intensity of 2.3e11 p/b and a transverse emittance of 2.1 μm injected from the SPS. In order not to exceed a pile up of 140 events/crossing, the luminosity is levelled at 5e34 cm^{-2}s^{-1} by gradually lowering the beta functions at the IPs (β^*) down to 15 cm while partially compensating for the crossing angle with the crab cavities. An ultimate goal of 320 fb^{-1}/year is also set assuming levelling at 7.5e34 cm^{-2}s^{-1}, allowing for a pile up of 200 events/crossing. Table 1 shows achieved and HL-LHC specified beam parameters at the SPS exit.

It is clear that both intensity and brightness of the LHC beams will need to be roughly doubled in the HL-LHC era. Looking back at Fig. 1, HL-LHC is basically targeting a point right in the middle of the currently inaccessible region.

ISBN: 978-3-95450-202-8 doi:10.18429/JACoW-HB2018-MOA1PL02

Table 1: Current and HL-LHC Beam Parameters Out of SPS

	N_b (10^{11} p/b)	$\epsilon_{x,y}$ (μm)
Achieved	1.3	2.7
HL-LHC target	2.3	2.1

LIU CHALLENGES TO REACH THE HL-LHC BEAM PARAMETERS

Figure 1 directly suggests the path to reach the challenging beam parameters specified in the second row of Table 1. We will discuss first how to achieve the desired brightness and we will focus later on the intensity reach.

Achieving the future brightness relies on two main pillars:

- Reduction of the slope of the PSB brightness line by at least a factor two;
- Mitigation of the space charge effect in the PS.

The space charge in the SPS does not seem to limit the performance even for the future beams, as its limitation curve clearly lies below the HL-HLC target point. The two goals listed above will be realised within the LIU project by means of the following actions. Firstly, the PSB brightness line with half slope will be made possible by using Linac4 with H^- charge exchange injection into the PSB at 160 MeV. It has been simulated that if Linac4 provides 40 mA within 0.4 μm, the future LHC beams can be injected in about 20 turns and the desired transverse emittance is compatible with the blow up due to space charge at the new injection energy (as was expected from a naive $\beta^2\gamma$ scaling) [12]. If the current from Linac4 is lower (compatibly with the goal set for the future fixed target beams), the number of injected turns will have to be correspondingly increased. Secondly, the injection energy into the PS will be raised to 2 GeV, which alone guarantees a 63% intensity increase for a fixed transverse emittance while keeping the space charge tune spread the same as nowadays. Besides, the longitudinal beam parameters at the PSB-PS transfer will have to be optimised to further reduce the tune spread at PS injection and ensure that the PS space charge curve in the limitation diagram ends up in the shadow of the PSB brightness line. The longitudinal emittance will be blown up along the PSB cycle to provide longer bunches at the PS injection, while the larger momentum spread will also further reduce the space charge tune spread due to the increase of the average beam horizontal size through dispersion. The longitudinal emittance blow up can be reproducibly applied in the PSB via either phase modulation of a higher harmonic or injection of band limited phase noise on the main harmonic, as has been demonstrated in MDs in 2017 [6] and 2018.

The achievement of the future intensity relies on:

- Longitudinal stabilisation of the beam along the PS accelerating ramp and at top energy;
- Increase of the available power of the 200 MHz RF system in the SPS in combination with a program of longitudinal impedance reduction;
- E-cloud mitigation in the SPS.

The main longitudinal limitation for LHC-type beams in the PS are dipolar coupled-bunch instabilities. A dedicated broad-band feedback system using a Finemet cavity as a longitudinal kicker has been installed and commissioned in the PS. Extensive tests with beam have been performed since 2016 to explore the intensity reach with this system. The maximum intensity with nominal longitudinal emittance at PS extraction has been measured to be above 2.0e11 p/b [13]. Due to quadrupolar instabilities and incoherent longitudinal emittance growth, it is not yet clear whether a higher harmonic system will be required eventually to keep the beam longitudinally stable with the desired longitudinal emittance at the design intensity for HL-LHC reported in table 1.

The LIU baseline for the SPS includes an upgrade of the low-level RF and a major upgrade of the 200 MHz RF system [14]. The low-level RF upgrade will allow pulsing the RF amplifiers with the revolution frequency (the LHC beam occupies less than half of the SPS circumference) leading to an increase of the available RF power from the existing power plant up to about 1.05 MW per cavity. The main upgrade consists of the re-arrangement of the four existing cavities and two spare sections into two 4-section cavities and four 3-section cavities, and the construction of two additional power plants providing 1.6 MW each. This will entail a reduction of the beam loading per cavity, an overall increase of the available RF voltage and a reduction of the peak beam coupling impedance at the fundamental frequency. With all this massive upgrade in place, the SPS will be able to provide LHC beams with up to about 2e11 p/b, still limited by coupled bunch longitudinal instabilities on the ramp and at top energy [15]. To achieve 2.3e11 p/b it is necessary to reduce the SPS longitudinal impedance. LIU has foreseen shielding of the vacuum flanges between the focusing quadrupoles and the adjacent straight sections as well as installation of High Order Mode (HOM) couplers to improve the damping of the HOMs of the 200 MHz cavities. Numerical simulations have shown that these two measures will allow matching the HL-LHC beam requirement [16]. Finally, the e-cloud in the SPS is a potential limiting factor for operation with higher intensity. Accelerating the present LHC beam without significant degradation from the e-cloud has required an integrated time of several days of dedicated scrubbing distributed over several years. Scrubbing is preserved from year to year in the SPS regions not exposed to air during the stop, while it is partially lost, but usually quickly recovered, where there has been air exposure. Studies of e-cloud build up in the different SPS chambers have revealed that the Secondary Electron Yield (SEY) thresholds will not change significantly when going to the HL-LHC intensity for most cases [17]. Although instability simulations showed that the beam becomes more sensitive to the e-cloud in the dipoles when increasing the beam intensity, it is believed that scrubbing will work also up to the HL-LHC bunch intensity. Recent experience with beams with 2e11 p/b already injected into the SPS has indeed revealed that scrubbing can be efficiently carried out over few days and results in a clear reduction of the e-cloud induced emittance growth

ISBN: 978-3-95450-202-8 doi:10.18429/JACoW-HB2018-MOA1PL02

(see Fig. 2). Coating with amorphous carbon (a-C) [18] will be applied to the chambers of the focusing quadrupoles (QF) and adjacent drift chambers during LS2 in synergy with the impedance reduction campaign, which will also gain an extra margin on the instability threshold.

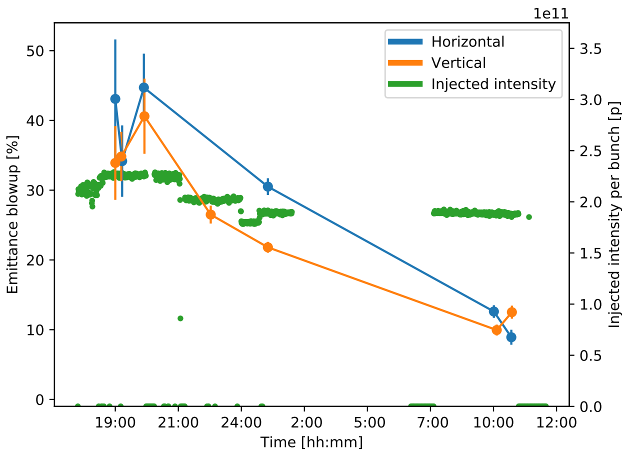

Figure 2: Evolution of emittance growth in SPS during high intensity run. Courtesy of H. Bartosik and M. Carlà.

Putting together all the points discussed in this section, we can draw the new brightness and intensity curves representing the projected limitations after the implementation of the LIU upgrades or actions, obtaining the limitation diagram in Fig. 3. The HL-LHC required point from Table 1 is also shown in yellow, demonstrating that the LIU upgrades are indeed compliant with the achievement of this final goal.

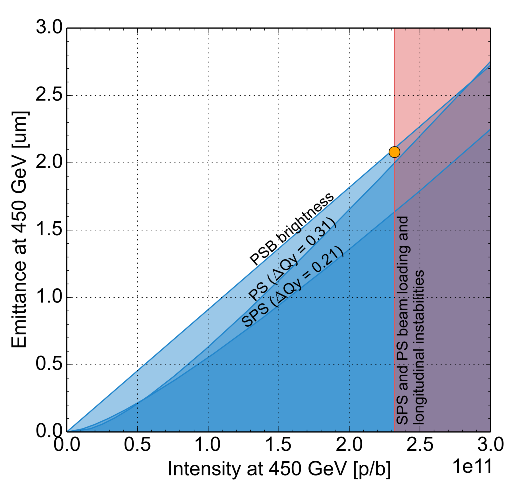

Figure 3: Limitation diagram for the standard LHC beam in the injectors' chain after the LIU upgrades.

HL-LHC CHALLENGES

The HL-LHC layout is based on the nominal LHC ring configuration, in which about 1.2 km of beam line will be changed. The nominal configuration is designed for a realistic, cost-efficient and achromatic implementation of the low β^* collision optics, based on the deployment of the Achromatic Telescopic Squeeze (ATS) scheme [19]. The installation of triplet quadrupoles of larger aperture is needed to safely accommodate the beams, which reach large dimensions (peak beta functions >20 km), and the shielding to limit the energy deposition and radiation in the SC coils and cold mass [3]. Single particle stability in HL-LHC is challenged by the large beta functions in the triplets and in the adjacent arcs, which enhance the effect of linear and non-linear errors in those regions leading to potentially low Dynamic Aperture (DA) in absence of correction. Even to allow for basic optics measurements pre-computed corrections based on accurate magnetic measurements will have to be used. Besides, the β^* levelling during many hours of operation at constant luminosity will require the commissioning of a large number of optical configurations. This further challenges the efficiency of the optics measurement and correction tools, needed to fulfil the tight tolerances coming from DA or coherent stability constraints [20].

In terms of effects related to the collective beam dynamics, running HL-LHC with double intensity and brightness will pose notable challenges, such as beam stability, beam induced heat loads in the cold regions and beam-beam [21]. (1) Transverse instabilities have been observed in the LHC with different types of beams and during different machine processes, and have required operation with quite extreme settings, e.g. with Q'=+15, octupole strength close to the maximum, as well as with maximum gain and maximum bandwidth of the transverse feedback (50 turns and 20 MHz, respectively) at high energy. The instabilities observed at injection energy (450 GeV), which are also cured by high chromaticity and octupole strength, are ascribed to e-cloud. Due to some features (such as symmetry between the transverse planes, heat load measurements on single magnets, simulated electron distributions with different magnetic fields), the e-cloud forming in the quadrupoles is likely to be the main culprit. Combined e-cloud build up and instability simulations show that the electron density in quadrupoles decreases for higher bunch currents and therefore these instabilities should become less critical for HL-LHC intensities. The underlying assumption is of course that all beam chambers will scrub for the higher HL-LHC beam intensities at least as much as they have for the present intensity. To gain margin in the octupole strength needed for suppressing instabilities driven at least partly by impedance, impedance reduction will be applied to the main existing contributors (i.e. the collimators) and to new elements in high beta regions (e.g. crab cavities). In particular, all secondary betatron collimators will be replaced with new ones based on a low-impedance design. The present baseline foresees using Mo-Graphite jaws coated with a 5μm Mo layer. This material exhibits comparable robustness as the present carbon-based secondary collimators, but has an electrical resistivity 5 (uncoated) to 100 times (coated) lower [22]. Through an iterative process between the RF and the impedance teams, the HL-LHC crab cavities have been already designed with attention to minimise the impact of HOMs on beam stability. (2) Within HL-LHC, the SEY in the insertion regions will

ISBN: 978-3-95450-202-8 doi:10.18429/JACoW-HB2018-MOA1PL02

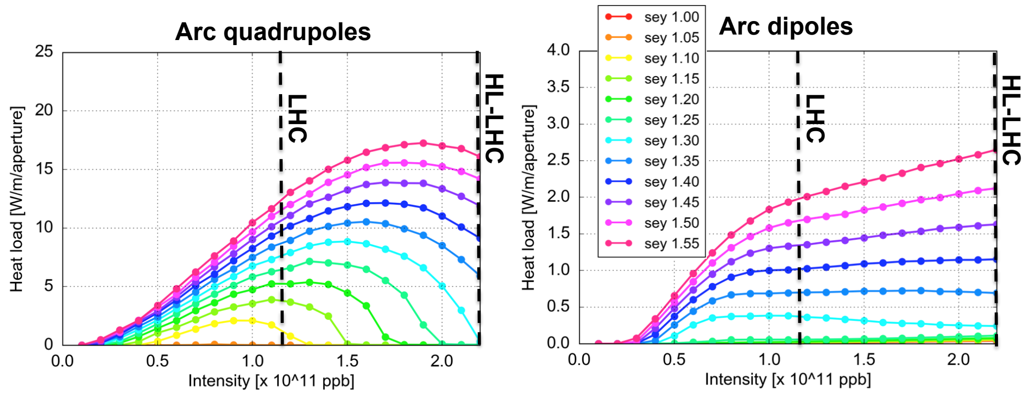

Figure 4: E-cloud generated heat load as a function of bunch intensity in LHC arc dipoles (left) and quadrupoles (right) for different SEYs, as labeled. Courtesy of G. Iadarola and G. Skripka.

be actively reduced by surface treatments (a-C coating [18] or laser treatment [23]), with an expected reduction of the heat load due to e-cloud in these regions. However, no intervention is foreseen on the beam screen of the arcs, which cover more than two thirds of the whole machine. When operating with 25 ns beams, the measured heat loads in the arcs have been consistently much larger than those expected from impedance and synchrotron radiation and they exhibited a still unexplained spread between arcs, being very close to the nominal cryogenics limits in the "hottest" arcs [24]. In future operation, we will be faced with two main issues. First, when moving to HL-LHC intensities and 7 TeV, the contribution of impedance and synchrotron radiation will become three-fold, which roughly halves the available margin of the cryogenic system for additional heat loads. Second, the scaling with intensity of the observed additional heat loads is quite uncertain. Making the educated assumption that e-cloud is the most plausible source of these heat loads (since it is compatible with a number of observations), we can however predict the heat load in the new parameter regime, as displayed in Fig. 4. For SEYs in the 1.2-1.4 range, as inferred from the present excess heat load in the various sectors, e-cloud build up simulations foresee a relatively mild change of e-cloud generated heat load when increasing the bunch intensity to HL-LHC values. This scaling needs to be validated experimentally after LS2 (when LIU will make higher intensity beams available from the injectors [25]). When summing up all the heat load contributions from the e-cloud in the different regions and those from impedance and synchrotron radiation, one finds out that, while the heat load in low-load sectors would be below 8 kW/arc and thus compatible with HL-LHC, the heat load in high-load sectors exceeds the maximum value by at least 20%. If this is confirmed, a back-up filling scheme featuring several 125 ns gaps within the bunch trains will be used for keeping the heat load in the high-load sectors within the capacity of the cryogenic plant. This will be at the expense of a 10-30% lower number of bunches in LHC.
(3) The beam-beam interaction introduces additional strong nonlinearities in the particle motion and leads to resonance excitation as well as a large tune spread, potentially resulting in a significant restriction of the DA and thus beam degradation. Operational experience and machine studies have proven that the present LHC has surpassed the head-on beam-beam tune shift limit, which was assumed based on experience from past colliders [26, 27]. However, the HL-LHC represents yet another jump into an unexplored parameter range, furthermore with a baseline configuration of luminosity β^* levelling and crossing angle compensation with crab cavities. The beam-beam studies for HL-LHC are performed by tracking the particles over a few million turns under the weak-strong approximation for the beam-beam interaction and for HL-LHC baseline parameters. The DA is calculated and compared with the target value of 6σ over 1e6 turns. Simulations seem to confirm so far that the target DA is comfortably achieved during the whole levelling process and including the chromaticity and octupole settings necessary for beam stability. This gives room to crossing angle adjustments during the levelling process to reduce the pile-up density and the radiation on the inner triplets [28]. A global exploration of the impact on DA of all the related parameters, including possible compensation of the long-range beam-beam effects with wires or electron lenses, is underway to refine operational scenarios and optimise the projected HL-LHC performance.

ACKNOWLEDGEMENTS

This paper summarises the enormous and excellent work carried out by the LIU and HL-LHC beam dynamics teams. Special thanks to H. Bartosik, G. Iadarola and R. Tomás. Then, I would also like to thank S. Albright, R. Alemany, S. Antipov, F. Antoniou, G. Arduini, M. Beck, E. Benedetto, N. Biancacci, R. Bruce, O. Brüning, X. Buffat, M. Carlà, H. Damerau, G.P. Di Giovanni, R. Di Maria, S. Fartoukh, V. Forte, M. Fraser, B. Goddard, K. Hanke, A. Huschauer, V. Kain, A. Lasheen, K. Li, M. Meddahi, L. Mether, E. Métral, B. Mikulec, Y. Papaphilippou, T. Pieloni, D. Quartullo, S. Redaelli, J. Repond, A. Romano, L. Rossi, B. Salvant, M. Schenk, R. Scrivens, E. Shaposhnikova, G. Skripka, F. Velotti, C. Zannini.

ISBN: 978-3-95450-202-8 doi:10.18429/JACoW-HB2018-MOA1PL02

REFERENCES

[1] J. Coupard *et al.*, "LIU Technical Design Report - Volume I: Protons", CERN, Geneva, Switzerland, Rep. CERN-ACC-2014-0337, Dec. 2014.

[2] J. Coupard *et al.*, "LIU Technical Design Report - Volume II: Ions", CERN, Geneva, Switzerland, Rep. CERN-ACC-2016-0041, Apr. 2016.

[3] G. Apollinari, I. Béjar Alonso, O. Brüning, P. Fessia, M. Lamont, L. Rossi, and L. Tavian, "High-Luminosity Large Hadron Collider (HL-LHC): Technical Design Report V. 0.1", CERN, Geneva, Switzerland, CERN Yellow Reports: Monographs, Rep. CERN-2017-007-M, April 2017, `doi:10.23731/CYRM-2017-004`

[4] M. Benedikt *et al.*, "Summary of Session 7: Accelerators and non LHC Experiment Areas Consolidation up to LS3", in *Proc. Chamonix 2014 Workshop*, Chamonix, France, Sep. 2014, CERN-ATS-2015-002, pp. 31-32.

[5] G. Rumolo *et al.*, "Expected Performance in the Injectors at 25 ns Without and With Linac4"', in *Proc. Review of LHC and Injector Upgrade Plans (RLIUP) Workshop*, Archamps, France, Oct. 2013, CERN-2014-006, pp. 17-24.

[6] S. Albright, E. Shaposhnikova and D. Quartullo, "Longitudinal emittance blow up and production of future LHC beams", in *Proc. Injector MD days 2017*, Geneva, Switzerland, March 2017, CERN-Proceedings-2017-002.23, pp. 23-26.

[7] G. Arduini *et al.*, "Fast vertical single-bunch instability at injection in the CERN SPS - an update", in *Proc. PAC'07*, Albuquerque, New Mexico, US, Jun. 2007, paper FRPMN065, pp. 4162-4164.

[8] H. Bartosik, "Beam dynamics and optics studies for the LHC injectors upgrade", Ph.D. thesis, CERN, Geneva, Switzerland, CERN-THESIS-2013-257, Nov. 2013.

[9] R. Garoby, *IEEE Transactions on Nuclear Science*, vol. 32, no. 5, pp. 2332 - 2334, Oct. 1985, `doi:10.1109/TNS.1985.4333903`

[10] H. Damerau *et al.*, "LIU: Exploring alternative ideas", in *Proc. Review of LHC and Injector Upgrade Plans (RLIUP) Workshop*, Archamps, France, Oct. 2013, CERN-2014-006, pp. 127-138.

[11] H. Bartosik and G. Rumolo, "Beams in the injectors", in *Proc. 5th Evian Workshop on LHC beam operation*, Evian-les-Bains, France, June 2014, CERN-ACC-2014-0319, pp. 93-98.

[12] E. Benedetto *et al.*, "Space charge effects and mitigation in the CERN PS-Booster, in view of the upgrade", in *Proc. HB'16*, Malmö, Sweden, Jul. 2016, paper THPM9X01, pp. 517-522.

[13] H. Damerau and L. Ventura, "Longitudinal coupled-bunch instability studies in the PS", in *Proc. Injector MD days 2017*, Geneva, Switzerland, March 2017, CERN-Proceedings-2017-002.59, pp. 59-62.

[14] E.Shaposhnikova, E. Chapala and E. Montesinos, "Upgrade of the 200 MHz RF System in the CERN SPS", CERN, Geneva, Switzerland, Rep. CERN-ATS-2011-042, Aug. 2011.

[15] M. Meddahi *et al.*, "LHC Injectors Upgrade (LIU) project at CERN", in *Proc. IPAC'15*, Richmond, VA, USA, May 2015, paper THPF093, pp. 3915-3918.

[16] E. Shaposhnikova *et al.*, "Identification and reduction of the SPS impedance", in *Proc. HB'16*, Malmö, Sweden, July 2016, paper TUAM3X01, pp. 260-265.

[17] G. Iadarola and G. Rumolo, "Electron cloud in the CERN accelerators (PS, SPS, LHC)", in *Proc. ECLOUD'12*, Elba Island, Italy, June 2012, CERN-2013-002, pp. 19-26.

[18] C. Yin Vallgren *et al.*, "Amorphous carbon coatings for the mitigation of electron cloud in the CERN Super Proton Synchrotron", vol. 14, p. 071001, Jul. 2011, `doi:10.1103/PhysRevSTAB.14.071001`

[19] S. Fartoukh, "Achromatic telescopic squeezing scheme and application to the LHC and its luminosity upgrade", *Phys. Rev. ST Accel. Beams*, vol. 16, p. 111002, Nov. 2013, `doi:10.1103/PhysRevSTAB.16.111002`.

[20] F. Carlier *et al.*, "Optics Measurement and Correction Challenges for the HL-LHC", CERN, Geneva, Switzerland, Rep. CERN-ACC-2017-0088, Nov. 2017.

[21] G. Arduini *et al.*, *JINST* vol. 11, p. C12081, Dec. 2016, `doi:10.1088/1748-0221/11/12/C12081`.

[22] E. Quaranta *et al.*, "Towards optimum material choices for the HL-LHC collimator upgrade", CERN, Geneva, Switzerland, Rep. CERN-ACC-2016-0062, May 2016.

[23] R. Valizadeh *et al.*, "Low secondary electron yield of laser treated surfaces of copper, aluminum and stainless steel", in *Proc. IPAC'16*, Busan, Korea, Jun. 2016, paper TUOCB02, pp 1089-1092.

[24] G. Iadarola, G. Rumolo, P Dijkstal, and L. Mether "Analysis of the beam induced heat loads on the LHC arc beam screens during Run 2", CERN, Geneva, Switzerland, Rep. CERN-ACC-Note-2017-0066, Dec. 2017.

[25] G. Rumolo *et al.*, "Update on the HiLumi/LIU parameters and performance ramp up after LS2", presented at HiLumi Collaboration meeting, Madrid, Spain, Nov. 2017, unpublished.

[26] W. Herr *et al.*, "Observations of beam-beam effects in the LHC in 2011", in *Proc. Chamonix Workshop 2012 on LHC Performance*, Chamonix, France, Jan. 2012, CERN-2012-006, pp. 99-104.

[27] T. Pieloni *et al.*, "Colliding high brightness beams in the LHC", in *Proc. HB'12*, Beijing, China, Sep. 2012, paper MOP250, pp. 180-182.

[28] Y. Papaphilippou *et al.*, "Long Range Beam-Beam effects for HL-LHC", presented at LHC Performance Workshop (Chamonix 2018), Chamonix, France, Jan. 2018, unpublished.

61st ICFA ABDW on High-Intensity and High-Brightness Hadron Beams HB2018, Daejeon, Korea JACoW Publishing
ISBN: 978-3-95450-202-8 doi:10.18429/JACoW-HB2018-MOA1PL03

LINAC4 COMMISSIONING STATUS AND CHALLENGES TO NOMINAL OPERATION

G.Bellodi* for the Linac4 team, CERN, Geneva, Switzerland

Abstract

Linac4 will be connected to the Proton Synchrotron Booster (PSB) during the next long LHC shutdown in 2019 and it will operationally replace Linac2 as provider of protons to the CERN complex as of 2021. Commissioning to the final beam energy of 160 MeV was achieved by the end of 2016. Linac4 is presently undergoing a reliability and beam quality test run to meet the beam specifications and relative tolerances requested by the PSB. In this paper we will detail the main challenges left before achieving nominal operation and we will report on the commissioning steps still needed for final validation of machine readiness before start of operation.

INTRODUCTION

Linac4 is a 160 MeV H- linear accelerator that will replace Linac2 as injector of the CERN PS Booster (PSB) and provider of protons to the whole CERN complex as of 2021. The pre-injector part is composed of a RF volume source producing a 45 keV beam at 2 Hz maximum repetition rate, followed by a Low Energy Beam Transport section (LEBT), a Radio Frequency Quadrupole (RFQ) accelerating the beam to 3MeV, and finally a Medium Energy Beam Transport Line (MEBT), matching the beam to the linac. The MEBT is composed of 11 quadrupoles, 3 bunchers and a chopper, formed by two sets of deflecting plates, which are used to selectively remove micro-bunches in the 352 MHz sequence, in order to optimise injection into the 1 MHz CERN PSB RF bucket. The nominal scheme currently envisaged is to chop 133 bunches out of 352, with a consequent current reduction by 40%. After the MEBT, the linac consists of three distinct sections: a conventional Drift Tube Linac (DTL) accelerates the beam to 50 MeV. It is divided in 3 tanks and is equipped with 111 Permanent Magnet Quadrupoles (PMQs). This is followed by a Cell-Coupled Drift Tube Linac (CCDTL), made up of 21 tanks of 3 cells each, accelerating the beam to 100 MeV. The CCDTL was constructed by the Russian Scientific Research Institute for Technical Physics (VNIITF) and the Budker Institute of Nuclear Physics. Focusing is provided by Electro-Magnetic Quadrupoles (EMQs) placed outside each module, and PMQs between coupled tanks. Final acceleration to 160 MeV is done through a PI-Mode Structure (PIMS), composed of 12 tanks of 7 cells each, interspersed with 12 EMQs for beam focusing. The PIMS were constructed within a CERN-NCBJ-FZ Julich collaboration and assembled and tuned at CERN. Both CCDTL and PIMS represent the first such cavities to work in an operational machine. A 70 m long transfer line, including 17 EMQs, 5 dipoles (3 horizontal and 2 vertical) and a PIMS-like debuncher cavity connects Linac4 to the present injection line into the PSB, which will be only slightly modified for the remaining 110 m to the PSB entrance. A sketch of Linac4 is shown in Fig. 1.

COMMISSIONING

The commissioning of Linac4 was organised in six different phases over 3 years, alternating hardware installation and beam validation periods at increasing energy values. The commissioning was prepared and accompanied by extensive beam simulations, which turned out to be crucial to successfully optimise beam transmission and quality. A key decision was to start simulations with a particle distribution obtained by measuring the beam in the LEBT under different solenoid focusing and back-tracing the measurements to the start of the line.

In the first commissioning stage a dedicated 3 MeV test stand was used for a systematic beam measurement campaign that lasted 6 months. The following stages at higher energies (12 MeV, 50 MeV, 100 MeV and 160 MeV) lasted on average 3 weeks each. Two diagnostics test benches were used during commissioning. The low energy one (used at 3 and 12 MeV), allowed direct measurements of transverse emittance and energy spread via a slit-and-grid system and a spectrometer arm respectively. The high energy bench (used at 50 and 100 MeV) contained 3 profile harps and wire-scanners at 60 deg phase advance from each other for emittance reconstruction; a Bunch Shape Monitor (BSM) and lasing station for beam stripping and two Beam Position Monitors for Time-Of-Flight (TOF) and trajectory measurements.

Table 1: Energy and Beam Intensity Milestones

Energy [MeV]	Date (beam energy)	Record peak current	Date (record current)	2017 operational current
0.045	2013	50 mA	11/2015	40 mA
3	03/2013	30 mA	10/2015	26 mA
12	08/2014	24 mA	11/2016	20 mA
50	11/2015	24 mA	11/2016	20 mA
105	06/2016	24 mA	06/2016	20 mA
160	10/2016	24 mA	10/2016	20 mA

A very important result of the low energy commissioning was the agreement between direct measurements of the beam transverse emittance via the slit-and-grid method and indirect measurements based on emittance reconstruction from profiles, using either a “forward-method” technique or a tomographic reconstruction method [1].

* Giulia.Bellodi@cern.ch

61st ICFA ABDW on High-Intensity and High-Brightness Hadron Beams HB2018, Daejeon, Korea JACoW Publishing
ISBN: 978-3-95450-202-8 doi:10.18429/JACoW-HB2018-MOA1PL03

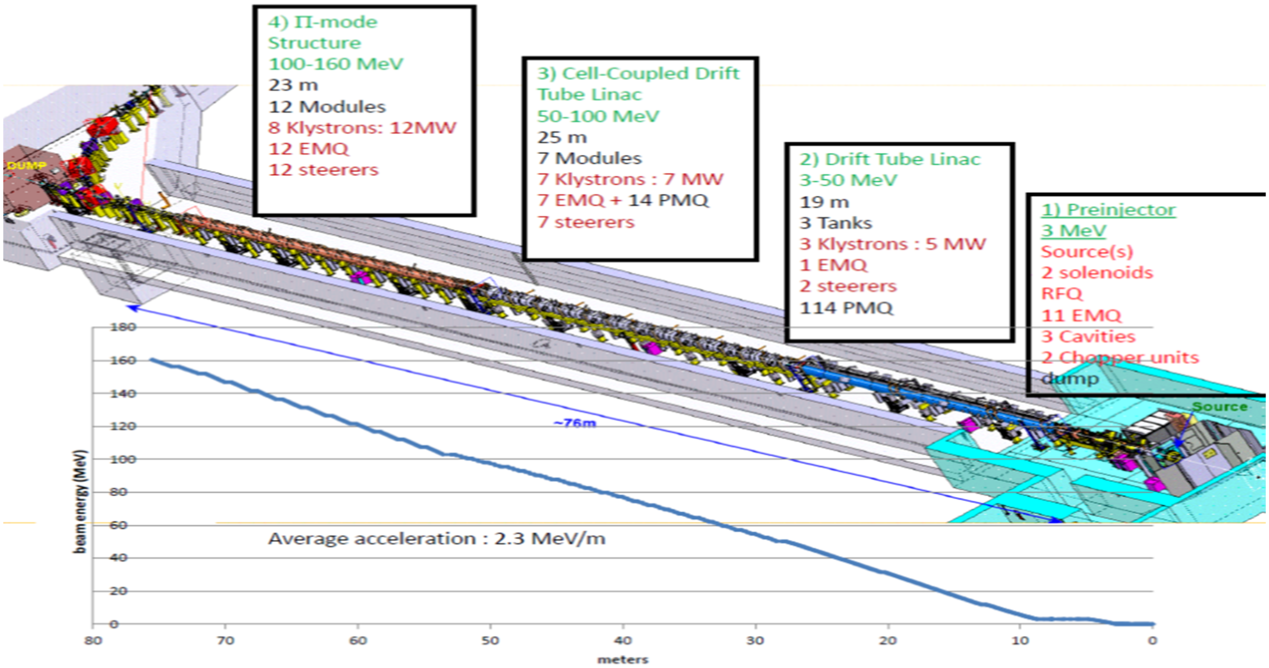

Figure 1: Sketch of Linac4.

We refer to past publications for a more complete description of commissioning measurements [2]; timelines and main milestones of the different commissioning stages are summarised in Table 1. Note that record peak currents were not always taken during the measurement campaign at the corresponding energy. Beam commissioning to the final energy of 160 MeV was successfully completed by the end of 2016.

HALF SECTOR TEST

After achieving this milestone, the 160 MeV beam was used for a few months at the end of 2016 to feed a test set-up of the PSB injection chicane, the Half Sector Test (HST). The purpose of this test was to gain information about the H^-→proton stripping system, to help reduce risks and facilitate the commissioning during the Long-Shutdown-2 (LS2, 2019-2020), when many modifications are foreseen in the framework of the LHC Injectors Upgrade (LIU) programme, and to ensure that the new equipment works according to specifications. The Linac4 connection requires a complete renewal of the PSB injection scheme, due to the energy increase from 50 to 160 MeV and the injection of H^- ions instead of protons as currently done from Linac2. Protons are presently injected via a multi-turn injection process using kickers and an injection septum. After connection, the H^- ions from Linac4 will be injected through a stripping foil located in the centre of the injection bump. Fast kicker magnets will be used for phase-space painting. The new injection scheme will benefit from reduced space charge effects and injection losses (from the current 50% to ~2% due to unstripped or partially stripped particles). The high complexity of integration in a limited space availability, however, justified the proposal for a test installation in the Linac4 transfer line, consisting of a half injection chicane of one PSB ring (see Fig. 2). The installation was composed of:

- a stripping foil system with a loader containing 6 foils and a screen with radiation-hard camera
- half of the injection chicane
- a monitor measuring partially and unstripped particles (H^0/H^-) and the H^0/H^- dump
- beam-loss monitors in vicinity of the dump
- beam current transformers upstream and downstream of the HST for stripping efficiency measurements
- a screen for beam profile and position measurements.

A separate stripping foil test stand was installed at the beginning of the Linac4 transfer line in order to:

- test foil changing mechanisms and interlock functions
- gain experience on foil handling
- test different foil materials and thicknesses
- gain information on foil lifetime.

The HST received first beam at the end of October 2016 and stopped operation in April 2017. Stripping efficiency was confirmed to be >99% for 200 μg/cm^2 thick carbon foils, fulfilling the design specifications.

A few foil breakages were observed, possibly due to interference with the Beam Televison (BTV) screen, used for beam observation (see a sample measurement in Fig. 3). All the main functionalities were checked and validated. Input was gained on possible design changes to improve measurement precision and stability and for noise reduction. The operational experience gained with equipment handling, controls and interlocks, was crucial for future commissioning phases.

ISBN: 978-3-95450-202-8 doi:10.18429/JACoW-HB2018-MOA1PL03

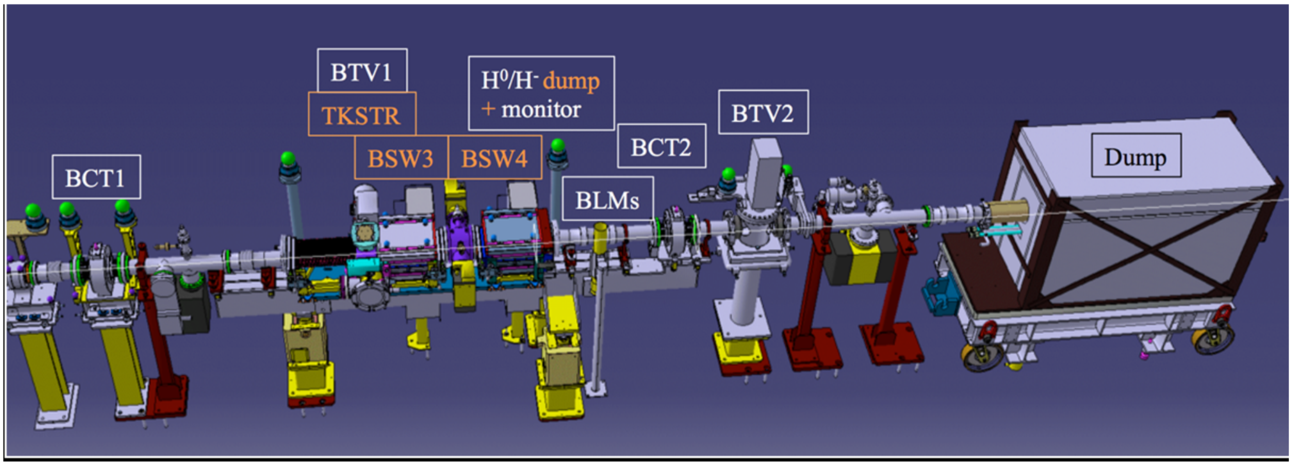

Figure 2: Sketch of the half-sector test installation.

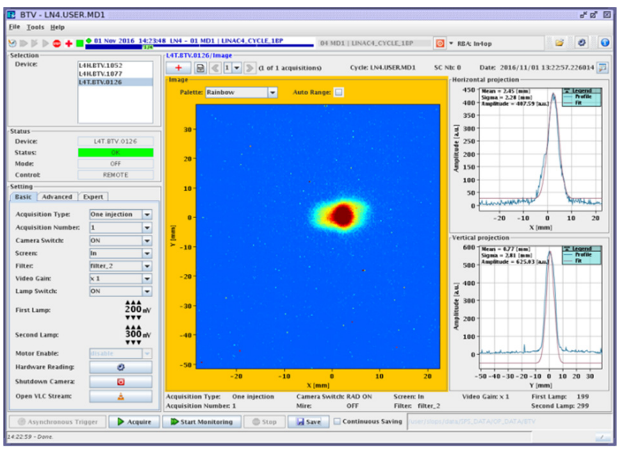

Figure 3: Transverse profile of the beam at 160 MeV measured on the Beam Television (BTV) screen.

RELIABILITY RUN

Once connected to the PSB, Linac4 will be the sole provider of protons to the whole CERN accelerator complex. This sets very high requirements in terms of machine availability, which will ultimately need to match the current performance of Linac2, running today, after 40 years, with an average availability of more than 98%. After successful completion of machine commissioning, a Reliability Run was therefore planned, intended also as a transitional period towards operation. The main aim of the run was essentially consolidation of routine operation and identification of potential recurring problems, thus providing a unique opportunity for early identification of weak points and for improving procedures. The Reliability Run took place from June to the end of December 2017, and it was divided in two phases to allow for scheduled Technical Stops for maintenance and technical interventions. The first phase lasted until the end of September, and it was composed of short periods of operation followed by repairs and optimization. The second phase took place from the end of October to the end of the year, with longer periods of operation followed by technical interventions, to approach more realistic operating conditions. In total, 19 weeks were dedicated to the Reliability Run. The Accelerator Fault Tracking system [3], initially developed for the LHC, was also adopted for Linac4 fault tracking, with some ad hoc adjustments, needed to account for the fact that Linac4 is not yet an operational machine (hence call-out support is not available on a round-the-clock basis). Machine availability and beam-on time was thus calculated manually from logbook entries during working hours only, subtracting scheduled interventions and machine studies.

The analysis of the weekly availability is shown in Fig. 4. The average machine availability over the 19 weeks of the run exceeded 90%. There were 2 specific weeks where long faults were recorded: 1) week 36, with a controls timing issue and a RF cavity cooling problem , and 2) week 47, with the failure of a power converter anode module needing replacement. Apart from these two occurrences, most of the down-time was due to short and recurrent faults, mainly affecting the RF systems, power converters, the pre-chopper and the source. A full fault distribution covering the entire run period is shown in Fig. 5. Some of the problems identified were addressed and fixed immediately during the ensuing End-of-the-Year-Technical-Stop, while others will be corrected during the Extended Technical Stop foreseen in summer 2018.

BEAM QUALITY RUN

The last Linac4 operational period took place between February and May 2018. Substantial RF interventions had taken place during the previous End-of-Year-Technical-Stop (LLRF upgrades, maintenance of high-power RF systems, upgrades of the RF restart procedures etc). The focus of this run was therefore placed on recommissioning all the changes implemented and on the validation of a series of beam quality requirements that had been agreed amongst different groups as necessary for future Linac4 operation with the PSB.

ISBN: 978-3-95450-202-8 doi:10.18429/JACoW-HB2018-MOA1PL03

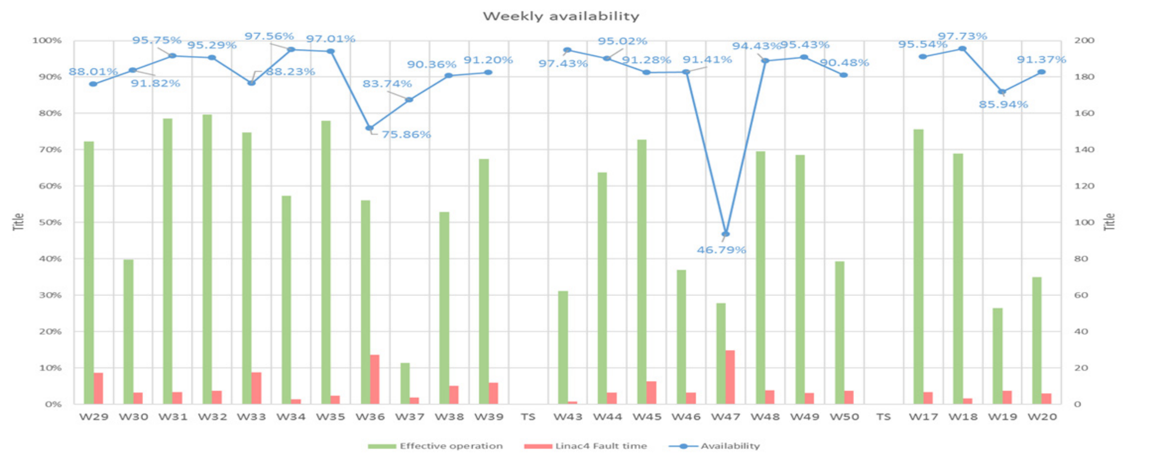

Availability	Fault Count	Operation	Suspended OP	Effective Operation	Fault Mean Time to Repair
91.5%	**449**	23 weeks	~ 8 weeks	~15 weeks	~29 min

Figure 4: Linac4 weekly availability during the 2017/2018 reliability run.

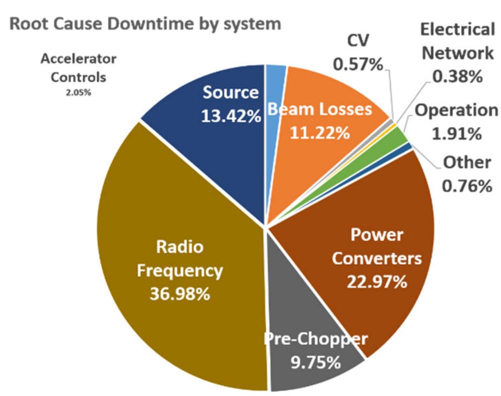

Figure 5: Linac4 fault distribution by system.

The following list of measurements can be earmarked as main achievements of the run:

i) Beam intensity flatness along the pulse and shot-to-shot stability were both confirmed to be within ±2% (excluding the initial current rise time due to space charge compensation build-up at low energy), which is comparable or slightly better than the current performance from Linac2.

ii) Similarly, the horizontal and vertical position variations along the pulse were measured to be contained within ±1 mm (requested margin at the entrance of PSB not to exceed a transverse emittance of 1.7 μm for LHC beams, see Table 3).

iii) The chopper performance was tested in depth, by operating with different (and sometimes extreme) chopping patterns on two parallel users in the machine supercycle. In the first case a LHC-type test beam was used, with a pulse length of 160 μs and a chopping factor of 60% at 352 MHz (equivalent to a ~625 ns long bunch train being accelerated and ~375 ns long bunch train being chopped off and deflected onto the 3 MeV dump). In the second case a substantially different chopping pattern was implemented (3.6 μs beam transmitted, 2.4 μs chopped off), with a longer pulse length. This validated the pulse-to-pulse use of the chopper and was a test exercise to mimic production of different beams in parallel for the LHC and fixed target physics experiments. The remnant current transmitted when the chopper is activated was measured to be ~0.15 mA, which is at the limit of resolution of the measuring devices and amounts to ~1% of the total transmitted beam intensity. Rise and fall times of the chopper signals were confirmed to be within a few ns, in agreement with the technical specifications of the pulse amplifier and PSB requests to minimize losses and reduce activation of the vertical injection septum.

Dedicated time was also set aside to progress with the commissioning of several beam diagnostics devices, particularly the laser emittance monitor [4] and the Bunch Shape Monitor (BSM) [5]. The laser emittance monitor uses a pulsed laser beam delivered to the tunnel by optical fibres to detach electrons from the H^- ions, which are then deflected into an electron multiplier. The resulting neutral H^0 atoms are separated from the main beam and recorded downstream by diamond-strip detectors. By scanning the laser through the H^- beam, transverse profiles can be obtained from the signals on the electron multiplier. The H^0 profiles on the diamond detector allow to determine the beam divergence, which in combination with the laser position, allows the H^- transverse emittance to be reconstructed (see Fig. 6).

ISBN: 978-3-95450-202-8 doi:10.18429/JACoW-HB2018-MOA1PL03

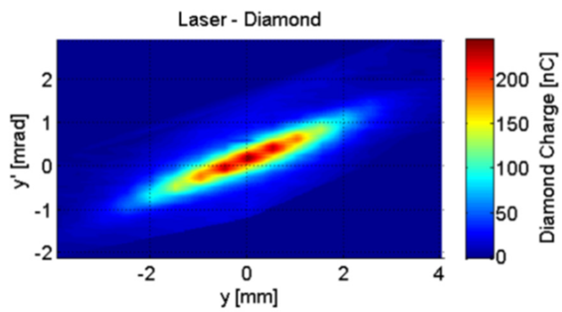

Figure 6: Beam phase space reconstruction at 160 MeV in the Linac4 transfer line using the laser emittance monitor.

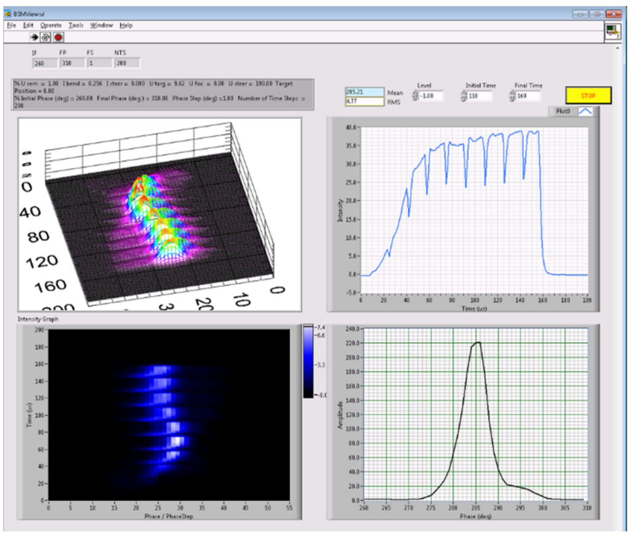

Figure 7: Screenshot from a BSM measurement at Linac4 showing clockwise:1) beam intensity along the pulse length (top right); 2) longitudinal beam phase profile (bottom right); evolution of the phase profile along the pulse length (mountain and cascade plots on the left).

The BSM was developed and fabricated at INR in Russia, to make longitudinal beam profile measurements with a phase resolution of 1° (over a full range of 180° at 352 MHz). Two such devices are installed at Linac4: the first one after the PIMS in the straight line to the dump, and the second one after the debunching cavity in the transfer line to the PSB. Hardware and beam commissioning were successfully completed in varied measurement conditions (changing chopping pattern, pulse length etc- see Fig. 7).

OUTLOOK AND FUTURE PLANNING

Table 2 shows a comparison of the nominal Linac4 beam parameters with the results achieved during the 2017 reliability run. The beam current amounts to 60% of the target value. This intensity limitation occurs in the low-energy pre-injector section and is due to the fact that the beam extracted from the currently installed cesiated RF volume source has an emittance exceeding the transverse aceptance of the RFQ. Target performance for Linac4 after connection to the PSB is to inject via charge-stripping up to $1x10^{13}$ protons per ring at 160 MeV. The current performance is still sufficient to guarantee the production of LHC-type and fixed-target-physics-type beams (see Table 3), by compensating the lower intensity with a higher number of injected turns [6].

Table 2: Linac4 Design Targets vs Today's Achievements

	Linac4 design targets	Linac4 achieved
Peak current in the linac	40 mA	24 mA
Routine current in the linac	40 mA	20 mA
Transverse emittance at 160 MeV	0.4 π mm mrad	0.3 π mm mrad
Energy at PSB injection	160 MeV	160 MeV
Pulse length / rep rate	400 µs/ 1 Hz	Up to 600 µs/ 1 Hz

Table 3: Beam Specifications at the PSB

Beam	Intensity (protons/ring)	Emittance at PSB – [mm mrad]	N° turns at 20 mA beam current
LHC-type	$3.4 x10^{12}$	1.7	45
Fixed target physics	$1\text{-}1.2 x10^{13}$	10	110-150

A R&D programme has however been launched in parallel on a separate dedicated ion source test stand to study alternative source extraction geometries and plasma generators in order to maximise the current in the RFQ acceptance. This will open the way to upgrades and will allow to exploit the full potential of the linac.

Linac4 has now entered a phase of Extended Technical Stop (ETS) for 3 months until September 2018 to allow the RF team to complete a series of scheduled upgrade and maintenance activities. This will be followed by a re-commissioning run until the end of the year with the aim of validating all changes implemented.

Linac4 will be connected to the PSB during the first semester of 2019, and further commissioning periods are being planned in the following to complete validating the whole installation and its beam performance before the start of official operation in 2021.

REFERENCES

[1] V.A.Dimov *et al*, "Emittance reconstruction techniques in presence of space charge applied during the Lina4 beam commissioning", in *Proc. HB'16*, Malmö, Sweden, Jul. 2016, paper WEPM1Y01, pp. 433-438.

[2] A.M. Lombardi, "The Linac4 project", in *Proc. HB'16*, Malmö, Sweden, Jul. 2016, paper MOAM2P20, pp. 1-5.

61st ICFA ABDW on High-Intensity and High-Brightness Hadron Beams HB2018, Daejeon, Korea JACoW Publishing
ISBN: 978-3-95450-202-8 doi:10.18429/JACoW-HB2018-MOA1PL03

[3] C. Roderick *et al.*, “Accelerator Fault Tracking at CERN”, in *Proc. ICALEPCS’17*, Barcelona, Spain, Oct. 2017, paper TUPHA013, pp. 397-400.

[4] T.Hofmann *et al.*, “Results from the laserwire emittance scanner and profile monitor at CERN’s Linac4”, in *Proc. 28th Linear Accelerator Conf. (LINAC’16)*, East Lansing, MI, USA, Sep. 2016, pp. 715-719.

[5] A. V. Feshenko, “Methods and instrumentation for bunch shape measurements”, in *Proc. 2001 Particle Accelerator Conf. (PAC’01)*, Chicago, IL, USA, Jun. 2001, pp. 517-521.

[6] V. Forte *et al*, “Multi-Particle Simulations of the Future CERN PSB Injection Process With Updated Linac4 Beam Performance”, presented at HB’18, Daejeon, Korea, Jun. 2018, paper WEP2PO007, this conference.

ISBN: 978-3-95450-202-8 doi:10.18429/JACoW-HB2018-WEA1PL01

WHAT IS MISSING FOR THE DESIGN AND OPERATION OF HIGH-POWER LINACS?

A. Shishlo†, Oak Ridge National Laboratory, Oak Ridge, TN 37831, USA

Abstract

The design process, tuning, and operation of high-power linacs are discussed. The inconsistencies between the basic beam physics principles used in the design and the operation practices are considered. The missing components of the beam physics tools for the design and operations are examined, especially for negative hydrogen ion linacs. The diagnostics and online models necessary for tuning and characterization of existing states of the linac are discussed.

INTRODUCTION

The design process of a new high power linac is always a combination of two simultaneous and interacting processes [1]. The first is an engineering design where the available technologies (normal temperature or superconducting) are chosen for each section of the linac; the feasibility, availability, and cost of cavities and magnets are analysed; the limitations of the real estate are considered; and so forth. This part of the design process is mostly related to hardware choice, and it should minimize the overall cost of the new linac construction. The second part is related to the beam physics. The new linac should deliver a beam with necessary properties, and, at the same time, beam loss should be low enough to allow "hands on" maintenance of the linac equipment. Also, this low beam loss requirement will define the necessary tolerance limits for hardware and electronics influencing the final cost of the project. These two parts of the whole design process interact, and usually several iterations between them are necessary to get a good design.

The linac operation cycle can be broken onto three parts: maintenance/upgrade, commissioning/tuning, and production. In this paper I will only consider the tuning component of this cycle, and its dependency on the design and simulation model.

In my opinion, there are several deficiencies in the design and operation processes

- During the physical and engineering design, not enough attention is given to the procedures and hardware for tuning/commissioning of the linac in the operation cycle. With the increasing number of components in future projects this could be a bottleneck for the availability of future linacs.
- The model-based beam loss simulations for tolerance limits in the engineering design should use more realistic models and tuning algorithms.
- The beam loss reduction during operation should be model-based not only for the initial stage of tuning. The final empirical beam loss tuning should also be replaced with a model-based one. For this, we need benchmarked models.

It is possible that some of these problems cannot be solved for a long time, but we have keep them in mind as our goals. In this paper the examples describing these deficiencies are discussed mainly for the Oak Ridge Spallation Neutron Source (SNS) linac [2].

SNS LINAC

The SNS linac structure is shown in Fig. 1. It has both a normal temperature and a superconducting cold linac. The normal conducting part includes front end, RFQ, medium energy beam transport part (MEBT), drift tube linac (DTL), and coupled cavities linac (CCL). It accelerates beam to 186 MeV. The superconducting linac (SCL) includes 81 cavities and accelerates beam to 1 GeV.

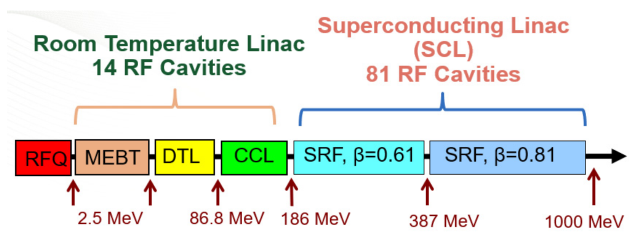

Figure 1: The SNS linac.

SNS LINAC TUNING/COMISSIONING

In this section the three examples related to the SNS linac tuning are discussed: two examples about RF set up procedures, and one about the orbit correction in CCL. The SNS linac diagnostics includes Beam Position Monitors (BPMs) which are also capable to measure the bunch phase proportional to the bunch arrival time. These BPMs are used for "time-of-flight" measurements.

SCL RF Tuning

The initial design of SCL suggested 100 us beam for superconducting cavities tuning [3]. The process was based on the RF cavity response to a beam loading with occasional "time-of-flight" measurements to avoid accumulating errors. The procedure should be repeated for all cavities one by one. At the beginning all cavities are detuned, and, as the process moves on, they will be brought to the resonant frequency. The whole tuning procedure was expected to give an uncertainty of ±20 MeV in the final beam energy which was a static error.

During the commissioning of the SNS SCL this approach was modified to avoid uncontrollable spraying of superconducting structures with 100 us beam. In addition to that, the process of bringing the detuned cavity to the

† email address: shishlo@ornl.gov

61st ICFA ABDW on High-Intensity and High-Brightness Hadron Beams HB2018, Daejeon, Korea JACoW Publishing
ISBN: 978-3-95450-202-8 doi:10.18429/JACoW-HB2018-WEA1PL01

resonant frequency takes 10-15 minutes including the bureaucratic overhead, and the total tuning time would be about two 8-hour shifts. Eventually the following modification to the SCL tuning procedure and linac hardware were implemented:

- All SCL cavities are on the resonance frequency all time. To avoid beam acceleration, initially all cavities are at 59 Hz repetition rate of RF pulses. The beam repetition rate for tuning is 1 Hz. The cavities are tuned one by one by switching to 60 Hz and performing "time-of-flight" energy measurements with all available BPMs.
- To avoid the beam loading of the cavities an attenuation system has been installed in MEBT to reduce the beam peak current by 80% or more.
- To reduce the beam loading even further, the Low Energy Beam Transport (LEBT) chopper at the RFQ entrance is used to provide only 1-5 us of beam.
- The SNS ring is used to calibrate the beam final energy with accuracy about 100 keV.
- The tuning process is automated. Now it takes about 45 minutes to tune all RF cavities in SCL.
- In the case of a cavity failure, the SCL can be retuned based on the model without any additional measurements. The cavities' phases will be changed to return the final beam energy to the initial value.

The fast tuning/retuning technique for new superconducting linacs becomes more important for high availability, because they have hundreds of cavities. The model-based retuning is especially significant for user facilities that need a fast reconfiguration for different experiments.

Warm Linac RF Setup

The SNS normal temperature linac includes 10 long RF structures: 6 DTL and 4 CCL cavities. To setup design values of amplitudes and phases for such type of cavities, the Delta-T procedure was developed at Los Alamos National Lab [4]. This procedure uses only a narrow phase range around the design value (~10°), because it is based on a linear model. A more general approach called "Phase scan signature matching" was developed at Fermilab [5]. At SNS both these algorithms were implemented in the high level tuning applications. The scheme describing these methods is shown in Fig. 2. To tune the cavity's amplitude and phase they use a phase scan of this cavity and data from two BPMs in the next cavity. The downstream cavity should be in the "off resonance" state.

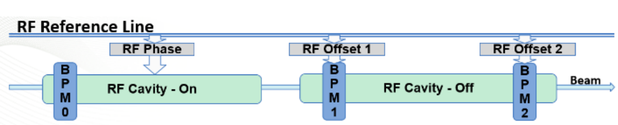

Figure 2: Warm linac RF tuning: DTL and CCL cavities.

During the SNS normal conducting linac commissioning and operations, it was found that tuning applications always needed an expert presence and "try and miss" iterations, because the working region around the design RF amplitude and phase is very narrow. The BPM 1 and 2 (see Fig. 2) should be calibrated for the "time-of-flight" bunch phase measurements. Later another tuning method was developed which uses only one BPM inside the tuning cavity (BPM0 in Fig. 2). We were lucky to have these inner BPMs at the right positions in the cavities with just a few accelerating RF gaps after the cavity entrance. This configuration allows to perform the cavity phase scan from -180° to +180° without BPM's signal interruptions for all cavity amplitudes. An example of a resultant BPM's phase as a function of the cavity's phase is shown in Fig. 3.

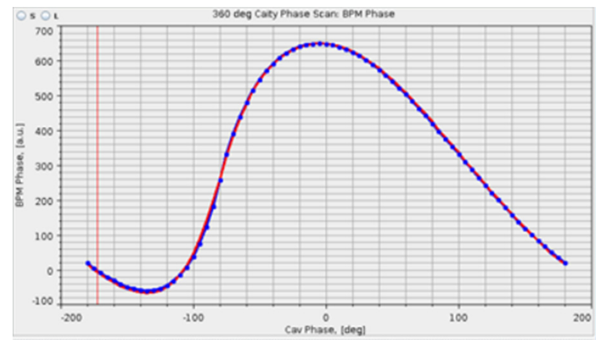

Figure 3: DTL3 phase scan. Blue points are BPM phases. Red line is the model calculation. The vertical red line is a cavity phase working point.

Comparing this data with the model calculation we know how far we are from the cavity design parameters. This method uses only one BPM, so there is no need for the timing calibration. It is also faster than initial methods, and it was easily automated allowing to tune RF in the whole warm linac in 22 minutes. Unfortunately, the initial design did not provide us with the inner BPM in the first DTL cavity, so for this case we still use the phase scan matching method. This example shows the importance to have the right diagnostics at the right places during the design stage.

CCL Orbit Correction

The SNS coupled cavity linac has 48 quadrupole magnets and only 10 BPMs to measure the beam transverse positions. The initial design included more BPMs, but during the cost optimization some BPMs were removed from the CCL lattice. During the commissioning it was found that a standard orbit correction application can easily make BPMs readings close to zero, but beam loss was still too high. To see the real orbit quadrupole gradient scans were performed, and they showed that the orbit between BPMs has ± 3 mm deviation from the quad centres. The quad gradient scans procedure cannot be a part of the routine orbit correction, because it is disruptive and too slow.

The situation was resolved by the development of a more comprehensive model for the beam center motion in the CCL. The new model includes possible transverse offsets of quadrupoles and BPMs from the beam pipe center. The unknown offset parameters were found after several quadrupole gradient scans, and then they were narrowed down by analysis of several hundreds of trajectories in CCL for different quadrupole and dipole corrector fields combinations. The values of the vertical offsets of the quadrupoles

ISBN: 978-3-95450-202-8 doi:10.18429/JACoW-HB2018-WEA1PL01

are shown in Fig. 4. The maximal offsets shown in Fig. 4 (±1 mm) are too big to be real, but they work very well for the new orbit correction algorithm. The new algorithm includes three steps. First, we use beam positions measured by BPMs to figure out the beam position and angles at the CCL entrance. Next we use the inverted transport matrices generated from the magnet fields and offsets to calculate the beam trajectory is in the whole CCL. In the third step, we apply the standard orbit correction algorithm for all significant points in the CCL lattice using the simulated trajectory. After correction, the orbit deviation from the center usually is less than 1 mm. This case demonstrates that deficiencies during the design will result in some additional studies and developments needed to provide a reliable and fast beam loss tuning.

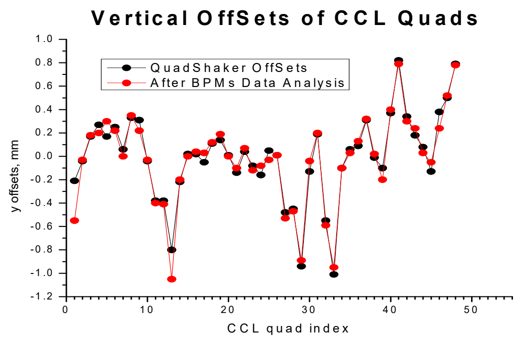

Figure 4: The vertical offsets of the CCL quads used in the model for the specialized orbit correction application.

OPTIMAL TOLERANCE DESIGN PROBLEM

Tolerance limits in the engineering design have a significant impact on the final price tag of the project. The usual procedure to check the acceptable tolerance on beam related parameters includes multiple “end-to-end” simulations with randomly distributed parameters errors. The main goal of the simulations is to estimate if beam losses are on the acceptable level. To get beam loss estimation, the linac model for simulations should be a Particle-In-Cell (PIC) code. In this section of the paper we discuss manly the RF system errors. The usual numbers for cavities tolerances are 1% in the amplitude and 1° for the phase.

The parameter errors are divided onto two different parts: static and dynamic. The distinction between them is very clear for the mechanical alignment errors in lattice components like magnets, RF cavities, apertures etc. If we apply the significant alignment errors to the model, beam loss will show up in the simulations due to the orbit distortion. Then these losses will be eliminated or significantly reduced by the orbit correction with the dipole correctors included in the engineering design. The dynamic errors usually are not compensated in hadron linacs. The source of the static errors is the positioning of the lattice elements during the construction, and for the dynamic errors that could be, for instance, mechanical vibrations. Tolerance limits will be different for static and dynamic errors in the case of the alignment errors. For the RF parameters tolerances, the situation is not so clear.

This section discusses the following topics related to the tolerance of RF parameters

- The SNS experience with the RF parameters vs. the design values.
- The recent development in the TraceWin code [6] related to the RF tolerances and the tuning procedure simulations.
- The deficiencies in the PIC codes related to beam loss calculations.

SNS RF Settings vs. Design. Static Errors.

Using SNS as an example we consider three types of situations. The first is a MEBT buncher phase setting procedure where we do not have the capability to distinguish between two possible setpoints. The second is the SCL cavities' field gradients where we do not have a choice, because they are defined by the maximal achievable value. And the third case is for synchronous phases of the SCL cavities that are set to get the local minimum of beam loss.

To setup non-accelerating phases of RF bunchers in the SNS MEBT (see Fig. 1) we use the RF phase scans for different RF amplitudes and the phase signals from downstream BPMs. If the RF phase is the non-accelerating one, the phases from the BPMs will be the same for all RF buncher amplitudes. The result of such scans for one of the BPMs is shown in Fig. 5. The MEBT attenuation system was used for these measurements, so there were no space charge effects. This figure clearly demonstrates the stationary RF phase point with accuracy around 1°. The problem is that different BPMs give different set-points in the range of ±4°. The possible reason for that is a non-symmetrical longitudinal shape of the bunch, and its transformation along the MEBT. At this moment, we have no means to verify which value is the correct one, and settings found for different BPMs can be used as a stating point for final beam loss tuning. So, this ±4° spread could be considered as a legitimate static error of the MEBT RF.

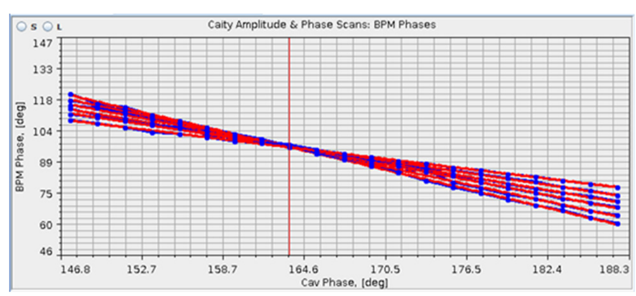

Figure 5: The MEBT buncher #2 phase scans for different amplitudes. Blue points are BPM phases, and red lines are linear fits for different RF amplitudes.

Another example of unexpected deviations from the design parameters is the field gradients of the SCL cavities. Figure 6 shows the measured SNS SCL cavity field gradients and the design values for the medium and high beta sections of the superconducting linac. As we can see, for most cavities in the medium beta region the gradients are above the design by 20-40%, and for the high beta they are lower than the design by approximately the same amount. To get the final linac energy near the design we had to keep gradients as high as possible. Figure 6 describes the SNS situation several years ago, but even at that time the linac delivered 1 MW beam with acceptable losses.

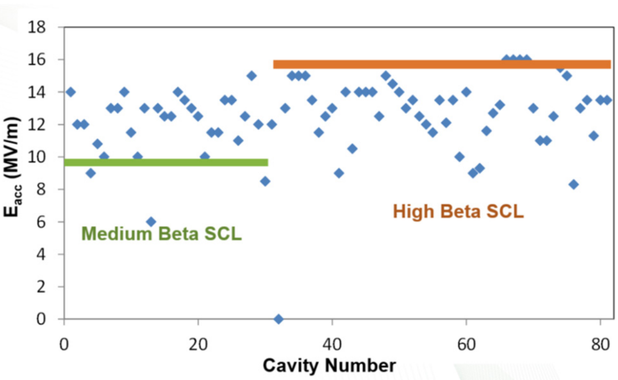

Figure 6: The real field gradients of the SNS SCL cavities. The lines are the design values.

The next example shows the synchronous phases of the SCL cavities during the SNS production run in 2014 (see Fig. 7). These synchronous phases provide a low beam loss tune in SCL despite their significant deviation from the design value of -18°. They were a result of the empirical beam loss tuning after initially setting all of them to the design values. At this moment, we do not understand the reason why the low loss tune needs this behaviour of the synchronous phases along SCL.

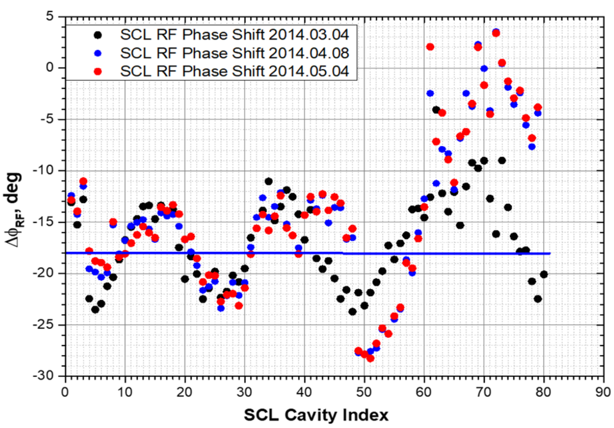

Figure 7: The measured synchronous phases of the SCL cavities for the low beam loss tune. The blue line is the design value.

All the discussed examples show that the realistic static tolerances for RF amplitudes and phases could be much higher than the 1%, 1° standard limits. For dynamics errors, the SNS experience gives 1.5% and 2° values for the SCL RF system which are close to the standard.

RF Static Errors Treatment in Simulations

The big deviations of the RF parameters from the design values in the operational high power linac with acceptable beam loss shows that our usual treatment of the static errors in the RF system must be reconsidered. As an example of this approach we have a recent modification of the TraceWin code related to this topic [6]. In [6] the longitudinal beam dynamics simulation method has been improved by including more "close-to-real" models for cavities tuning procedure. A specific command has been implemented in TraceWin code to simulate this tuning process. The new method was tested with the MYRRHA linac [7] model. The application of this new method to the simulations reduced the estimation of total beam loss by factor 60.

Despite some logical inconsistencies and unrealistic expectation of the BPM positions accuracy (±1 mm) in [6], this more realistic approach to the static errors treatment should be welcomed by the community and should encourage more studies in this direction.

Code Deficiencies in Beam Loss Simulations for H^- Linacs

We can look at the paper [6] results from another angle. If the change of the static error interpretation method in the model significantly reduced expected beam loss, can we trust these simulations with respect to the beam halo description? We are going to consider this issue in the next section. Here the simulation of the recently discovered Intra-Beam-Stripping (IBSt) mechanism of beam loss in H^- linacs [8, 9] is discussed.

The IBSt induced beam losses are important for all high-power H^- linacs, and they were not considered in any design of existing H^- linacs. At this moment, there is only one code that includes the model for such type of beam loss calculations – TRACK [10]. TRACK is a PIC code, so it is more computationally expensive to use than envelope codes. IBSt induced beam losses are defined by the bunch core, so it should be easily implemented into envelope codes. For now, these losses are usually calculated by using postprocessing scripts analysing the RMS beam sizes along the linac. Incorporating this mechanism into the modern envelope and PIC codes would benefit the community.

OPERATIONS : MODEL BASED BEAM LOSS TUNING

As we mentioned before, the operation cycle includes tuning the accelerator parameters to provide necessary beam properties and the acceptable level of beam loss. Usually the initial tuning is performed by using the online model right in the control room or with precalculated data. The final tuning of high power linacs is always an empirical beam loss reduction by slightly tweaking parameters known to be effective from previous experience. Unfortunately, at this moment we do not have reliable and benchmarked PIC codes capable of beam loss prediction on necessary level of 10^{-4} or less. Also, this type of simulation should include not only the code itself, but also a realistic initial distribution of the bunch particles. At SNS there are plans for studies related to these topics.

ISBN: 978-3-95450-202-8 doi:10.18429/JACoW-HB2018-WEA1PL01

Bunch 6D Initial Distribution Studies

To test a new RFQ for the SNS accelerator, a functional copy of the SNS Front End with the H^- Ion Source, LEBT, RFQ, and MEBT has been built at SNS. From the beginning this installation was dedicated for beam physics studies, and it is called the Beam Test Facility (BTF). The first accomplished study on BTF was the measurements of the 6D phase space distribution of the particles in the H^- bunches from the RFQ [11]. The data analysis is still in progress. The knowledge of the 6D distribution is a necessary step in the experimental benchmark of any PIC code. The next step is a study of halo development for different optics.

Plans for FODO Lattice at SNS BTF

In addition to the existing beam line of BTF, there is a plan to install a FODO lattice with the necessary diagnostics for beam halo formation studies [11]. The combination of known 6D distribution at the entrance of this FODO line, and halo measurements at the exit, will give us a useful instrument for a full benchmark of PIC models.

Backtracking Feature of Codes

The 6D phase space measurement is an ultimate solution for the initial distribution problem, but even right now many linacs have an emittance measuring station somewhere in the lattice. The data from these measurements could be used for the bunch generation in PIC codes assuming zero correlation between planes. Beam diagnostics also can include Bunch Shape Monitors (BSM), but usually they are at different locations. If BSMs are upstream of the transverse emittance stations (the case at SNS), and we want to combine the data, then we need the ability of the code to track the bunch backwards in the lattice. This feature of the code can serve many purposes, but not many codes have it. From the theoretical point of view there is no obstacle for the backward tracking, because all our equations of motion are time reversable.

CONCLUSION

Briefly summarizing the arguments about the missing components in design and operations of the high power linacs, I want to highlight the following

- In the design process, more attention should be paid to the tuning procedures of the linacs including hardware and algorithms.
- To estimate tolerance in engineering design the realistic models and algorithms for beam loss calculations are needed.
- The same realistic models are needed for beam loss tuning during the operations.

ACKNOWLEDGMENTS

This manuscript has been authored by UT-Battelle, LLC, under Contract No. DE-AC0500OR22725 with the U.S. Department of Energy. This research was supported by the DOE Office of Science, Basic Energy Science, and Scientific User Facilities. The United States Government retains and the publisher, by accepting the article for publication, acknowledges that the United States Government retains a non-exclusive, paid-up, irrevocable, world-wide license to publish or reproduce the published form of this manuscript, or allow others to do so, for the United States Government purposes. The Department of Energy will provide public access to these results of federally sponsored research in accordance with the DOE Public Access Plan (http://energy.gov/downloads/doe-public-access-plan).

APPENDIX

Author deeply appreciate very useful advices from A. Aleksandrov (ORNL), P. Ostroumov (FRIB), and B. Mustafa (ANL) during the preparation of this paper.

REFERENCES

[1] P. Ostroumov, F. Gerigk, “Superconducting Hadron Linacs,” *Rev. Accel. Sci. Tech.*, vol. 6, pp. 171-196, 2013.

[2] S. Henderson *et al*., “The Spallation Neutron Source accelerator system design”, *Nucl Instrum Meth A*, vol. 763, pp. 610-673, 2014.

[3] J. Stovall *et.al.*, “Superconducting linac for the SNS”, in *Proc. LINAC’00*, Monterey, CA, USA, Aug. 2000, p. 605.

[4] K.R.Crandall, "The Delta-T Tuneup Procedure for the LAMPF 805-MHz Linac", LANL Report LA-6374-MS, June 1976.

[5] T.L. Owens, M.B. Popovic, E.S. McCrory, C.W. Schmidt, and L.J. Allen, “Phase Scan Signature Matching for Linac Tuning”, *Particle Accelerators*, vol. 48, pp. 169-179, 1994.

[6] D. Uriot, “Improvement of the RF field phase & amplitude errors simulation in TraceWin code,” in *Proc. IPAC’18*, Vancouver, Canada, April 2018, paper THPAF017.

[7] D. Vandeplassche *et al*., “The MYRRHA Linear Accelerator”, in *Proc. IPAC’11*, San Sebastian, Spain, Sep. 2011, pp. 2718-2720.

[8] V. Lebedev *et al*., “Intrabeam Stripping in H-Linacs”, in *Proc.* LINAC’10, Tsukuba, Japan, September, 2012, pp. 929-931.

[9] A. Shishlo *et al*., *Phys.* Rev. *Lett*., vol 108, p. 114801, 2012.

[10] V. Aseev *et al*., “TRACK *:* The new beam dynamics code”, in *Proc. PAC’05*, Knoxville, Tennessee, USA, 2005, pp. 2053-2055.

[11] A. Aleksandrov *et al*., “6D Beam Measurement, Challenges and Possibilities”, in *Proc. IPAC’18*, Vancouver, Canada, April 2018, paper THXGBE1.

4 Workshop and Conference Reports

4.1 The 7th International Beam Instrumentation Conference (IBIC 2018)

Yongbin Leng, SSRF/SINAP
Mail to: leng@sianp.ac.cn

The 7th International Beam Instrumentation Conference (IBIC 2018, https://indico.sinap.ac.cn/event/3/) was held in Shanghai (China) between September 9th and 13th 2018. The International Beam Instrumentation Conference has a long and healthy history, dating back to 2012. The conference takes place every year with the most recent events being held in Grand Rapids, MI, USA (2017) and Barcelona, Spain (2016). The 2018 edition will be hosted by Shanghai Institute of Applied Physics. Like its predecessors, this conference is also dedicated to exploring the physics and engineering challenges of beam diagnostics and measurement techniques for charged particle beams.

The conference was hosted by Shanghai institute of applied physics (SINAP), which is the photon science center of China, operating two large scale facilities: SSRF and SXFEL. Dr. Zhentang Zhao, the director of SINAP, was invited to be the conference chair. The scientific program of the conference was set up by the International Organizing Committee, chaired by Yongbin Leng (Shanghai Institute of Applied Phyics and Shanghai Synchrotron Radiation Facility). The following nine topics were covered during this conference: Overview and machine commissioning, Beam charge and current monitors, Beam loss monitors and machine protection, Beam position monitors, Longitudinal diagnostic and synchronization, Transverse profiles and emittance monitors, Data acquisition systems, Feedback and beam stability, and Machine parameters measurements and others.

The 3.5 day programme of the 2018 IBIC conference included 15 invited and 23 contributed talks, and 1 public lecture. Furthermore, 149 posters were presented in the 3 poster sessions, and a 3 day long vendor exhibition with 19 exhibitors could be visited during the conference. In total, 234 participants coming from 18 countries gather around during the 3.5 days of the conference. The detail program and talks are available via the conference website. The conference proceedings will be published at JACoW.

4.2 The 23rd International Workshop on Ion Sources (ECRIS 2018)

Luigi Celona
INFN-LNS, Via S. Sofia 64, 95123 Catania, ITALY
Mail to: celona@lns.infn.it

The Electron Cyclotron Resonance ion sources (ECRIS) have a wide number of applications both in the accelerator facilities, increasing the beam energy and intensity, and in the industrial applications, making more efficient the industrial processes.

The workshop, organized by the Istituto Nazionale di Fisica Nucleare-Laboratori Nazionali del Sud (INFN-LNS), was aimed to highlight the state of the art in ECR Ion Sources Science&Technology, and to reinforce the common ground and synergies among the different actors in the field.

The workshop was held in the halls of the Catania Diocesan Museum, located in the heart of the old city with several archaeological and cultural attractions situated nearby. The venue is placed at the foot of the Etna - the highest and most active Volcano of Europe - in a city that is now experiencing its third millenium of history since its establishment in 730 BC.

The International Advisory Committee (13 members from 10 countries) set up a scientific program of 45 talks and 22 posters covering themes relevant to the production of beams.

Along with "traditional" applications of ECRIS such as Radioactive Ion Beams and charge breeders, Production of highly charged ion beams, Controls and diagnostics, Production of high intensity ion beams, Codes and simulations, Beam extraction and transport, several new developments in the field were presented at the workshop. Among those are the efforts in the commissioning of the first 4th generation ECRIS working at 45 GHz at IMP and the progress of the 3rd generation sources at LBNL, IMP, RIKEN and MSU. The results of the commissioning of new sources named HIISI (JYFL), AISHa (INFN-LNS) and PS-ESS (INFN-LNS) have been presented. The status and upgades of the ECR based ion sources in use on the major facilities worldwide (RIKEN, GANIL, CERN, Texas A&M, KVI, CERN, MedAustron, QST NIRS, KBSI, IMP, JYFL, LBNL, MSU, JINR, IAP-RAS) have been also reported. New ideas have been presented from different groups, in particular ATOMKI, JYFL and INFN-LNS teams presented innovative plasma diagnostic methods based on high resolution spectrometers and spectropolarimeters.

Three round tables have been also inserted in the program on subjects covering a key role in the future evolution of ECR ion sources: "Future magnetic system for ECRIS", "Future of ECRIS: beyond the scaling laws?", "Extraction and transport of intense beams" chaired respectively by D. Leitner (LBNL, USA), H. Koivisto (University of Jyvaskyla, Finland) and P. Spaedtke (GSI, Germany). A total of 97 participants from 15 countries have been recorded.

For the sixth successive time Pantechnik awarded the Geller prize. The prize has been established 10 years ago for the 18th ECRIS workshop in Chicago (2008), and it rewards an exceptional contribution of young talented researchers (under 41) to the development of ECR sources. This time the committee chaired by Mi Sook Won (KBSI, South Korea) and consisting of Santo Gammino (INFN-LNS, Italy), Takahide Nakagawa (RIKEN, Japan), Daniel Xie (LBNL, USA) and Hog-Wei Zhao (IMP, China) selected Vadim Skalyga (IAP-RAS, Russia) for his outstanding contribution to the field of ECRIS working in gasdynamic regime.

The detailed program is available at the workshop website (http://ecris18.lns.infn.it) and the proceedings will be published at JACoW. Moreover, some selected papers will be published soon in a special issue of Journal of Instrumentation.

Figure 1: ECRIS 2018 Workshop poster.

Figure 2: ECRIS 2018 Workshop photo.

4.3 29th Linear Accelerator Conference-LINAC18

Pei Gouxi
Mail to: peigx@ihep.ac.cn
IHEP, 19 Yuquanlu, Shijingshan, Beijing

29th Linear Accelerator Conference, LINAC 18, took place at the Friendship Hotel and Conference Venue in Beijing, China on 16-21 September 2018.

This conference was the main bi-yearly gathering for the world-wide community of linac specialists. It provided a unique opportunity to hear about the latest advances of projects and developments concerning hadron and lepton linacs, and their applications.

In the tradition of previous LINAC conferences, plenary sessions including invited speakers were scheduled every day. Poster sessions were held on Monday, Tuesday and Thursday afternoons. There were also two special events on Sunday, 16 September 2018 , namely a student poster session and an evening reception for registrants and their companions at the Friendship Hotel and Conference Venue. Participants were also warmly invited to join an outing to Summer Palace or Great Wall and the beautiful surroundings on Wednesday afternoon, and to visit IHEP major facilities (BEPCII, LINAC, etc.) or Compact Laser Plasma Accelerator (CLAPA) Lab at Peking University as well as Accelerator in Tsinghua University on Friday afternoon, after the formal end of the conference. On Thursday 20 September 2018, conference banquet was arranged at the Great Mansion Restaurant, Beijing.

Participants of LINAC 18 were included representatives of institutions and companies involved in the design, construction or use of linear accelerators. Companies interested in promoting their products were encouraged to hold a booth in the industrial exhibit and to apply for sponsorship.

The active participation of students who qualified the criteria was encouraged, with incentives and funding. Best three poster awards were distributed to encourage the students' research and presentation.

The detail program and talks are available via the conference website https://indico.ihep.ac.cn/event/7319/overview. The pre-proceedings are available at http://linac2018.vrws.de/. However, conference proceedings will be published at JACoW.

4.4 eeFACT2018

F. Zimmermann
CERN, BE Department, 1211 Geneva 23, Switzerland
Mail to: frank.zimmermann@cern.ch

From 24 to 27 September 2018 the Jockey Club Institute for Advanced Study of the Hong Kong University of Science and Technology (HKUST) organized the 62nd ICFA

Advanced Beam Dynamics Workshop on High Luminosity Circular e^+e^- Colliders (eeFACT2018). Like its predecessors eeFACT2016 at Daresbury in the UK, HF2014 in Beijing, and HF2012 at FNAL, eeFACT2018 was held under the auspices of ICFA, which is encouraging the global coordination of, and joint research on, factory-like circular colliders. eeFACT 2018 was co-sponsored by IHEP, KEK, and the EU's Horizon2020 ARIES project. The workshop was jointly chaired by Andrew Cohen (IAS, HKUST, the Local Committee Chair,), Yoshihiro Funakoshi (KEK), Qing Qin (IHEP), and Frank Zimmermann (CERN).

The eeFACT2018 workshop addressed numerous aspects of present and future e^+e^- factories: physics landscape and motivations, design concepts, optics issues, interaction region and machine detector interface, beam-beam issues, injectors and beam injection, impedance issues and beam instabilities, emittance control, polarization, beam instrumentation and beam diagnostics, superconducting RF, other technologies, and energy efficiency.

Among its 74 participants (see photo), 28 originated from mainland China, 16 from Japan, 8 from Russia, 7 from the US, 6 from Italy, 3 from CERN, 2 from Australia, and 1 each from Turkey, France and Hong Kong.

Participants of the ICFA workshop on High Luminosity Circular e+e- Colliders "eeFACT2018" are all smiles at Hong Kong UST's Institute for Advanced Study.

At eeFACT2018, Yifang Wang, the director of IHEP Beijing, gave an inspiring presentation on "The Future of High Energy Physics and China's Role". During the subsequent parallel sessions, different site options for a 100 km CEPC collider ring were reviewed. Qinhuangdao has proven the most-highly qualified site, but all the sites investigated in China would be acceptable. A detailed overview of CEPC civil engineering and technical infrastructures covered many aspects of the projects. Several test drills were already completed. The total construction period of the CEPC tunnel is expected to last 54 months, which includes preparatory work of 8 months, main work of 43 months, and completion work of 3 months. Experts from IHEP Beijing presented ongoing work related to the cooling and cryogenics infrastructure, and to other key technologies, including an ambitious development program for high-efficiency klystrons.

Other great news came from SuperKEKB, whose commissioning progress has been on schedule. The results from commissioning phase 2 do not indicate any showstoppers. In particular, there is no indication for an electron-cloud related blow up at the design bunch spacing, at least up to 60% of the design positron-bunch intensity. A peak luminosity of ~5.6×10^{33} cm^{-2}s^{-1} was reached. The specific luminosity more than doubled during the last month of commissioning, indicating further room for improvement.

The FCC-ee study is far advanced and well on track for completing the Conceptual Design Report by December 2018. Detailed optics correction and tuning simulations indicate that the target values for the vertical emittance can be reached with traditional magnet alignment tolerances of order 100 micron rms. The FCC CDR will be an important input to the upcoming update of the European Strategy for Particle Physics in 2019/20.

eeFACT2018 also featured latest updates from other lepton-collider projects and studies around the world, including DAFNE, ILC, CLIC, VEPP-2000 and muon colliders.

More details and all the presentations give can be found on the eeFACT2018 workshop web site http://eefact2018.ust.hk/ .

4.5 Workshop on Accelerator Operations: WAO2018

Gregory Marr
Mail to: gmarr@bnl.gov
Brookhaven National Laboratory
Collider-Accelerator Department
Upton, NY USA 11973

Introduction

This past autumn, Operations staff and managers from around the globe gathered in the Charles B. Wang Center at Stony Brook University, to participate in the 11th Workshop on Accelerator Operations – WAO2018. The Workshop, on New York's Long Island, was attended by nearly 120 participants coming from institutions in Europe, Asia, Australia, and North America over the week of September 30 to October 5, 2018.

WAO2018 was hosted by the Relativistic Heavy Ion Collider (RHIC) and National Synchrotron Light Source II (NSLS-II) facilities at Brookhaven National Laboratory (BNL). The Local Organizing Committee (LOC), co-chaired by P. Ingrassia and G. Marr, prepared the week's arrangements at the venue.

Proceedings

The agenda and presentation material followed the program plans prepared by the WAO International Program Committee (IPC), also chaired by G. Marr. Topics covered a range of subjects such as: basic operating organization and practices; operator training; the contributions of accelerator operators, within and outside the control room; operator interaction with physicists; issues with aging, new, or compact accelerator facilities; new technologies. The attending IPC members each took part chairing sessions and moderating discussions.

Attendees contributed 43 oral presentations and 25 posters to the Workshop. There were also plenary and parallel discussion periods where a range of topics were discussed at length, including: maintenance tracking, operator training programs, and operator/physicist interactions. The invited speaker, Dr. Ferdinand Willeke (BNL), offered his perspective on design considerations for reliable, highly available accelerators. Additionally, 3 live software demonstrations were presented during the poster session, which was a new addition to the WAO.

The workshop format is a popular arrangement for the attendees, with allotted time for discussion and interaction after every presentation. This, in combination with breaks and group lunches, afforded ample opportunities for discussion and collaboration amongst participants, in both formal and informal atmospheres.

Figure 1: WAO 2018 participants.

Outlook

All Workshop material remains on the website for future reference:

https://www.bnl.gov/wao18/

Additionally, the website contains links to previous Workshop materials, and a photo gallery of this year's event.

Looking ahead, the IPC has accepted the proposal to hold the next WAO in 2020 in Barcelona, Spain. WAO2020 will be hosted by the ALBA Synchrotron, managed by the

Consortium for the Construction, Equipping and Exploitation of the Synchrotron Light Source (CELLS).

4.6 The 26th Russian Particle Accelerator Conference, RuPAC–2018

Sergey Ivanov, NRC "Kurchatov Institute" – IHEP
Mail to: Sergey.Ivanov@ihep.ru

The 26th Russian Particle Accelerator Conference (RuPAC–2018) was held in Protvino, Moscow Region, Russia on October 1–5, 2018. It was co-organized by the Scientific Council of Russian Academy of Sciences for Charged Particle Accelerators, Joint Institute for Nuclear Research (JINR, Dubna), Budker Institute of Nuclear Physics SB RAS (BINP, Novosibirsk), and Institute for High Energy Physics of the National Research Center "Kurchatov Institute" (NRC KI – IHEP, Protvino).

Goal of the event was to facilitate information interchange and discussion of various aspects of accelerator science and technology, beam physics, new accelerator development, upgrade of existing facilities, and use of accelerators for basic and applied research.

The scientific program covered the conventional topics with a bias to domestic activity:

1. Modern trends in accelerators
2. Colliders
3. Particle dynamics in accelerators and storage rings, cooling methods, new methods of acceleration
4. High intensity cyclic and linear accelerators
5. Heavy ions accelerators
6. Synchrotron radiation sources and free electron lasers
7. Magnetic and vacuum systems, power supplies
8. Superconducting accelerators and cryogenics
9. RF power structures and systems
10. Control and diagnostic systems
11. Ion sources and electron guns
12. Medical and industrial applications
13. Radiation problems in accelerators
14. Special presentations (without classification)

RuPAC–2018 was attended by about 170 participants from 46 organizations, both home (32) and foreign (14) labs. 24 invited talks, 30 contributed oral reports and 135 posters (189 in total) were presented at the Conference.

The year of this Conference, 2018, is notable for the Russian accelerator community as it marks a few round-figure anniversary dates — 75 years to Kurchatov Institute (Moscow), 60 years to BINP (Novosibirsk) and 100 years to its founder and first director academician Gersh Budker, 55 years to IHEP (Protvino), and 50 years since convening the first national particle accelerator conference, the forerunner of the RuPAC series itself.

The Organizing Committee decided to maintain the Conference tradition of the best youth's scientific works award contest (for authors aged below 35, inclusive). The laureates were nominated by the Selection Committee summoned at the Conference and chaired by academician Vasiliy Parkhomchuk (BINP of SB RAS, Novosibirsk, Russia).

This year, the Selection Committee decided to award 5 full diplomas plus an encouraging diploma for a yet undergraduate student. The contest winners are listed alphabetically in Table 1.

Table 1: Winners of the RuPAC-–018 contest for young scientists and engineers.

Name	*Affiliation*	*Report*
Gorelyshev, Ivan	JINR, Dubna	Test Bench Measurements for the NICA Stochastic Cooling Pickup and Kicker
Maltseva, Yulia	BINP SB RAS, Novosibirsk	VEPP-5 Injection Complex Performance Improvement for Two-Collider Operation
Melnikov, Sergey (an encouraging diploma)	JINR, Dubna	Stability of Charged Particle Movement in a Storage Ring With Focusing by a Longitudinal Magnetic
Opekunov, Alexander	RFNC–VNIIEF, Sarov	Experimental Studies of Electron Beam Characteristics of High Power CW Resonance Accelerator
Paramonov, Yuri	TORIY, Moscow	C-Band High Power Amplifier Klystron Developed for Linear Electron Accelerators
Smygacheva, Antonina	NRC KI, Moscow	The Bunch Size Measurements in the Storage Ring "Siberia-2"

Processing of the electronic files of about 200 contributions, during and after the Conference, was accomplished by Maxim Kuzin and his team from BINP SB RAS. The final version of the Proceedings is published at the JACoW web-site (www.jacow.org), direct link to the conference proceedings being

http://accelconf.web.cern.ch/AccelConf/rupac2018/

The success of the RuPAC-2018 caп be attributed to the collaborative efforts of the Program and Organizing Committees, the local staff of the host institution – NRC KI – IHEP (Protvino), and, of course, to all of the participants themselves.

Participants of the Conference from Russian accelerator centers and Universities and from several accelerator centers from Germany, Italy, Sweden, Romania, Canada, and China enjoyed fruitful discussions at oral and poster presentations regardless of nasty and rainy weather that was followed by the third wave of sunny "Indian Summer" in the Moscow Region.

The conference of the RUPAC series is a traditional (since 1968) biennial meeting, the next one to be held in the autumn of 2020.

Figure 1: RuPAC–2018 Conference poster.

Figure 2: Participants of the RuPAC–2018 Conference.

4.7 12th International Workshop on Emerging Technologies and Scientific Facilities Controls (PCaPAC)

Reinhard Bacher
DESY, Hamburg, Germany
Mail to: reinhard.bacher@desy.de

Introduction

Recently, the PCaPAC International Program Committee has revised the mission of PCaPAC, keeping both the traditional aspects of PCaPAC as well as focusing on emerging technologies. This is reflected in PCaPAC's new official name "International Workshop on Emerging Technologies and Scientific Facilities Controls". However, the well-known acronym "PCaPAC" will be kept. Following the mission statement PCaPAC will place emphasis on discussing important issues of modern or emerging technologies for the control of scientific facilities or other large or distributed systems, as well as on presenting and discussing specific topics and projects of the hosting institute or country. Finally, PCaPAC will encourage institutes or countries outside of the traditional conference mainstream to host the workshop, and junior colleagues in the early stages of their career in the field of control systems development.

PCaPAC 2018

The 12th PCaPAC workshop was held at NSRRC in Hsinchu, Taiwan from October 16th to 19th, 2018 and and was attended by 102 participants representing institutions from Europe, Middle East, USA and predominately Asia.

The first day was devoted to 4 tutorial sessions focusing mainly on data science and machine learning. This emerging topic was further addressed and highlighted during the remaining workshop days by 3 keynote talks.

In total, 25 talks grouped in 6 plenary sessions and 60 poster presentations in 2 poster sessions were presented covering the topics "Control Systems", "User Interfaces and Tools" with particular emphasis on "GUI Technologies and Framework", "Hardware Technologies and Component Integration, System Modelling and Automation", "Data Acquisition and Data Storage, Data Analysis", and "Infrastructure and Networking, Management of IT Projects, Cyber Security".

In order to stimulate the exchange of ideas and experiences, 2 moderated and lively discussion sessions were held covering such things as GUI technology trends and the relevance of the IIoT (Industrial Internet of Things) approach for accelerator controls.

Finally, the workshop was completed by a guided visit of the NSRRC facilities and the awarding of the Isamu Abe prize to two young participants from NSRRC (Taiwan) and ELI (Czech Republic) for their outstanding presentations.

4.8 The 14th International Conference on Heavy Ion Accelerator Technology

Hongwei Zhao, Institute of Modern Physics, CAS
Mail to: zhaohw@impcas.ac.cn

Heavy ion accelerator technology plays a key role in basic researches and applications with heavy ions. Therefore, a platform to make global collaboration and present the state of the art heavy ion accelerator technologies as well as the update of the status of the existing facilities is very necessary for the heavy ion accelerator community and users' community. The HIAT conference provides a platform for scientists, engineers, students and industrial partners to present and discuss the latest developments in the heavy ion accelerator technologies. The last conference in the series was HIAT2018 (http://hiat2018.csp.escience.cn), hosted on the campus of IMP in Lanzhou, China from Oct. 22 to 26, 2018 and was attended by totally 123 participants representing institutions from Asia, Europe and North America. HIAT2018 was the fourteenth conference in the series started from 1973 in Daresbury, which was named as International Conference on Electrostatic Accelerators at that time.

The scientific program of the conference was set up by International Advisory Committee, chaired by Dr. Yuan He (IMP, CAS). The workshop was hosted by Institute of Modern Physics (IMP), CAS. Its Local Organizing Committee was chaired by L. Sun and included L. Li (conference secretary), Liang Lu, Teng Tan, Qiangjun Wu, Wentao Guo, Yao Yang, Weihua Guo, Xinchen Hou, Qinwen Chen, and Yulu Huang.

The scientific program includes mainly the oral contributions and posters. 41 invited and contributed talks have been presented at the conference. Traditional topics such as Heavy Ion Applications, Electrostatic Accelerators, Radioactive Ion Beam Facilities, Room Temperature and SC Cyclotrons, Room Temperature and SC Linacs, Accelerator System and Components, Ion Sources, Traps and Charge Breeding, Synchrotrons and Storage Rings, are presented and discussed during the 5 days' conference time. Following a review of larger accelerators (at IMP, CIAE, JINR, FAIR, MSU, RIKEN), detailed reports covered mid-to-small size facilities such as ATLAS (ANL), where simultaneous acceleration of stable and exotic beam is envisaged, SPIRAL (GANIL), SPES (INFN) and BRIF (CIAE). Regarding applications, the new DC130 cyclotron in Dubna will give beam time to space electronics tests, the Chinese ADS, aiming to be operational around 2024, completed the front end demo, CIAE finalized their compact 200 keV machine for AMS and NIRS their superconducting gantry for ion beam cancer therapy. In the closing session, on behalf of the IAC, Dr. Giovanni Bisoffi (INFN-LNL/Italy) gave a conclusion remarks of this conference.

As an important part of the scientific program, the lab tour gives the conference participants a guided tour of most of the existing facilities at IMP, which includes the HIRFL facility consisting of the injector superconducting ECR ion source SECRAL-II, 2 cascade cyclotrons, CSRm synchrotron ring and the CSRe spectrometer ring, CiADS demo linac facility that has accelerated CW proton beam up to 26.5 MeV, and the recently operational LEAF (Low Energy intense heavy ion Accelerator Facility) facility.

The conference presentations and proceedings will be published at JACoW. After light review process, qualified papers will be eventually published at Journal of Physics: Conference Series (IOP), which is also an open access journal to share research achievements and findings.

Figure 1: HIAT2018 Conference poster.

Figure 2: HIAT2018 Conference Photo (IMP, Lanzhou, Oct. 22, 2018).

4.9 APEC2018

G. Franchetti[1] and F. Zimmermann[2]

[1] GSI, Darmstadt, Germany
[2] CERN, BE Department, 1211 Geneva 23, Switzerland
Mail to: g.franchetti@gsi.de or frank.zimmermann@cern.ch

The Accelerator Performance and Concept workshop (APEC2018) was held in Frankfurt am Main from 10 to 12 December 2018. It attracted 60 participants, 23 of whom hailed from Germany, 8 each from Switzerland and from the US, 7 from China, 3 each from Italy and France, 2 each from the UK, Austria and Sweden, respectively, 1 one Belgium and 1 from Finland. Participants included 8 students and 9 women. GSI and the EC-cofunded ARIES project were the joint co-organizers of this event.

Snapshot of APEC2018 organizers and participants.

APEC2018 reviewed the state of the art in (1) beam quality control in hadron storage rings and synchrotrons, along with performance limitations; (2) reliability and availability of particle accelerators; and (3) improved beam stabilization.

After a warm welcome by the GSI division head Mei Bai, Axel Brachmann from SLAC discussed the performance and reliability issues in large-scale facilities, taking the LCLS-II as an example. The following talks addressed the operation and performance limits of other present and future large-scale facilities, with excellent overviews from the CERN LHC complex, SIS18, FAIR, RHIC, and HIAF. A tantalizing talk discussed the possibility of 4D phase-space painting to arrive at a self-consistent distribution without halo formation under study for the SNS.

Workshop participants then had the chance to visit the GSI accelerator control room, walk around existing machines like the UNILAC and the ESR, and to observe the impressive FAIR construction site.

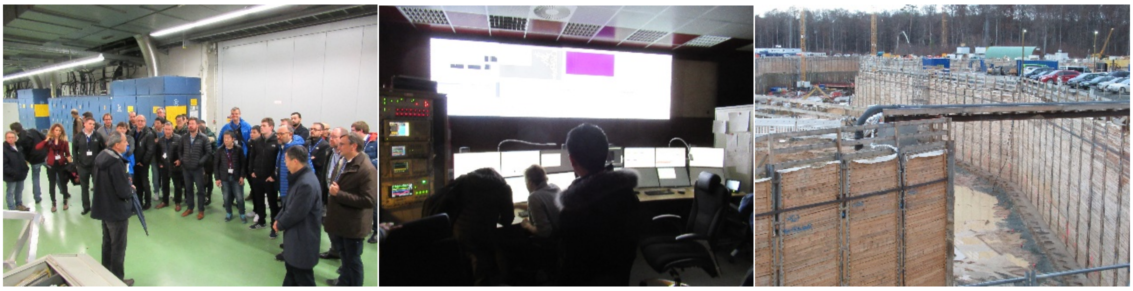

Participants of the APEC2018 workshop visiting the GSI UNILAC, the accelerator control room, and the FAIR construction site.

All talks in the afternoon addressed the performance challenges for various versions of the Future Circular Collider, including beamscreen design, resistive wall instability, HOM heating, RF beam loading, electron-cloud suppression, handling of synchrotron radiation, and future beam tests at the DAΦNE test facility in Frascati.

The morning of the second day reviewed the application of optimization algorithms and machine learning tools to accelerator controls, with applications to SIS18, SNS, MYRRHA, Chinese ADS, and ESS. The rest of the day covered new types of Landau damping, real-time diagnostics for collider performance, the state of the art in accelerator feedback systems, and RF control, including automated phase tuning and cavity recovery. The survey of accelerator feedback systems ranged from extremely narrow-band dampers for multibunch mode 0, via wideband intrabunch feedback systems, to stabilization against ground motion.

The last day of APEC2018 focused on optimal RAMS characteristics for particle accelerators, modeling accelerator performance, and the route towards an open data infrastructure for accelerator reliability. Medical accelerators will serve as an important first test bed, and reliability database compiled by the fusion community as an example.

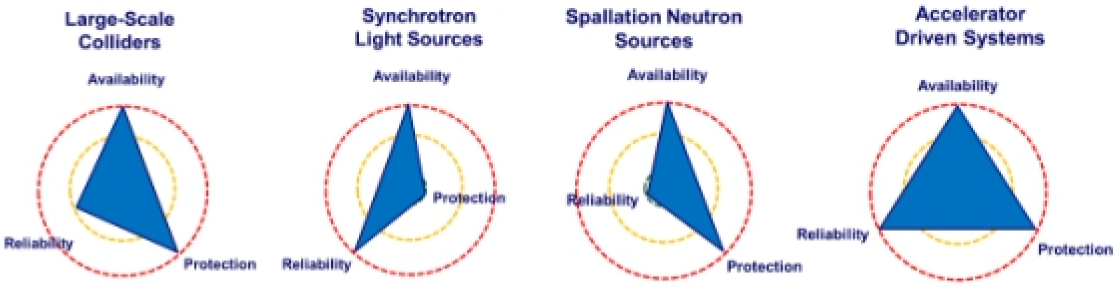

RASP charts illustrating the variation of requirements with the type of accelerator (Andrea Apollonio, CERN).

The final APEC2018 talk, by Suzie Sheehy of Oxford, presented intriguing results from reliability and failure-mode studies of medical LINACs "in challenging environments".

More details and all the presentations are available on the APEC2018 workshop web site https://indico.gsi.de/event/7510/ .

During discussions at APEC2018, the participants agreed on a community survey of the mechanisms limiting accelerator performance and the pertinent mitigation measures.

5 Forthcoming Beam Dynamics Events

5.1 10th International Particle Accelerator Conference (IPAC2019)

In this age, when we are more globally connected through digital technology than ever before, humans still find there is a great need and desire to meet in person. Considering this need, the 10th International Particle Accelerator Conference will take place 19-24 May 2019 at the Melbourne Convention & Exhibition Centre (MCEC) in Melbourne, Australia.

IPAC is the main international event for the worldwide accelerator community and related industry partners. Attendees will be presented with cutting-edge accelerator research and development results and gain the latest insights into accelerator facilities across the globe. The conference is an annual event cycling between Asia, Europe and the Americas, with the most recent events being held in Vancouver (2018) and Copenhagen (2017). The 2019 edition will be hosted by the Australian Nuclear Science and Technology Organisation (ANSTO) Australian Synchrotron, together with the University of Melbourne, the City of Melbourne and the Melbourne Convention Bureau.

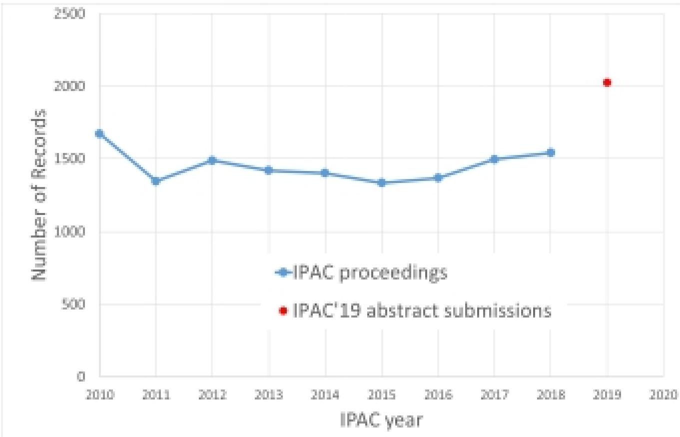

At IPAC'19, you will have the opportunity to meet and interact with accelerator scientists, engineers, students and vendors while experiencing one of the world's most livable city. A record number of 2,024 abstract submissions were received, so the conference promises to be well attended. Along with the usual JACoW proceedings, IPAC'19 will continue with the option for delegates to have a selected number of papers peer reviewed before the conference and published in the IOP Journal of Physics Conference Series.

Guided tours of the Australian Synchrotron, which located is located about 20 km from the venue, and of ANSTO in Sydney will be available to participants of the conference. The scientific equipment covered in the tours include the electron accelerators and photon beamlines at the Australian Synchrotron and the research reactor and neutron beamlines at ANSTO. The tours will have unprecedented access to the facilities and a chance to see firsthand some of the research being done. Visit he conference website for more information and registration.

http://ipac19.org

Mark Boland, Chair IPAC'19 Organising Committee

5.2 ICFA mini-Workshop on “Mitigation of Coherent Beam Instabilities in Particle Accelerators” (MCBI2019)

After the ICFA mini-Workshop on “Electromagnetic Wake Fields and Impedances in Particle Accelerators" held in 2014 in Erice, Sicily, and the ICFA mini-Workshop on "Impedances and Beam Instabilities in Particle Accelerators", held in 2017 in Benevento, Italy, the third workshop of this series will be organised jointly between CERN and EPFL and it will take place from September 23 to 27, 2019, in Zermatt, Switzerland.

This workshop will focus on all the mitigation methods for all the coherent beam instabilities, reviewing in detail the theories (and underlying assumptions), simulations and measurements on one hand, but on the other hand trying to compare the different mitigation methods (e.g. with respect to other effects such as beam lifetime) to provide the simplest and more robust solutions to the operators of the control rooms.

The workshop site

https://indico.cern.ch/e/MCBI2019

will be regularly updated to include the latest information as it becomes available.

Elias Métral, Tatiana Pieloni and Giovanni Rumolo, IOC Chairs MCBI2019

6 Announcements of the Beam Dynamics Panel

6.1 ICFA Beam Dynamics Newsletter

6.1.1 Aim of the Newsletter

The ICFA Beam Dynamics Newsletter is intended as a channel for describing unsolved problems and highlighting important ongoing works, and not as a substitute for journal articles and conference proceedings that usually describe completed work. It is published by the ICFA Beam Dynamics Panel, one of whose missions is to encourage international collaboration in beam dynamics.

Normally it is published every April, August and December. The deadlines are 15 March, 15 July and 15 November, respectively.

6.1.2 Categories of Articles

The categories of articles in the newsletter are the following:

1. Announcements from the panel.

Reports of beam dynamics activity of a group.

Reports on workshops, meetings and other events related to beam dynamics.

Announcements of future beam dynamics-related international workshops and meetings.

Those who want to use newsletter to announce their workshops are welcome to do so. Articles should typically fit within half a page and include descriptions of the subject, date, place, Web site and other contact information.

Review of beam dynamics problems: This is a place to bring attention to unsolved problems and should not be used to report completed work. Clear and short highlights on the problem are encouraged.

Letters to the editor: a forum open to everyone. Anybody can express his/her opinion on the beam dynamics and related activities, by sending it to one of the editors. The editors reserve the right to reject contributions they judge to be inappropriate, although they have rarely had cause to do so.

The editors may request an article following a recommendation by panel members. However anyone who wishes to submit an article is strongly encouraged to contact any Beam Dynamics Panel member before starting to write.

6.1.3 How to Prepare a Manuscript

Before starting to write, authors should download the template in Microsoft Word format from the Beam Dynamics Panel web site:

http://icfa-bd.kek.jp/icfabd/news.html

It will be much easier to guarantee acceptance of the article if the template is used and the instructions included in it are respected. The template and instructions are expected to evolve with time so please make sure always to use the latest versions.

The final Microsoft Word file should be sent to one of the editors, preferably the issue editor, by email.

The editors regret that LaTeX files can no longer be accepted: a majority of contributors now prefer Word and we simply do not have the resources to make the conversions that would be needed. Contributions received in LaTeX will now be returned to the authors for re-formatting.

In cases where an article is composed entirely of straightforward prose (no equations, figures, tables, special symbols, etc.) contributions received in the form of plain text files may be accepted at the discretion of the issue editor.

Each article should include the title, authors' names, affiliations and e-mail addresses.

6.1.4 Distribution

A complete archive of issues of this newsletter from 1995 to the latest issue is available at

http://icfa-usa.jlab.org/archive/newsletter.shtml.

Readers are encouraged to sign-up for electronic mailing list to ensure that they will hear immediately when a new issue is published.

The Panel's Web site provides access to the Newsletters, information about future and past workshops, and other information useful to accelerator physicists. There are links to pages of information of local interest for each of the three ICFA areas.

Printed copies of the ICFA Beam Dynamics Newsletters are also distributed (generally some time after the Web edition appears) through the following distributors:

John Byrd	jmbyrd@lbl.gov	North and South Americas
Rainer Wanzenberg	rainer.wanzenberg@desy.de	Europe++ and Africa
Toshiyuki Okugi	toshiyuki.okugi@kek.jp	Asia**and Pacific

++ Including former Soviet Union.

** For Mainland China, Jiu-Qing Wang (wangjq@mail.ihep.ac.cn) takes care of the distribution with Ms. Su Ping, Secretariat of PASC, P.O. Box 918, Beijing 100039, China.

To keep costs down (remember that the Panel has no budget of its own) readers are encouraged to use the Web as much as possible. In particular, if you receive a paper copy that you no longer require, please inform the appropriate distributor.

6.1.5 Regular Correspondents

The Beam Dynamics Newsletter particularly encourages contributions from smaller institutions and countries where the accelerator physics community is small. Since it is impossible for the editors and panel members to survey all beam dynamics activity worldwide, we have some Regular Correspondents. They are expected to find interesting activities and appropriate persons to report them and/or report them by themselves. We hope that we will have a "compact and complete" list covering all over the world eventually. The present Regular Correspondents are as follows:

Liu Lin	*Liu@ns.lnls.br*	*LNLS Brazil*
Sameen Ahmed Khan	Rohelakan@yahoo.com	SCOT, Middle East and Africa

We are calling for more volunteers as Regular Correspondents.

6.2 ICFA Beam Dynamics Panel Members

Name	eMail	Institution
Rick Baartman	baartman@lin12.triumf.ca	TRIUMF, 4004 Wesbrook Mall, Vancouver, BC, V6T 2A3, Canada
Marica Biagini	marica.biagini@lnf.infn.it	INFN-LNF, Via E. Fermi 40, C.P. 13, Frascati, Italy
John Byrd	jbyrd@anl.gov	Accelerator Systems Division Argonne National Laboratory 9700 S. Cass Ave Building 401-C4263, Argonne, IL 60439, U.S.A.
Yunhai Cai	yunhai@slac.stanford.edu	SLAC, 2575 Sand Hill Road, MS 26 Menlo Park, CA 94025, U.S.A.
Yong Ho Chin	yongho.chin@kek.jp	KEK, 1-1 Oho, Tsukuba-shi, Ibaraki-ken, 305-0801, Japan
Jie Gao	gaoj@ihep.ac.cn	Institute for High Energy Physics, P.O. Box 918, Beijing 100039, China
Ajay Ghodke	ghodke@cat.ernet.in	RRCAT, ADL Bldg. Indore, Madhya Pradesh, 452 013, India
Eliana Gianfelice-Wendt	eliana@fnal.gov	Fermilab, Mail Station 312, PO Box 500, Batavia IL 60510-5011, U.S.A.
Ingo Hofmann	i.hofmann@gsi.de	High Current Beam Physics, GSI Darmstadt, Planckstr. 1, 64291 Darmstadt, Germany
Sergei Ivanov	sergey.ivanov@ihep.ru	Institute for High Energy Physics, Protvino, Moscow Region, 142281 Russia
In Soo Ko	isko@postech.ac.kr	Pohang Accelerator Lab, San 31, Hyoja-Dong, Pohang 790-784, South Korea
Elias Metral	elias.metral@cern.ch	CERN, CH-1211, Geneva 23, Switzerland
Peter Ostroumov	Ostroumov@frib.msu.edu	FRIB, National Superconducting Cyclotron Laboratory, Michigan State University, 640 S. Shaw Lane East Lansing, Michigan 48824, U.S.A.
Mark Palmer	mpalmer@bnl.gov	Brookhaven National Lab, Upton, NY 11973, U.S.A.
Chris Prior	chris.prior@stfc.ac.uk	ASTeC Intense Beams Group, STFC RAL, Chilton, Didcot, Oxon OX11 0QX, U.K.
Ji Qiang	jqiang@lbl.gov	Lawrence Berkeley National Laboratory (LBNL), MS 71J-100a, One Cyclotron Road, Berkeley, California, CA 94720-8211 USA
Yuri Shatunov	Yu.M.Shatunov@inp.nsk.su	Acad. Lavrentiev, Prospect 11, 630090 Novosibirsk, Russia
Yoshihiro Shobuda	yoshihiro.shobuda@j-parc.jp	Japan Proton Accelerator Research Complex (J-PARC), Shirakata-Shirane 2-4, J - Tokai-Mura, Naka-Gun, Ibaraki-Ken 319-1195
Jiu-Qing Wang	wangjq@ihep.ac.cn	Institute for High Energy Physics, P.O. Box 918, 9-1, Beijing 100039, China
Rainer Wanzenberg	rainer.wanzenberg@desy.de	DESY, Notkestrasse 85, 22603 Hamburg, Germany
Zhentang Zhao	zhaozhentang@sinap.ac.cn	SINAP, Jiading campus: 2019 Jia Luo Road, Jiading district, Shanghai 201800, P. R. China Zhangjiang campus: 239 Zhang Heng Road, Pudong New District, Shanghai 201203, P. R. China